STUDY OF SOME ALPHA INDUCED REACTIONS AT THE CYCLOTRON ENERGIES

ABSTRACT

THESIS SUBMITTED IN PARTIAL FULFILMENT
OF THE REQUIREMENTS FOR THE AWARD
OF THE DEGREE OF

Doctor of Philosophy

IN

PHYSICS

ISAR AHMAD RIZVI

DEPARTMENT OF PHYSICS
ALIGARH MUSLIM UNIVERSITY
ALIGARH (INDIA)

1988

A B S T R A C T

As far as alpha-particle interaction with a nucleus is concerned the mode of reaction mechanism has been a point of interest for several years. Sufficient evidences are present to believe that the mode of reaction is not merely through compound nucleus formation. Hence the emphasis on the type, non-equilibrium reaction mechanism which is taking part in such type of nuclear reaction, has to be given a due consideration. The experimental data on alpha-particle interaction show a high energy tail in the excitation function, which is inexplicable in the framework of equilibrium (compound) model. When the pre-equilibrium emission of particles prior to the equilibrium formation is taken into consideration, the experimental trend is somehow explained. Several semi-classical models have been proposed which take care of above considerations. One of these models is the geometry dependent hybrid (GDH) model which is relatively simpler to handle.

With the availability of high-resolution and large volume semi-conductor detectors, and of good quality beams, the excitation function measurement business has entered into a new era. The knowledge of excitation functions is important not only for nuclear physics research, but also for practical applications as in the production of radio-nuclides and for solid-state research. One of the interesting features of (α,xpyn) reaction is that alpha-particles bring in a large amount of angular momentum in

the compound nucleus. This results in a population of moderately high spin states. The work reported in this thesis deals with the study of some alpha induced reactions at the cyclotron energies. The thesis has been ramified into five chapters. In Chapter - I, a general introduction regarding nuclear reactions, including different theories and models, is presented. In this chapter, a brief view of the present work is also given.

In Chapter-II, the various nuclear reaction theories are discussed. Chapter-III contains the nuclear model code which is used in the present investigation. In Chapter-IV, experimental technique and details of measurements are described. The experiments were done at the Variable Energy Cyclotron Centre (VECC), Calcutta (India). Excitation functions for the reactions $^{55}Mn(\alpha,n)^{58}Co$, $^{55}Mn(\alpha,2n)^{57}Co$, $^{55}Mn(\alpha,3n)^{56}Co$, $^{55}Mn(\alpha,4n)^{55}Co$, $^{55}Mn(\alpha,\alpha n)^{54}Mn$ + $^{55}Mn(\alpha,2p3n)^{54}Mn$, $^{55}Mn(\alpha,\alpha 3n)^{52g}Mn$, $^{63}Cu(\alpha,n)^{66}Ga$ $^{63}Cu(\alpha,2n)^{65}Ga$ + $^{63}Cu(\alpha,pn)^{65}Zn$, $^{65}Cu(\alpha,n)^{68}Ga$, $^{65}Cu(\alpha,2n)^{67}Ga$, $^{65}Cu(\alpha,3n)^{66}Ga$, $^{69}Ga(\alpha,n)^{72}As$, $^{69}Ga(\alpha,2n)^{71}As$, $^{69}Ga(\alpha,3n)^{70}As$, $^{69}Ga(\alpha,p3n)^{69}Ge$, $^{71}Ga(\alpha,n)^{74}As$, $^{71}Ga(\alpha,4n)^{71}As$, $^{209}Bi(\alpha,3n)^{210}At$ and $^{209}Bi(\alpha,4n)^{209}At$ have been measured by the activation method using 'Stacked foil' technique, the alpha-particle energies ranging from 7 to 60 MeV. Bombardments were made with the alpha particle beam of 40 MeV and 60 MeV. The beam was collected in a 'Faraday-cup' and the total charge was measured by a current integrator. The induced gamma activities in each foil were recorded by a 100 cc Ge(Li) spectrometer.

Chapter-V deals with results and discussion of the measurements. Measured excitation functions are compared with the earlier reported values, whatsoever available, and also with those evaluated theoretically on the basis of both equilibrium and pre-equilibrium reactions using the nuclear model code 'ALICE/LIVERMORE-82' in the framework of geometry dependent hybrid (GDH) model. Present analysis indicates clearly the presence of considerable amount of pre-equilibrium contributions in alpha induced reactions. Pure equilibrium reaction mechanism is unable to explain the high energy tail of the measured excitation functions and a proper admixture of equilibrium and pre-equilibrium processes is needed to reproduce the experimental excitation functions in full energy range. The initial exciton configuration n_o = 4(2 neutrons plus 2 protons, no hole) gives the satisfactory reproduction of experimental data and supports the finding of many earlier investigations. The pre-equilibrium fraction (f_{PE}) is found to be dependent on the projectile energy and increases very fast as the energy of alpha particle increases and then at a higher excitation energy when the multiplicity of the outgoing particles increases, the pre-equilibrium fraction becomes more or less constant.

STUDY OF SOME ALPHA INDUCED REACTIONS AT THE CYCLOTRON ENERGIES

THESIS SUBMITTED IN PARTIAL FULFILMENT
OF THE REQUIREMENTS FOR THE AWARD
OF THE DEGREE OF

Doctor of Philosophy

IN

PHYSICS

ISAR AHMAD RIZVI

DEPARTMENT OF PHYSICS
ALIGARH MUSLIM UNIVERSITY
ALIGARH (INDIA)

1988

Dedicated

To My

Parents

Certified that the work presented in this thesis is the original work of Mr. Isar Ahmad Rizvi, done under my supervision.

(A.K. Chaubey)

READER AND INCHARGE,
NUCLEAR PHYSICS LABORATORY
DEPARTMENT OF PHYSICS
ALIGARH MUSLIM UNIVERSITY
ALIGARH 202 002, INDIA.

A_C_K_N_O_W_L_E_D_G_E_M_E_N_T

I have great pleasure in acknowledging my deep sense of gratitude to my supervisor, Dr. A.K. Chaubey, Reader in the Department of Physics and Incharge, Nuclear Physics Laboratory Aligarh Muslim University, Aligarh (India) for his invaluable guidance, unfailing help and encouragement during the course of this work. I am also greatly indebted to the late Prof. M.L. Sehgal, my former Supervisor and ex-Chairman of our Department from whom I got the initial inspiration to go ahead with this research.

I would like to thank Prof. M. Shafi, Chairman, Department of Physics, Aligarh Muslim University, Aligarh for providing the necessary research facilities to me in the Department. Prof. M.Z.R. Khan, the Coordinator, D.S.A. (Physics) Programme, has also been a source of constant encouragement to me throughout this work.

I also wish to thank the Director and technical staff of the Variable Energy Cyclotron Centre (VECC), Calcutta (India) for providing me the experimental facilities and hospitality during my stay there. I must place on record the tremendous support extended to me by Dr. R.K. Bhandari of the same establishment.

Comments and suggestions on the Computer Code 'ALICE/LIVERMORE-82' by Prof. M. Blann of Lawrence Livermore National Laboratory, University of California, Livermore (USA) and Dr. S.B. Garg of Bhabha Atomic Research Centre, Bombay (India) are also gratefully acknowledged.

I am grateful to Dr. M. Afzal Ansari, Lecturer, Department of Physics, Aligarh Muslim University, Aligarh for his

continuous help and many stimulating discussions on the subject throughout the course of this work. I must thank all my colleagues and friends especially, Dr. R.K.Y. Singh, Dr. R.P. Gautam, Dr. Ahrar Hussain, Mr. M.Q.R. Khan, Mr. M.S. Ahmad, Mr. M.K. Bhardwaj and Mr. Harvans Singh, for their valuable suggestions at various stages of this work. The occasional help of general nature provided by Mr. Naeemuzzaman Khan, my hostel colleague, during the completion of this work is also highly acknowledged.

The financial assistance from the University Grants Commission, New Delhi (India) and Aligarh Muslim University, Aligarh in the form of fellowships, is also deeply acknowledged.

Finally, I must thank Mr. I. Salim, S.T.A. in the Department of Physics, who deserves my hearty gratitude for his help and technical support, as also Mr. Mohd. Rashid who extended his full cooperation in typing the thesis expeditiously and Mr. Naeem Ahmad who took care to draw the figures accurately.

Isar Ahmad Rizvi

(ISAR AHMAD RIZVI)

Dated : 31·X·88

A B S T R A C T

As far as alpha-particle interaction with a nucleus is concerned the mode of reaction mechanism has been a point of interest for several years. Sufficient evidences are present to believe that the mode of reaction is not merely through compound nucleus formation. Hence the emphasis on the type, non-equilibrium reaction mechanism which is taking part in such type of nuclear reaction, has to be given a due consideration. The experimental data on alpha-particle interaction show a high energy tail in the excitation function, which is inexplicable in the framework of equilibrium (compound) model. When the pre-equilibrium emission of particles prior to the equilibrium formation is taken into consideration, the experimental trend is somehow explained. Several semi-classical models have been proposed which take care of above considerations. One of these models is the geometry dependent hybrid (GDH) model which is relatively simpler to handle.

With the availability of high-resolution and large volume semi-conductor detectors, and of good quality beams, the excitation function measurement business has entered into a new era. The knowledge of excitation functions is important not only for nuclear physics research, but also for practical applications as in the production of radio-nuclides and for solid-state research. One of the interesting features of (α,xpyn) reaction is that alpha-particles bring in a large amount of angular momentum in

the compound nucleus. This results in a population of moderately high spin states. The work reported in this thesis deals with the study of some alpha induced reactions at the cyclotron energies. The thesis has been ramified into five chapters. In Chapter - I, a general introduction regarding nuclear reactions, including different theories and models, is presented. In this chapter, a brief view of the present work is also given.

In Chapter-II, the various nuclear reaction theories are discussed. Chapter-III contains the nuclear model code which is used in the present investigation. In Chapter-IV, experimental technique and details of measurements are described. The experiments were done at the Variable Energy Cyclotron Centre (VECC), Calcutta (India). Excitation functions for the reactions $^{55}Mn(\alpha,n)^{58}Co$, $^{55}Mn(\alpha,2n)^{57}Co$, $^{55}Mn(\alpha,3n)^{56}Co$, $^{55}Mn(\alpha,4n)^{55}Co$, $^{55}Mn(\alpha,\alpha n)^{54}Mn$ + $^{55}Mn(\alpha,2p3n)^{54}Mn$, $^{55}Mn(\alpha,\alpha 3n)^{52g}Mn$, $^{63}Cu(\alpha,n)^{66}Ga$, $^{63}Cu(\alpha,2n)^{65}Ga$ + $^{63}Cu(\alpha,pn)^{65}Zn$, $^{65}Cu(\alpha,n)^{68}Ga$, $^{65}Cu(\alpha,2n)^{67}Ga$, $^{65}Cu(\alpha,3n)^{66}Ga$, $^{69}Ga(\alpha,n)^{72}As$, $^{69}Ga(\alpha,2n)^{71}As$, $^{69}Ga(\alpha,3n)^{70}As$, $^{69}Ga(\alpha,p3n)^{69}Ge$, $^{71}Ga(\alpha,n)^{74}As$, $^{71}Ga(\alpha,4n)^{71}As$, $^{209}Bi(\alpha,3n)^{210}At$ and $^{209}Bi(\alpha,4n)^{209}At$ have been measured by the activation method using 'Stacked foil' technique, the alpha-particle energies ranging from 7 to 60 MeV. Bombardments were made with the alpha particle beam of 40 MeV and 60 MeV. The beam was collected in a 'Faraday-cup' and the total charge was measured by a current integrator. The induced gamma activities in each foil were recorded by a 100 cc Ge(Li) spectrometer.

Chapter-V deals with results and discussion of the measurements. Measured excitation functions are compared with the earlier reported values, whatsoever available, and also with those evaluated theoretically on the basis of both equilibrium and pre-equilibrium reactions using the nuclear model code 'ALICE/LIVERMORE-82' in the framework of geometry dependent hybrid (GDH) model. Present analysis indicates clearly the presence of considerable amount of pre-equilibrium contributions in alpha induced reactions. Pure equilibrium reaction mechanism is unable to explain the high energy tail of the measured excitation functions and a proper admixture of equilibrium and pre-equilibrium processes is needed to reproduce the experimental excitation functions in full energy range. The initial exciton configuration n_o = 4(2 neutrons plus 2 protons, no hole) gives the satisfactory reproduction of experimental data and supports the finding of many earlier investigations. The pre-equilibrium fraction (f_{PE}) is found to be dependent on the projectile energy and increases very fast as the energy of alpha particle increases and then at a higher excitation energy when the multiplicity of the outgoing particles increases, the pre-equilibrium fraction becomes more or less constant.

C_O_N_T_E_N_T_S

		Page
CHAPTER - I	INTRODUCTION	01
	References	11
CHAPTER - II	NUCLEAR REACTION THEORIES	
2.1	Compound nucleus theory	17
2.2	Pre-equilibrium theory	24
2.2.1	Intranuclear Cascade Model ...	26
2.2.2	Harp-Miller and Berne Model ...	28
2.2.3	Exciton Model	30
2.2.4	Hybrid Model	37
2.2.5	Geometry Dependent Hybrid Model ...	40
	References	44
CHAPTER - III	NUCLEAR MODEL CODE	
3.1	Types of calculation available in code ...	49
3.2	Formulations	51
3.3	Code subroutines	59
3.4	Use of the code	63
	References	65
CHAPTER - IV	EXPERIMENTAL TECHNIQUE AND MEASUREMENTS	
4.1	Formulation	69
4.2	Calibration and Detector Efficiency ...	72
4.3	Irradiations	76

4.4 Counting 80

4.5 Measurements 81

4.5.1 Target Nucleus: ^{55}Mn 82

4.5.2 Target Nucleus: $^{63,65}Cu$ 108

4.5.3 Target Nucleus: $^{69,71}Ga$ 123

4.5.4 Target Nucleus: ^{209}Bi 141

4.6 Errors 153

References 156

CHAPTER - V RESULTS AND DISCUSSION

5.1 Experimental Results 159

5.2 Model Calculations 167

5.3 Discussion 170

5.4 Conclusions 188

References 192

List of Publications 196

- oOo -

CHAPTER - I

I N T R O D U C T I O N

The study of nuclear reaction is of paramount importance from the point of view of understanding the nuclear reaction mechanism. With the advent of the high-energy accelerating machines, such as the Van de Graaff generator, the Cockroft-Walton accelerator, the cyclotron, and the pelletron, the high-energy particles like protons, deuterons, alpha particles and heavy ions have become available to produce nuclear reactions in all elements of the periodic table. Progress in accelerator technology has helped fundamental research tremendously, apart from giving spin-off benefits in applied fields. Modern accelerators play an effective complementary role to nuclear reactions, for they produce radioactive isotopes which have various applications. While nuclear reactors can produce neutron-rich isotopes mostly around the line of β-stability, nuclear reactions induced by ions enable the production of very useful radioactive isotopes on both sides from the line of β-stability. With ever increasing use of these radioactive isotopes in various applied fields, there is a growing demand to provide knowledge of the 'Excitation function' of nuclear reactions, in order, that the production of selected isotopes could be maximized. From the physics point of view, the shape of the excitation function reveals the reaction mechanism.

Nuclear reactions are classified under two categories, depending upon the time at which they occur and are accordingly called direct reactions, or compound nucleus reactions. The direct reactions are supposed to be initiated and completed at the very first projectile-target collision, and hence are thought to occur within the time ($\sim 10^{-22}$ sec.) taken by projectile to cross the nuclear diameter. On the other hand, compound nucleus reactions continue to the end of a very large number of internal collisions, and therefore take a comparatively longer time ($\sim 10^{-16}$ sec.). Again, the particles emitted in the direct and compound stages may be recognised by their energies and angular distributions. The particles from the direct reactions are emitted predominantly in the same direction as the incident particle, with similar energies. On the other hand, particles emitted via a compound nucleus, are emitted in all directions, with an angular distribution symmetric of about 90°, and when the final states merge into continuum, the angular distributions have a characteristic Maxwellian energy distribution. Also, the compound reaction mechanism is more likely to take place at relatively lower excitation energies, while the direct process is more probable at higher excitations.

As isochronous cyclotrons came into wide usage in the 1960s and higher projectile energies became available for nuclear reaction studies[1)], several new experimental features emerged from systematic investigations. Thus, there has been increasing evidence to show that some reactions take place with intermediate

time scales between the two extremes. They manifest themselves in the high energy tails of excitation functions, non-Maxwellian hard components in the particle spectra, and a gradually changed pattern of angular distributions, from forward peaking to fore-and-off symmetry. These new experimental features were neither consistent with the compound nucleus model[2] nor with the direct reaction model[3]. This may be explained with the help of Fig. 1.1, in which the general nature of observed energy spectrum of particles, in a high energy nuclear reaction, at a particular angle and for a specific residual nucleus, is shown. The broad peak in the lower energy corresponds to evaporation from a compound nucleus, while the sharp peaks in the high energy tail of the spectrum correspond to population of low-lying states in the residual nucleus and can be attributed to the direct reactions. The smooth distribution in between the broad and the sharp peaks has no explanation in these two approaches. This portion may be attributed to some intermediate processes called 'Pre-compound' or 'Pre-equilibrium processes[1,4,5].

The pre-equilibrium concept may be considered a bridge between the two extremes[1,4-9]. A series of complicated collisions inside the nucleus follows the initial interaction, and there is a certain probability of particle emission after each one of these collisions. In these intermediate processes, selectivity of the direct reactions is lost. Also, only some degree of freedom is involved, i.e., the number of excited particles and holes which share the excitation energy of intermediate system is small. The study of pre-equilibrium

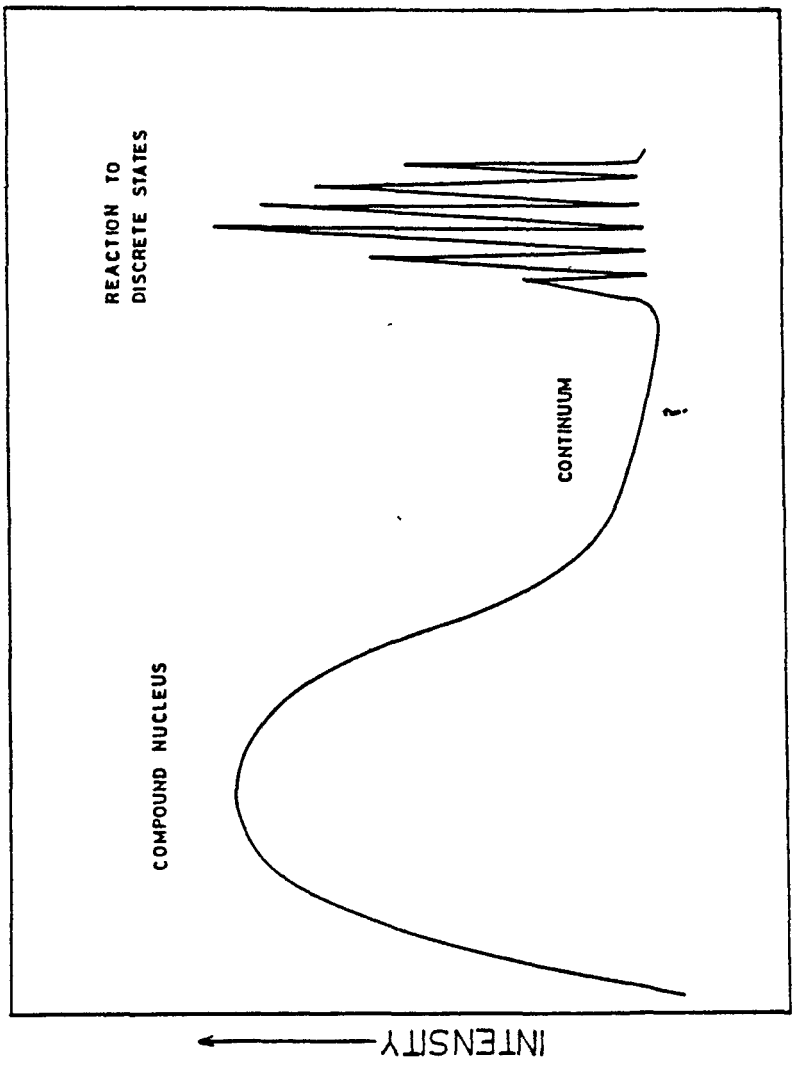

Fig. 1.1 Typical particle spectrum obtained in a high energy nuclear reaction.

phenomena is useful in radiotherapy[10], space explorations[11], fusion reactor design[12] and astrophysics[13,14].

Since the basic work of Griffin[15] in 1966, a variety of different pre-equilibrium models have been developed[16]. The most widely used models are the intranuclear cascade model (INC), the Harp-Miller-Berne (HMB) model, but more particularly, the exciton (EM) and the hybrid/geometry dependent hybrid (GDH) models.

The intra-nuclear cascade model provides a classical approach to pre-compound decay[17,18]. In this model, the trajectories of particles inside the nucleus are followed in coordinate space by means of Monte Carlo methods[16]. The numerical simulation of the scattering process is based on experimental free nucleon-nucleon (N-N) scattering cross-sections, and the angular distributions. Upto 1975, there was the only pre-equilibrium model able to predict angular distributions of emitted particles.

The Harp-Miller-Berne model[19] has its energy divided into bins and the average number of occupied single particle levels in each bin is computed, usually in the framework of the Fermi gas model. In course of time, the occupation of nucleons in each bin changes due to the intranuclear collisions. The evolution of this excited nuclear Fermi gas is followed through numerical calculation of the relative occupation of each bin, as a function of time, by solving a set of coupled differential equations. The transition rates are obtained from experimental

free nucleon-nucleon scattering cross-sections. In contrast to the intra-nuclear cascade model, this model permits a quantum statistical treatment, though in practice, the transition rates are computed in a classical manner. However, it cannot predict angular distributions. Yet another practical disadvantage of the Harp-Miller-Berne model is its computational complexity. To deal with such situations additional assumptions have to be introduced. This has been done in the exciton and hybrid models, which now have become the most popular pre-equilibrium models for applications in nuclear data evaluation[16].

The exciton and hybrid models, originate from the work of Griffin[15] and are closely related. In these models, the nuclear state is characterized by the excitation energy E and the total number(n)of particles p above holes h below the Fermi surface. Also, in the exciton model, it is assumed that all possible ways of sharing the excitation energy between different particle-hole configurations, with the same exciton number n, have equal a priori probability. Instead of tracing the evolution of the occupation of each energy bin, as in the Harp-Miller-Berne model, one merely traces the temporal development of the exciton number n, which changes in time, as a result of intranuclear collisions. This assumption makes pre-equilibrium theory amenable to practical calculations.

In the hybrid model an attempt is made to retain some more elements from the Harp-Miller-Berne model, e.g., by using the concept of mean free path in nuclear matter, internal transition

rates are related to the free nucleon-nucleon scattering cross-section. A further refinement is introduced in the geometry dependent hybrid (GDH) model by taking into account the variation of nuclear density at the nuclear surface[1].

More recently, several quantum-mechanical theories have been proposed[20]. These quantum-mechanical theories provide in principle, a way of calculating the cross-sections of pre-equilibrium processes without the uncertainties of the semi-classical approximations. These theories are based on detailed expressions for the microscopic processes occuring in the nucleus in which a statistical averaging is done. Some of the important theories are proposed by Feshbach et al.[5], Agassi et al.[21], McVoy and Tang[22], Tamura et al.[23-25] and Udagawa et al.[26-29]. At present these theories are applicable only for the nucleon induced reactions[16] because, for a complex particle the quantum mechanical treatment of the initial projectile-target interaction becomes very much complex. Therefore, measured excitation functions have been calculated theoretically with and without the inclusion of pre-equilibrium emission using semi-classical models.

In order to test pre-equilibrium theories, it is reasonable to have extensive studies on excitation functions, energy and angular distributions, etc., of particles emitted in nuclear reactions at higher excitation energies. The study of excitation functions of α-induced reactions can give some informations about the reaction mechanism[30-34]. The presence of pre -

equilibrium component in any reaction can be observed from the high energy tail of the excitation function, which cannot be reproduced by the compound (statistical) model. The study of excitation functions is also important from the point of view of nucleo-synthesis[30].

The alpha particle was used in the earliest determination of nuclear size, and it is still regarded as one of the most useful probes for learning the shape of the nucleus. It is a complex particle, and interacts with matter (or nuclei) in a more complicated way than nucleons do. However, its attenuation in nuclear matter restricts the interaction to the low-density surface region of the nucleus, particularly if the alpha particle bombarding energy is not too high. At high energies, the alpha particle is regarded as an important projectile for nuclear reaction studies. It can impart[31] considerable angular momentum to the target nucleus and hence relatively high angular momentum states can be populated and consequently, various type of nuclear reaction studies are possible. From these reaction studies some information about nuclear structure such as shell effect[35,36], nucleon densities[39] and nuclear reaction mechanism[31-38] can be obtained. These studies are also useful in the construction of nuclear level schemes[40-44].

A lot of work has been done on the study of excitation functions of α-induced reactions for various target nuclides[45], over a wide range of energy, and over a wide range of periodic table. However, the situation is still unsatisfactory, as

there are large discrepancies in the reported values[45], even for a single specific reaction. Moreover, the data are incomplete and contain considerable errors. Besides, analysis of these excitation functions, in the past, has been carried out on the basis of the compound nucleus (statistical equilibrium) model[46,47], and, in general, this mechanism of the reaction could not account for the high energy tails of the excitation functions[48-51].

In the present work, excitation functions for α-induced reactions have been experimentally measured in the energy range from ≲7-60 MeV for nineteen reactions covering a relatively wide mass region from 55 to 209. The stacked foil activation technique has been used for the irradiations of target foils. The irradiation of the stacks was carried out at the Variable Energy Cyclotron Centre (VECC), Calcutta (India). The activity produced in foils was measured using a 100 cc ORTEC Ge(Li) detector, in conjunction with a 4K multichannel analyser. The excitation functions have also been evaluated theoretically using the computer code 'ALICE/LIVERMORE-82'[52] which is based on compound and pre-equilibrium models. In this code the calculations based on compound nucleus are due to a Weisskopf-Ewing model[53], while pre-equilibrium calculations are based on hybrid/geometry dependent hybrid models[54-56]. The experimental results have been compared with the theoretical predictions based on the widely used pre-equilibrium geometry dependent hybrid model[55]. Theory and

experiment were found, in general, in agreement. The pre-equilibrium fraction (f_{PE}) of the total reaction cross-section nas also been calculated at different energies. To the best of our knowledge excitation functions for the $^{55}Mn(\alpha,\alpha 3n)^{52g}Mn$, $^{69}Ga(\alpha,n)^{72}As$, $^{69}Ga(\alpha,2n)^{71}As$, $^{69}Ga(\alpha,3n)^{70}As$, $^{69}Ga(\alpha,p3n)^{69}Ge$, $^{71}Ga(\alpha,n)^{74}As$ and $^{71}Ga(\alpha,4n)^{71}As$ reactions, have been reported for the first time.

The details of nuclear reaction theories, nuclear model code and experimental measurements have been given in Chapter II, III and IV respectively. Chapter - V deals with results and discussion of the measurements.

References

1) M. Blann : Ann. Rev. Nucl. Sci. 25 (1975) 123.

2) N. Bohr : Nature 137 (1936) 344.

3) A.M. Lane : Nucl. Phys. 11 (1959) 625.

4) E. Gadioli and E. Gadioli Erba : Nuclear Theory for Applications 1980, IAEA - SMR - 68/1, Vienna (1981) p. 3.

5) H. Feshbach, A.K. Kerman and S. Koonin : Ann. Phys.(N.Y.) 125 (1980) 429.

6) P.E. Hodgson : Heavy Ion Collisions - Proc. of Inter. Summer School, La - Rabida, Spain, 1982, p. 220.

7) H. Jahn : Nuclear Theory for Applications - 1982, IAEA - SMR - 93, Vienna (1984) 39.

8) V.E. Bunakov : Nuclear Theory for Applications - 1978, IAEA - SMR - 43, Vienna (1980) 255.

9) H. Jahn : Nuclear Theory for Applications - 1978, IAEA - SMR - 43, Vienna (1980) 239.

10) U. Klein, G. Buche, W. Kluge, H. Matthay and G. Mechtersheimer : Nucl. Phys. A329 (1979) 339.

11) V.V. Verbinski and W.R. Burrus : Phys. Rev. 177 (1969) 1671.

12) BNL Report BNL - NCS - 50681, 1977 (Unpublished)

13) C.K. Garret and A.L. Twikervich : Phys. Rev. C8 (1973) 594.

14) R.P. Gautam : Ph.D. Thesis, Aligarh Muslim University, Aligarh (1986).

15) J.J. Griffin : Phys. Rev. Lett. 17 (1966) 478.

16) H. Gruppelaar, P. Nagel and P.E. Hodgson : Revista del Nuo. Cim. 9 No. 7.1 (1986).

17) H.W. Bertini, G.D. Harp and F.E. Bertrand : Phys. Rev. C10 (1974) 2472.

18) K. Chen, G. Friedlander, G.D. Harp and J.M. Miller : Phys. Rev. 166 (1968) 949.

19) G.D. Harp, J.M. Miller and B.J. Berne : Phys. Rev. 165 (1968) 1166.

20) P.E. Hodgson : Lecture given in 'Workshop on Applied Nuclear Theory and Nuclear Model Calculations for Nuclear Technology Applications' 15 February - 18 March, 1988, ICTP, Trieste (Italy).

21) D. Agassi, H.A. Weidenmuller and G. Mantzouranis : Phys. Rev. C22 (1975) 145.

22) K.W. McVoy and X.T. Tang : Phys. Rep. 94 (1983) 140.

23) T. Tamura, T. Udagawa, D.H. Feng and K.K. Kan : Phys. Lett. B68 (1977) 109; T. Tamura and T. Udagawa; ibid : B78(1978) 189.

24) T. Tamura, H. Lenske and T. Udagawa; Phys. Rev. C23 (1981) 2769.

25) T. Tamura, T. Udagawa and H. Lenske : Phys. Rev. C26 (1982) 379.

26) T. Udagawa, T. Tamura and B.T. Kim : Phys. Lett. B82 (1979) 349.

27) T. Udagawa and T. Tamura : In continuum spectra in Heavy Ion Reactions, edited by T. Tamura, J.B. Natowitz and D.H. Youngblood (Harwood, New York, N.Y., 1980) p. 155.

28) T. Udagawa, D. Price and T. Tamura : Phys. Lett. B116 (1982) 311.

29) T. Udagawa, K.S. Low and T. Tamura : Phys. Rev. C28 (1983) 1033.

30) M.R. Anderson, L.W. Mitchell, M.E. Sevior and D.G. Sargood: Nucl. Phys. A405 (1983) 170.

31) T. Matsuo, J.M. Matuszek, Jr. N.D. Dudey and T.T. Sugihara: Phys. Rev. B139 (1965) 886.

32) E.T. Chulick and J.B. Natowitz : Nucl. Phys. A173 (1971) 487.

33) A. Djaloeis, P. Jahn, H.J. Probst and C. Mayer - Boricke : Nucl. Phys. A250 (1975) 149.

34) C.L. Branquinho, S.M.A. Hoffmann, G.W.A. Newton, V.J. Robinson, H.Y. Wang and I.S. Grant : J. Inorg. Nucl. Chem. 41 (1979) 617.

35) M. Blann and G. Merkel : Phys. Rev. B137 (1965) 367.

36) W.W. Bowman and M. Blann : Nucl. Phys. A131 (1969) 513.

37) P. Misaelides and H. Munzel : J. Inorg. Nucl. Chem. 42 (1980) 937.

38) G.W.A. Newton, V.J. Robinson and E.M. Shaw : J. Inorg. Nucl. Chem. 43 (1981) 2227.

39) A.R. Barnett and J.S. Liley : Phys. Rev. C9 (1974) 2010.

40) W.F. Davidson, R.M. Lieder, H. Beuscher, A. Neskakis, G.A. Varley, J.C. Willmolt, F. Kearns and J.C. Lisla : J. Phys. G (Nucl. Phys.) 2 (1976) 199.

41) N.E. Sanderson and R.G. Summers-Gill : Nucl. Phys. A261 (1976) 93.

42) K.O. Zell, W. Gast, D. Hippe, W. Schuh and P. Von Bentano : Z. Phys. A202 (1979) 135.

43) T. Morek, H. Beuscher, B. Bochev, D.R. Haenni, T. Kutsarova, R.M. Lieder, M. Muller - Veggian and A. Neskakis : Nucl. Phys. A391 (1982) 269.

44) A.J. Krenier, C. Alonso Arias, M. Detray, D. Digregorie, A. Pachece, J. Davidson and M. Davidson : Nucl. Phys. A425 (1984) 397.

45) EXFOR Library, Nuclear Data Section, IAEA, Vienna (1986).

46) W. Hauser and H. Feshbach : Phys. Rev. 87 (1952) 336.

47) J.M. Blatt and V.F. Weisskopf : Theoretical Nuclear Physics (Wiley, New York, 1952).

48) R.E. Vande Vijver : Physica 29 (1963) 1214.

49) D. Vinciguerra, K. Kotajime and R.E. Van de Vijver : Nucl. Phys. 77 (1966) 337.

50) F.M. Lanzafame and M. Blann : Nucl. Phys. A142 (1970) 545.

51) H.E. Kurz, E.W. Jasper, K. Fischer and F. Hermes : Nucl. Phys. A168 (1971) 129.

52) M. Blann and J. Bisplinghoff : ALICE/LIVERMORE-82, Lawrence Livermore Laboratory Report UCID-19614 (1982).

53) V.F. Weisskopf and D.H. Ewing : Phys. Rev. 57 (1940) 472.

54) M. Blann : Phys. Rev. Lett. 27 (1971) 337, 27 (1971) 700(E) 27 (1971) 1550(E).

55) M. Blann : Phys. Rev. Lett. 28 (1972) 757.

56) R.K.Y. Singh : Ph.D. Thesis, Aligarh Muslim University, Aligarh (1985).

CHAPTER - II

NUCLEAR REACTION THEORIES

Nuclear reactions, according to the time on which they occur, may be classified into two categories i.e., direct reactions and compound nucleus reactions. The direct reactions are supposed to take place at the very first target-projectile collision and hence they occur within the time taken ($\sim 10^{-22}$ sec) by the projectile to cross the nuclear diameter. On the other hand, the compound nucleus reaction takes place at the end of very large number of internal collisions and therefore takes comparatively a long time ($\sim 10^{-16}$ sec).

However, in recent years, there has been an increasing evidence to point out that some reactions take place with intermediate time scales between two extremes. They manifest themselves in the 'high energy regions' of the excitation functions, non-Maxwellian hard components in the particle spectra and a gradually changed pattern of angular distributions from forward peaking to fore-and-off symmetry. These new experimental features were inexplicable[1] by existing direct reaction or compound nucleus models. A large body of such experimental data at high energies has successfully been explained by a new set of models called the 'Pre-compound' or 'Pre-equilibrium' models.

Most of these models are semi-classical[2] in nature and have been used with considerable success in describing experimental

data pertaining to the equilibration process, mainly the forward peaked hard component observed in the continuous spectra of light ejectiles and the high energy 'tails' seen in the excitation functions of activation cross-sections. More elaborate quantum mechanical theories[3-5] which are not easily applied to routinely calculate measurable pre-equilibrium cross-sections, have tended to support the foundations on which the semi-classical models are built. This has prompted a continued interest in these models as tools to predict cross-sections for a number of practical purposes and to test the adequacy of the underlying physics.

2.1 Compound nucleus theory

Bohr[6], in 1936, proposed the compound-nucleus theory of nuclear reactions. According to this concept, the nuclear reaction takes place in two steps : (i) the incident particle together with the target nucleus forms the compound nucleus in which energy is shared among all the nucleons; (ii) the compound nucleus then decays to the final products. Since the life-time of the compound nucleus is much greater than the time taken by the incident particle to traverse the nucleus ($\sim 10^{-22}$ sec), it is assumed that the mode of decay of the compound nucleus is independent of the mode of its formation, except for the requirements of the various conservation laws[7,8]. Thus, to calculate the cross-section of a nuclear reaction, it is necessary to determine the cross-sections of the two processes, that is, the

formation of the compound nucleus and its decay.

Compound-nucleus processes[9] may conveniently be divided according to the number of compound-nuclear states excited by the reaction, and this depends on the energy spread ΔE of the incident beam and on the widths Γ and spacings D of the compound nuclear states. If $\Delta E<\Gamma<D$, so that the levels are well separated, the corresponding resonances in the cross-sections may be analysed by the Breit-Wigner formalism. This formalism may be extended to the case $\Delta E<\Gamma\backsim D$ where two levels overlap, but becomes impracticable when more than two states are excited at the same energy. When $\Gamma>D$ so that the levels overlap strongly and the energy resolution $\Delta E<\Gamma$, the measured cross-sections fluctuate as a function of energy, but in so complicated way that it is not possible to identify the contributing resonances. If the energy spread $\Delta E>\Gamma$, many states are excited simultaneously but the fluctuations are no longer apparent. The resulting energy-averaged cross-sections may be analysed by the statistical theory.

The basic assumptions of the statistical theory are almost the same as proposed by Bohr[6]. These are (i) the reaction proceeds via a compound nucleus whose excitation is high enough to allow a statistical average over all possible phases of the nuclear states, (ii) the decay mode of the compound nucleus is independent of the mode of its formation. However, since the number of particles in the nucleus is finite and much smaller than the numbers required for the application of the laws of

statistics, accurate agreement between theory and experiments is hardly to be expected[8].

The Weisskopf-Ewing statistical model[10] gives the following relation for the average reaction cross-section ($\bar{\sigma}_{jk}$) :

$$\bar{\sigma}_{jk} = [\sigma_{comp}(j)] \left[\frac{G_k}{G} \right] \quad \ldots \quad (2.1)$$

where j and k represent the incident and outgoing particles. The first factor on the right hand side of equation (2.1) depends only on the reactants and is called the cross-section for the formation of the compound nucleus which may be calculated using the transmission coefficients for the partial waves. The second factor, called the branching ratio, depends only on the final products (k).

With the application of compound nucleus formation condition and with the conservation of total angular momentum J and parity π the average total cross-section for the reaction I(j,k)L averaged over many resonance structures may be given as[6,11]:

$$\bar{\sigma}_{jk} \equiv \sum_{J,\pi} \sigma_{jk}{}^{J^\pi} \quad \ldots \quad (2.2)$$

By applying the assumption of compound nucleus formation we have,

$$\bar{\sigma}_{jk} \equiv [\sigma_{comp}{}^{J^\pi}(j)] \left[\frac{G_t J^\pi}{\sum_t G_t J^\pi} \right] \quad \ldots \quad (2.3)$$

The sum over t runs over all reaction alternatives available to

the compound nucleus. Since Equation (2.3) is now valid for each J,π separately, the factorization of the cross-section as in Equation (2.3) does not imply that the compound nucleus forgets its total angular momentum and parity[12].

The connection between compound-nucleus cross-sections and branching ratio is established by the following reciprocity theorem :

$$k_j^2 \, \bar{\sigma}_{jk}^{J^\pi} = k_k^2 \, \bar{\sigma}_{kj}^{J^\pi} \qquad \ldots \qquad (2.4)$$

where k_j and k_k are the wave numbers for the relative motion of the pair j and k.

Combining Equations (2.3) and (2.4), we find

$$G_j^{J^\pi} = k_j^2 \, \sigma_{comp}^{J^\pi}(j) \qquad \ldots \qquad (2.5)$$

Finally we obtain each $\sigma_{comp}(j)$ from the optical-model absorption cross-section σ_j (abs) for the pair j. In terms of the complex phase shifts δ_{jl} of the optical model we have

$$\sigma_j(\text{abs}) = \frac{\pi}{k_j^2} \sum_l (2l+1)(1-|e^{2i\delta_{jl}}|^2) \qquad \ldots \qquad (2.6)$$

$$\equiv \sum_{J,\pi} \frac{\pi}{k_j^2} \frac{(2J+1)}{(2J_j+1)(2J_I+1)} \sum_{l=J-S}^{J+S} \sum_{S=J_I-J_j}^{J_I+J_j} (1-|e^{2i\delta_{jl}}|^2)$$

$$\equiv \sum_{J,\pi} \sigma_{comp}^{J^\pi}(j) \qquad \ldots \qquad (2.7)$$

where J_j is the spin of the incident particle j (in unit of ħ).

Comparison of Equations (2.5), (2.6), (2.7) yields :

$$G_j J^{\pi} = \sum_{s,l} T_l(j) \qquad \ldots \qquad (2.8)$$

where $T_l(j) = 1-|e^{2i\delta_{jl}}|^2$

Using Equations (2.3), (2.6) and (2.8) we get,

$$\sigma_{jk}^{-} = \frac{\pi}{k_j^2} \sum_{J,\pi} \frac{(2J+1)}{(2J_I+1)(2J_j+1)} \left[\sum_{s,l} T_l(j) \right] \left[\frac{\sum_{s',l'} T_{l'}(k)}{\sum_{t,s'',l''} T_{l''}(t)} \right]$$

$$\ldots \qquad (2.9)$$

The imprimed quantities s and l (where s is the channel spin and l is the orbital angular momentum) refer to the incoming channel j of the reaction, the primed quantities refer to the outgoing channels k and the double primed quantities in the denominator are summed over all channels (t) to which the compound nucleus can decay. Expression (2.9) can also be written as,

$$\sigma_{jk}^{-\mu\nu}(E_j^{\mu}) = \frac{\pi \lambda_j^2}{(2J_I^{\mu}+1)(2J_j+1)} \sum_{J,\pi} (2J+1) \frac{T_j^{\mu}(J^{\pi}) T_k^{\nu}(J^{\pi})}{T_{tot}(J^{\pi})}$$

$$\ldots \qquad (2.10)$$

where $\sigma_{jk}^{-\mu\nu}(E_j^{\mu}) = \sigma_{jk}^{-}$ is the average cross-section for the reaction I (in the state μ) $+j \longrightarrow$ L (in the state ν)$+k$ when I^{ν} and j interact with centre of mass energy E_j^{μ}. μ,ν indices representing bound states in target nucleus I and residual

nucleus L, respectively, $T_j^{\mu}(J^{\pi}) = \sum_{s,l} T_l(j)$ is the total transmission function for forming the state J^{π} in the compound nucleus by a combination of $I^{\mu}+j$, $T_k^{\nu}(J^{\pi}) = \sum_{s',l'} T_{l'}(k)$ is the transmission function for the decay of the J^{π} into $L^{\nu}+k$. $T_{tot}(J^{\pi}) = \sum_{t,s'',l''} T_{l''}(t)$ is the total transmission function for the decay of the compound nuclear state having spin J and parity π, that is

$$T_{tot}(J^{\pi}) = \sum_{i,\lambda} T_i^{\lambda}(J^{\pi})$$

where i is the particle in any combination of nucleus and particle to which the compound nuclear state can decay and λ is any state, bound or unbound, in the residual nucleus that is energetically accessible from $I^{\mu}+j$ interacting with energy E_j^{μ}.

The Equation (2.10) is the general expression for the total reaction cross-section of the reaction $I^{\mu}(j,k)L$, integrated over total solid angle, obtained in the framework of Hauser-Feshbach statistical theory of nuclear reactions[9,12,13].

In actual experiment, the target is generally in its ground state and μ is taken as zero. Further, the total cross-section $\bar{\sigma}_{jk}$ averaged overall energy states is given by

$$\bar{\sigma}_{jk} = \sum_{\nu} \sigma_{jk}^{\nu} = \frac{\pi \lambda_j^2}{(2J_I+1)(2J_j+1)} \sum_{J,\pi} (2J+1) \frac{T_j(J^{\pi}) T_k(J^{\pi})}{T_{tot}(J^{\pi})} \quad \ldots \quad (2.11)$$

where $T_j(J^{\pi}) = \sum_{l,s} T_j(J^{\pi},l,s)$ and $T_k(J^{\pi}) = \sum_{l',s'} T_k(J^{\pi},l',s')$.

The transmission functions in the particle (neutron, proton, and alpha) channels have been evaluated using an equivalent square-well representation of a Woods-saxon optical potential[14,15], using the relation

$$T_j^{\mu}(J^{\pi},l,s) = 1-\exp(-4\pi S_f P_l) \quad \ldots \quad (2.12)$$

where S is the strength function, which varies with energy only slowly except near resonance energy region, f is the reflection factor and is nearly energy independent and P_l is the penetration factor of the particle through the equivalent square-well potential and is nearly energy independent.

The photon transmission function has an entirely different form from that employed for neutrons, protons and alphas. By assuming that dipole transmission is the dominant one in the photon channel, the photon transmission function has been calculated from the following relation

$$T_k^{\nu}(J^{\pi}) = T_{\gamma}(J^{\pi}) = \sum_{\nu=0}^{\omega} [T_{\gamma}^{\nu}(EI)+T_{\gamma}^{\nu}(MI)] + \int_{\epsilon_c^{\omega}}^{\epsilon_c^{max}} \int_{J^{\nu},\pi^{\nu}} [T_{\gamma}^{\nu}(EI+T_{\gamma}^{\nu}(MI)] \times \rho(\epsilon_c^{\nu},J^{\nu},\pi^{\nu}) d\epsilon_c^{\nu} d\pi^{\nu} dJ^{\nu} \quad \ldots \quad (2.13)$$

where the superscript ν now indicates all excited states in the compound (residual) nucleus and where EI and MI indicate electric

and magnetic-dipole (transmission functions respectively and the sum and integrals are subject to tne appropriate dipole selection rules.

The nuclear level density formula used in the calculation was based on the 'Back-shifted Fermi Gas Model' and has the following form[16)]

$$\rho(\epsilon',J',\pi') = \rho_{tot}(\epsilon')f(\epsilon',J',\pi') \quad \ldots \quad (2.14)$$

where $\rho_{tot}(\epsilon')$ is the total nuclear level density in the nucleus of atomic mass A and moment of inertia 'ϑ' at the excitation energy ϵ', given as :

$$\rho_{tot}(\epsilon') = \frac{0.482}{A^{5/6}} \frac{\exp[2\sqrt{a(\epsilon'-\delta)}}{(\epsilon'-\delta)^{3/2}} \text{ MeV}^{-1}$$

and $f(\epsilon',J',\pi')$ is the distribution of spins and parities at that energy normalized so that the sum overall spins and parities is unity, and a and δ are two nuclear parameters to be determined emperically.

2.2 Pre-equilibrium theory

The statistical theory has been in use for more than half a century. The theory has very successfully explained the average behaviour of excitation function for nuclear reactions at intermediate energy. From the theoretical point of view also it is quite possible that compound nucleus of the statistical model does not live-long enough to sample all the possible

compound states, i.e., the compound system decays before the thermodynamical equilibrium has been reached. This possibility becomes more important at higher excitation energy and therefore, in nuclear reactions at high energies, it is necessary to consider the emission of particles during equilibration of the compound system itself. During the nineteen sixties, evidence accumulated indicating that it is possible for particles to be emitted after the first stage of a nuclear interaction but long before the attainment of statistical equilibrium; these are the pre-equilibrium particles and the process is known as the pre-equilibrium emission. The pre-equilibrium emission serves as a bridge between the two extremities, i.e., the direct and compound processes.

Many theories have been developed for accounting pre-equilibrium processes. The approach and the assumptions of most of the theories are quite different from each other. The ability of these theories to explain various experimental data such as angular distributions, excitation functions, etc., is also different.

A general view of the various theories is presented in the present work. The computer code 'ALICE/ LIVERMORE-82'[17] has been used to compute the excitation functions of α-induced reactions for comparison with our experimental values. The computer code has been developed on the basis of hybrid model[18] and the geometry dependent hybrid model[19,20]. These models belong to the semi- classical theories hence, in the following discussion

emphasis is given to semi-classical theories. Some of the important semi-classical theories are :

2.2.1 Intranuclear Cascade Model

2.2.2 Harp-Miller and Berne Model

2.2.3 Exciton Model

2.2.4 Hybrid Model

2.2.5 Geometry Dependent Hybrid Model

Most of these models are formulated with the core concept that the compound system initially involves only few degrees of freedom and passes through more complicated configurations until an equilibration is attained.

2.2.1 Intranuclear Cascade Model

The intranuclear cascade model (ICM) was first proposed by Serber[21] and modified by others[22-27] to explain various experimental nuclear reaction data. A simple diagramatic representation of the cascade model is shown in Fig. 2.1. Here it may be seen that the succession of two body interactions is followed in three dimensional geometry. In calculations, trajectories of the nucleons are followed one at a time during the cascade until some arbitrary energy generally considerably above the average equilibrium value has been attained by the nucleon. While, in principle, the time evolution of the reaction can be generated from such an approach, but the actual calculations

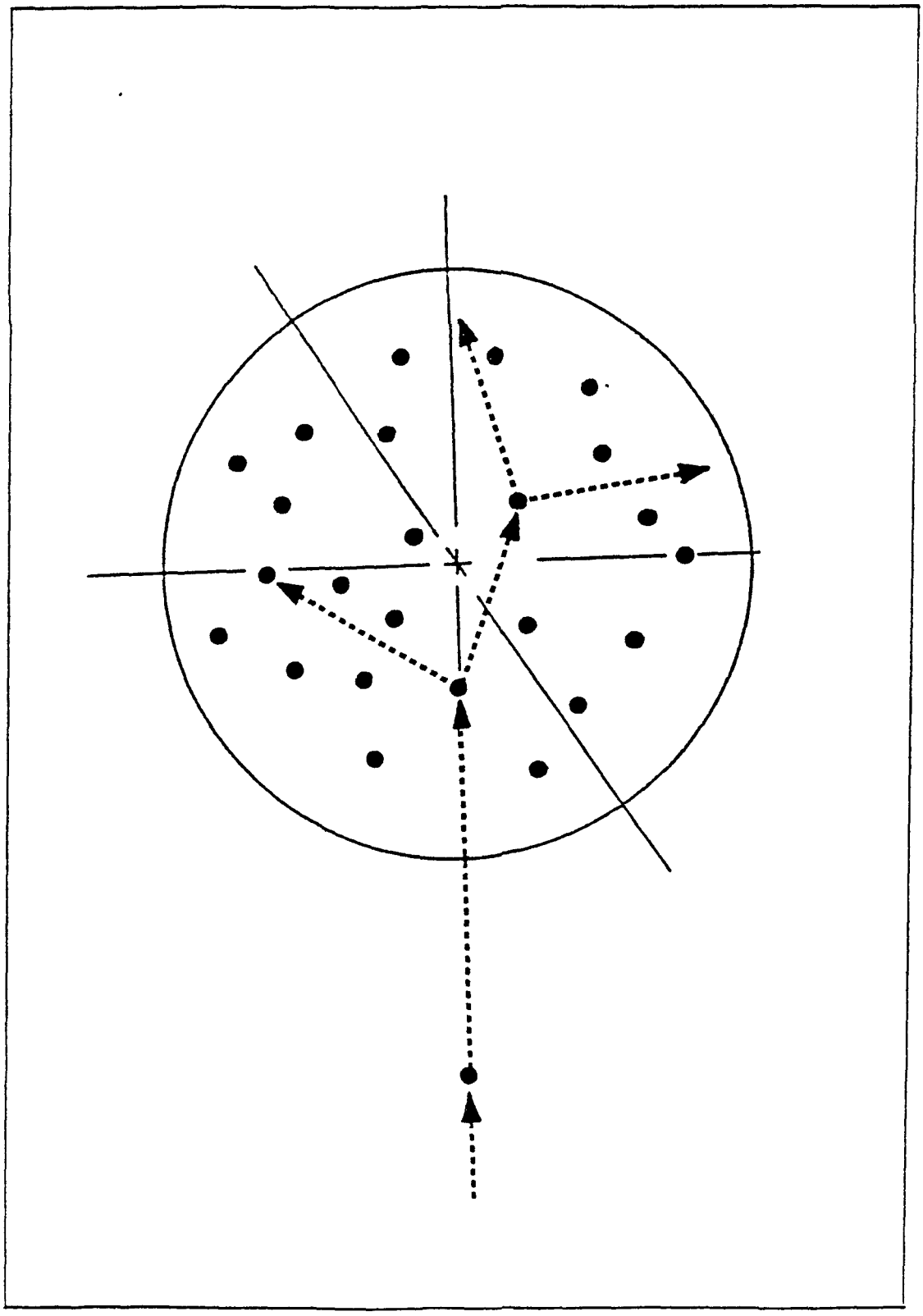

Fig. 2.1 Pictorial representation of the Intranuclear Cascade Model. The nature of the model in following classical trajectories following successive binary collisions is indicated. (Ref. 21)

become more involved after a few collision steps. Various forms for the nuclear potential wells, like square well, Fermi distribution from electron scattering data and nuclear density distributions have been used. The cascade model is the only model which predicts angular momentum of emitted particles. But, in the medium range energy, it does not predict them very well.

2.2.2 Harp-Miller and Berne Model

The physical description of the Harp-Miller-Berne (HMB) model[28], is given in Fig. 2.2 consider the initiation of the reaction at an initial time τ_0, as shown on the left of the figure. Energy bins of some width, e.g. 1 MeV, are defined and the number of available single particle levels in each bin are then calculated generally using a Fermi gas distribution and are stored. The calculation can be done either beginning with some initial arbitrary population of excited particles and holes, or with a nucleus in the ground state. The fractional occupation of each bin is followed in calculation as a function of time. For a given incident nucleon, the rate of allowed transitions with all nucleons in the nucleus is computed, as is the rate of emission of the particle into the continuum. Nucleon-nucleon scattering cross-sections are used for calculating the two-body transition rates with each energy partition being assigned equal-a-priori probability. Transmission rates into continuum are calculated using the free particle phase

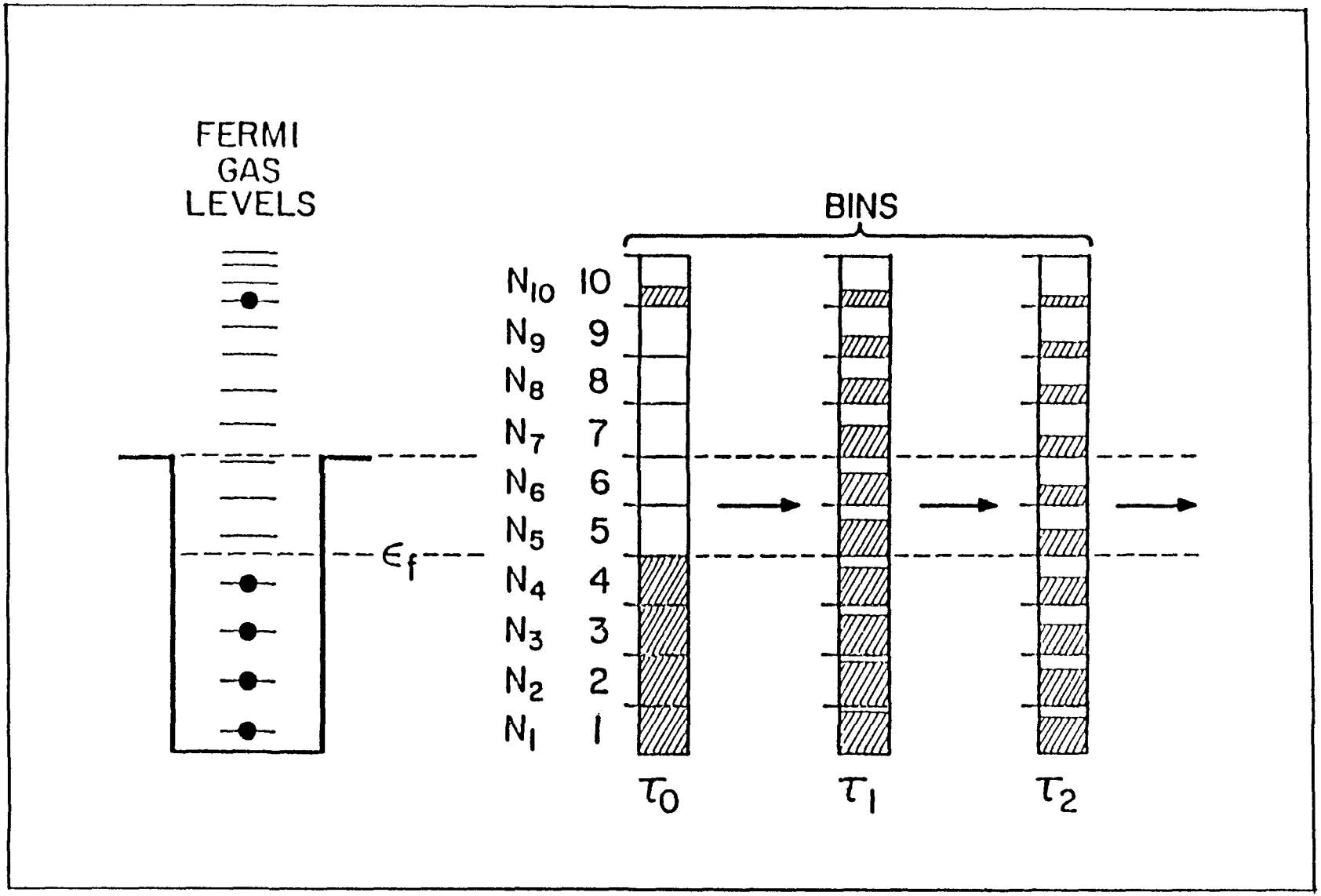

Fig. 2.2 Pictorial representation of the Harp-Millar-Berne Model. The shaded areas represent the occupied fraction of each bin, with occupations changing after each time interval. (Ref. 28)

space factors and inverse cross-sections. The particle flux is divided in proportion to be rate at which the particle may be emitted versus the rate at which it may make an internal transition.

After calculating the relative probabilities of scattering into and out of each bin and of emission from bins above the particle binding energies, populations of all bins are changed accordingly, as shown in the centre of Fig. 2.2. The calculation is repeated in units of time that are short with respect to the N-N collision time. The solution of equilibrium problem in this model depends on computer solution of a set of coupled differential equations.

Later, Harp and Miller[29] considered the nucleus to be composed of independent proton and neutron Fermi gases. The internal configuration of any nucleus at any instantaneous time is specified by the proton and neutron occupation numbers. It is also assumed that the equilibration of the gases takes place through binary nucleon-nucleon collisions. Correspondingly, a new set of master equations is obtained, the solution of which gives the proton and neutron occupation numbers.

2.2.3 Exciton Model

The Exciton Model (EM) was proposed by Griffin[30] and later modified by many workers[31-38] for explaining various experimental nuclear reaction data. In this model, it was

assumed that equilibration between target and projectile was acnieved by a succession of two-body interactions. Each state is characterized by the number of excited particles (p) plus holes (h) (or excitons, n=p+h) defined with respect to Fermi energy of the target. The physical concept of the exciton model is illustrated in Fig. 2.3. A nucleon is shown entering the nuclear potential on the left. All the fermions are in their ground state. The first interaction would, therefore, lead to a 2p1h (two particles plus one hole) state and it is assumed that any configuration is equally likely. This could be followed by a transition between one of the two excited particles and a particle in the ground state, or with the other excited particle. This could lead either to a 3p2h state, but to the original configuration, or to a different 2p1h state. The likehood of each occurance is assumed to be proportional to the density of the accessible final states. Since the initial simple configurations have far fewer than the equilibrium particle hole numbers, the level densities are rapidly increasing functions of increasing p-h number, and the system goes predominantly in the direction of equilibrium as indicated in Fig. 2.3 by the larger arrows in that direction.

For a given configuration specified by the particle-hole number, some fraction will have atleast one particle with energy in excess of its binding energy. The fraction of particles in a given exciton number state which one at a given energy ϵ+B above the Fermi energy (where B is the particle binding

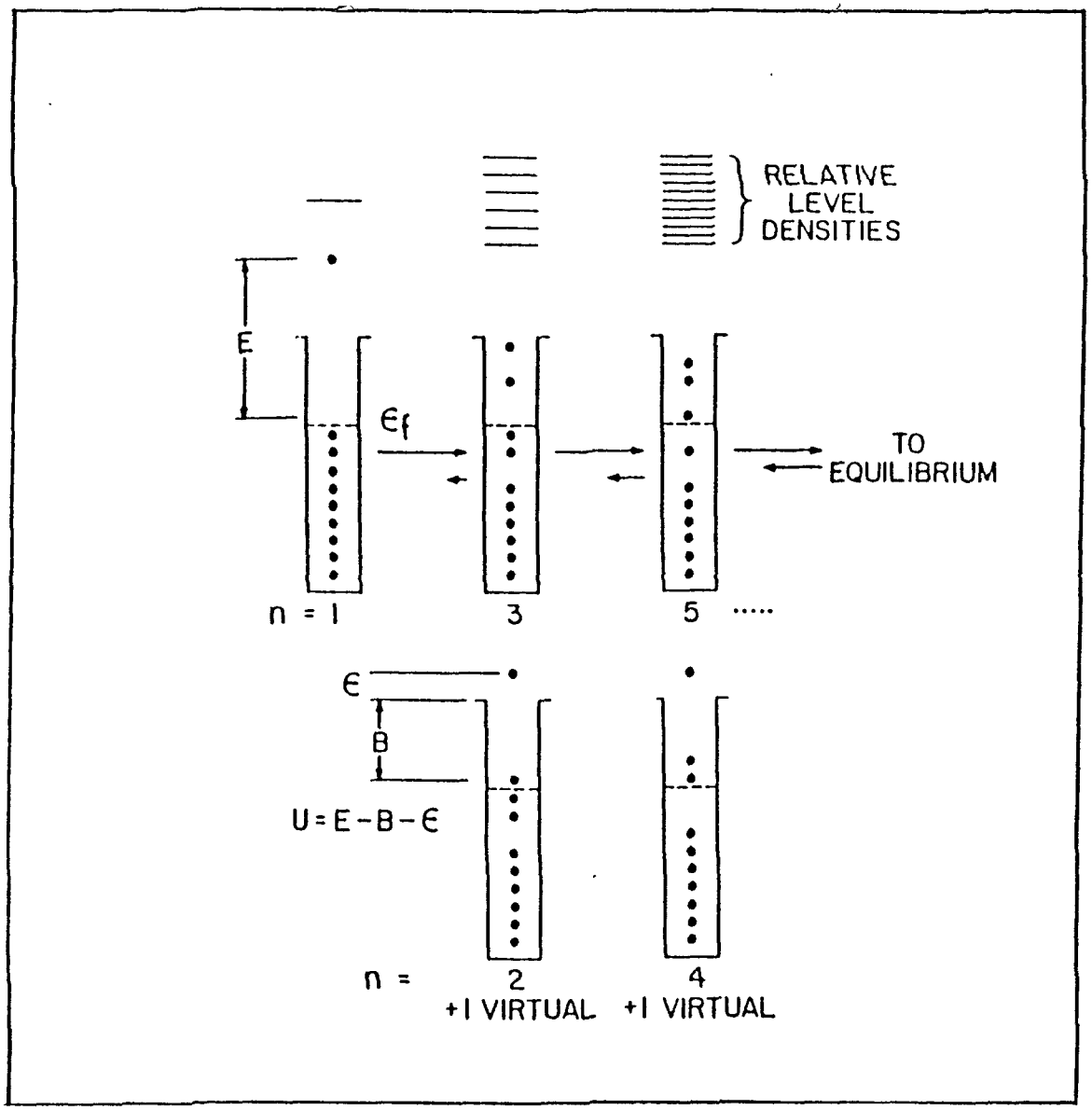

Fig. 2.3 Pictorial representation of the ideas inherent in the exciton model. Successive two-body interactions are indicated with some fraction of each exciton hierarchy having unbound particles. (Ref. 30)

energy and ϵ is the channel energy of the particle), can be computed and from it the relative probability of emission of a particle having such kinetic energy can be calculated.

Obviously, the initial states of simpler configurations have highest probability of emitting energetic particles. As the p-h number increases towards the equilibrium value, the probability that anyone particle has some high energy exponentially decreases and hence the emission rate for such process. Griffin[30] made the ad-hoc statistical assumption that every partition of energy for a given exciton number occured with equal a-priori probability during the equilibration process. It was further assumed that a pre-dominance of transitions to more complicated states relative to those simpler states, as the exciton state densities are rapidly increasing functions of the exciton number. The decay probability is computed in the exciton model as a sum over contributions from states from some initial exciton number n_o to the equilibrium value $\bar{n}$. Since all transitions are assumed to proceed by binary processes, each state has one particle and one hole more than the preceding state in the equilibration sequence (see Fig. 2.3), and the sum over states is taken in units of $\Delta n = +2$.

Intermediate state densities play an important role in exciton model. The first order approach to this density function is to assume that a nucleus behave like a degenerate Fermi gas and further that all levels are equally spaced. The density of states of a system p excited particles and h holes with

single-particle level density g at excitation E was given by Ericson[39] as

$$\rho_{p,h}(E) = \rho_n(E) = \frac{g(gE)^{n-1}}{p!h!(n-1)!} \quad \ldots \quad (2.15)$$

Another expression in which the Pauli principle is taken into consideration is given by Williams[40] as

$$\rho_n(E) = \frac{g[gE-A(p,h)]^{n-1}}{p!h!(n-1)!} \quad \ldots \quad (2.16)$$

where $A(p,h) = \frac{1}{4}(p^2+h^2+p-h) - \frac{1}{2}h$

and $n = p+h$

It will be assumed that the fraction of n-exciton states in which one particle is at an energy $\epsilon+B$ above the Fermi energy is given by the ratio

$$\rho_n(U,E)/\rho_n(E) = \rho_{p,h}(U,E)/\rho_{p,h}(E)$$

where U is the residual excitation if there is particle emission with channel energy ϵ. Then the probability of decay from an n exciton state is given by

$$P_n(\epsilon)\, d\epsilon = (2s+1)\left[\frac{\rho_n(U,\epsilon)}{\rho_n(E)}\right] \frac{4\pi p^2 dp}{h^3} \cdot \frac{\sigma v}{V} \tau_n \quad \ldots \quad (2.17)$$

where τ_n is the mean life time of an n exciton state, the other factors being the particle spin degeneracy, the phase

space and penetrability factors. The total decay probability is obtained from Equation (2.17) by substituting for the level densities from Equation (2.16) and summing it from initial exciton number n_o to the equilibrium exciton number ($\bar{n}$) in steps of $\Delta n = +2$.

$$P(\epsilon)d\epsilon = \sum_{\substack{n=n_o \\ n=+2}}^{\bar{n}} P_n(\epsilon)d\epsilon$$

$$= \frac{2s+1}{\pi^2\hbar^3 gE} \, m\epsilon\sigma \sum_{\substack{n=n_o \\ n=+2}}^{\bar{n}} \left(\frac{U}{E}\right)^{n-2} p(n-1)\,\tau_n d\epsilon \qquad \ldots \qquad (2.18)$$

The mean life-time τ_n may be evaluated on a relative basis[30], by the Golden rule of Fermi,

$$\lambda_{n,n'} = \frac{2\pi}{\hbar}|M|^2 \rho_{n'}(E) \qquad \ldots \qquad (2.19)$$

where $\lambda_{n,n'}$ is the transition rate from a given initial n exciton state to any of the accessible n' exciton final states, $|M|$ is the matrix element for the residual two-body interaction, and $\rho_{n'}(E)$ is the density of accessible final states.

William[40] has given formulas for the average number of accessible states for each types of transition as follows :

$$\lambda_+ = \frac{2\pi}{\hbar}|\bar{M}|^2 \frac{g^3U^2}{(p+h+1)} \qquad \ldots \qquad (2.20)$$

$$\lambda_- = \frac{2\pi}{\hbar}|\bar{M}|^2 g[p.h.(p+h-2)] \qquad \ldots \qquad (2.21)$$

$$\lambda_o = \frac{2\pi}{\hbar}|\bar{M}|^2 g\, U\left[\frac{3(p+h)-2}{4}\right] \quad \ldots \quad (2.22)$$

where g is the density of single-particle levels and λ_+, λ_-, λ_o are the average density of accessible states for transition in which the exciton number changes by +2, -2 and O. It may be seen from these results that $\lambda_{n+2} >> \lambda_{n-2}$ if $n << \bar{n}$. Assuming that $\lambda_{n+2} = \lambda_{n-2}$ at equilibrium ($n=\bar{n}$), it follows that

$$\bar{n} = \sqrt{2gE} \quad \ldots \quad (2.23)$$

Due to the fact that the two-body interaction matrix $|M|$ is not well known, the exciton model can give only the relative yields. As can be seen from Williams[40] expressions (2.20 - 2.22), the matrix element $|\bar{M}|$ has been used. At low excitation energies, it is reasonable to assume energy independent matrix element[35], while at higher excitations energy dependent matrix elements are used. According to Kalbach-cline[33], the following expression can be used for the energy dependence of matrix element

$$|\bar{M}|^2 = K.A^{-3}\, E^{-1} \quad \ldots \quad (2.24)$$

where A is the mass of the excited nucleus and E is the excitation energy. The value of K ranges from 95 to 7000 MeV[+3 41]. The following expressions for the residual two-body matrix element are proposed recently by Kalbach[34]

$$|\bar{M}|^2(n,E) = \frac{K}{A^3 e}\left(\frac{e}{7\ \text{MeV}}\right)^{1/2}\left(\frac{e}{2\ \text{MeV}}\right)^{1/2} \quad e<2\ \text{MeV} \quad \ldots \quad (2.25)$$

$$|\bar{M}|^2(n,E) = \frac{K}{A^3 e}\left(\frac{e}{7\ \text{MeV}}\right)^{1/2} \qquad 2\ \text{MeV} \leq e \leq 7\ \text{MeV}$$

... (2.26)

$$|\bar{M}|^2(n,E) = \frac{K}{A^3 e} \qquad 7\ \text{MeV} \leq e \leq 15\ \text{MeV}$$

... (2.27)

$$|\bar{M}|^2(n,E) = \frac{K}{A^3 e}\left(\frac{15\ \text{MeV}}{e}\right)^{1/2} \qquad 15\ \text{MeV} < e$$

... (2.28)

where $e = E/n$ is the average excitation energy per exciton.

The model due to Griffin[30] thus avoids the problem of following bin population by substituting density of states characterized by exciton number.

2.2.4 Hybrid Model

The hybrid model was proposed by Blann[18] in which the basic principles of the exciton model[30] and those of the Harp-Miller-Berne model[28] are incorporated. In this model, multiple pre-equilibrium particle emission alongwith the compound (equilibrium) decay is considered, whereas the spectra of emitted particles are calculated for each step in the energy dissipation process induced by the interaction between projectile and traget nucleons. The calculation starts with an initial number of excitons i.e., particle above and hole below the Fermi level induced by primary interaction and proceeds to states with an increasing exciton number. The energy brought

in by the interacting nucleon is shared among all the nucleons in different stages in a two-body nucleon-nucleon (N-N) collision process. Hence a pre-equilibrium decay of a single nucleon or a cluster of nucleons (multi-particles) are possible before the system is equilibrated.

The pre-equilibrium decay probability in the hybrid model is given by[1,42]

$$P_\nu(\epsilon)d\epsilon = \sum_{n=n_o}^{\bar{n}} [nP_\nu \frac{\rho_n(U,\epsilon)}{\rho_n(E)} g d\epsilon] \cdot [\frac{\lambda_c(\epsilon)}{\lambda_c(\epsilon)+\lambda_+(\epsilon)}] D_n$$

$$= \sum_{n=n_o}^{\bar{n}} nP_\nu(\epsilon)d\epsilon \qquad \ldots \qquad (2.29)$$

where $P_\nu(\epsilon)d\epsilon$ is the probability of finding a particle proton or neutron) in the channel energy range ϵ to $\epsilon+d\epsilon$, nP_ν is the number of particles of the type ν in them, if emitted into continuum, would have channel energy ϵ, $\rho_n(E)$ is the usual n-exciton state density. The quantity in the first set of brackets represents the number of particles of type ν which could be emitted in the energy range ϵ to $\epsilon+d\epsilon$ and $U=E-B_\nu-\epsilon$, where B_ν is the binding energy of particle type ν. The quantity in the second set of brackets represents the probability of those particles being emitted into continuum; $\lambda_c(\epsilon)$ is the rate of emission of the particles into continuum with channel energy ϵ and $\lambda_c(\epsilon)$ is the rate of intranuclear transitions for those particles. The factor D_n represents the fraction of the initial population surviving de-exitation by particle emission

prior to the n-exciton state under consideration.

The nucleon-nucleon scattering rate is based on either the imaginary optical potential, where the mean free path is given by[43)]

$$\lambda_+(E) = \frac{\hbar^2}{4m}\frac{1}{W^2}(E+V) + \sqrt{(E+V)^2 + W^2}^{1/2} \quad \ldots \quad (2.30)$$

$$\simeq \frac{\hbar^2}{2mW}\sqrt{\frac{2m}{\hbar^2}(E+V)} \quad \ldots \quad (2.31)$$

or on Pauli corrected nucleon-nucleon scattering cross-sections, where the mean free path is given by[43)]

$$\lambda_+(\epsilon) = \frac{1}{\rho\bar{\sigma}_o} \quad \ldots \quad (2.32)$$

where ρ is the density of nuclear matter and $\bar{\sigma}_o$ is the Pauli corrected nucleon-nucleon (N-N) scattering cross-section, approximately weighted for target neutron and proton number. The transition rate is the quotient of nucleon velocity divided by the mean free path. A closed form expression valid for nuclear matter of average density was given[44)]

$$\lambda_+(\epsilon) = 1.4\times10^{21}(\epsilon+B_\nu)-6\times10^{18}(\epsilon+B_\nu)^2/\text{sec.} \quad \ldots \quad (2.33)$$

where $\epsilon+B$ is the energy of nucleon ν above the Fermi energy. The continuum emission rate, $\lambda_c(E)$ is given by microscopic reversibility as

$$\lambda_c(\epsilon) = (2s+1)\frac{4\pi p^2 dp}{\hbar^3}\cdot\frac{dv}{\Omega g} \quad \ldots \quad (2.34)$$

wnere s is the nucleon spin, Ω is the laboratory volume, p is the nucleon momentum, g is the single particle level density in the nucleus, v is the nucleon velocity in the laboratory, and σ the inverse cross-section. With these two Equations (2.33) and (2.34) and the Ericson density expression (Equation 2.15), we can calculate absolute pre-equilibrium spectra with Equation (2.29). When we calculate N-N collision rates, there are two options, one is to use the imaginary optical potential given by Becchetti and Greenlees[45], the other is to use Equation (2.32) calculating σ_o based on expressions due to Kikuchi and Kewai[43] weighted for composite nucleus N and Z.

2.2.1.5 Geometry Dependent Hybrid Model

The geometry dependent hybrid (GDH) model[19] is a revised version of the hybrid model[18]. In the GDH model the diffused surface properties of nucleus are taken into consideration by employing the Fermi level density distribution function. To incorporate the diffused surface properties of nucleus in the GDH models the exciton state densities ρ_n and the intranuclear transition rates have been treated as a function of nuclear density. Therefore, the energy differential pre-equilibrium cross-section for particle emission in the GDH model is given by[42]

$$\frac{d\sigma_\nu(\epsilon)}{d\epsilon} = \pi\lambda^2 \sum_{l=o}^{\infty} (2l+1) T_l P_\nu(l,\epsilon) \quad \ldots \qquad (2.35)$$

where $P_\nu(l,\epsilon)\,d\epsilon$ is same as $P_\nu(\epsilon)\,d\epsilon$ but evaluated for l^{th} partial wave. When the system is equilibrated, its de-excitation is followed by the Weisskopf-Ewing[10] evaporation model while level density $\rho(U)$ is calculated using the Fermi gas level density formula.

In the geometry dependent hybrid model, the nuclear level density is given by a Fermi distribution[46] as

$$d(R_l) = d_s\,[\exp(R_l - C)/0.55\ \text{fm} + 1]^{-1} \quad \ldots \quad (2.36)$$

where d_s is the saturation density of nuclear matter and the charge radius C is given by

$$C = 1.07\ A^{1/3}\ \text{fm} \quad \ldots \quad (2.37)$$

taken from electron scattering results[47]. The radius for the l^{th} partial wave was defined by

$$R_l = \lambda\!\!\!^{-}(l + 1/2) \quad \ldots \quad (2.38)$$

The charge radius C of Equation (2.37) has been replaced in the present parameterization by a value characteristic of matter (rather than charge) radius based on the droplet model work of Myers[48], plus an ad-hoc projectile range parameter $\lambda\!\!\!^{-}$,

$$C = 1.18\ A^{1/3}\,[1-(1/(1.18\ A^{1/3})^2)]+\lambda\!\!\!^{-} \quad (2.39)$$

where $\lambda\!\!\!^{-}$ is the reduced de-Broglie wave-length of the projectile.

In the hybrid model the average nuclear density is calculated by integration and averaging Equation (2.35) between R=0 and R = C + 2.75 fm. The Fermi energy (ϵ_f) has been taken 40 MeV for saturation density and is assumed to vary as the average density to the two-thirds power. The value of ϵ_f so evaluated is used in defining the single particle level density 'g' for all calculations, hybrid and GDH. The single particle level densities have been defined by[46)]

$$g_n = \frac{N}{20} \left[\frac{\epsilon_f + B_n + \epsilon}{\epsilon_f} \right]^{1/2} \quad \ldots \quad (2.40)$$

$$g_p = \frac{Z}{20} \left[\frac{\epsilon_f + B_p + \epsilon}{\epsilon_f} \right]^{1/2} \quad \ldots \quad (2.41)$$

In the hybrid model, the Pauli corrected nucleon-nucleon cross-sections are used to evaluate the $\lambda_+(\epsilon)$ of Equation (2.29), the average value of the Fermi energy (usually = 30 MeV) and density is used to define the nucleon mean free path (MFP). In the geometry dependent hybrid model the Fermi energies and nuclear densities are defined according to impact parameter via Equation (2.38). Options have been employed using either the maximum density along each trajectory or an average.

The hybrid and geometry dependent hybrid models have been successful in reproducing a broad range of data[1)]. These models were able to reproduce experimental particle spectra as well as excitation functions of the reactions induced by α-particles.

Blann[1] calculated, the particle spectra for (α,p) reactions in medium and heavy mass nuclei at an α-particle energy of 55 MeV and compared the results with experimental results of Chevarier et al.[49] and found good agreement between the two. The author also compared the experimental particle spectra[49-51] for the ^{93}Nb reaction at α-particle energies of 30.5, 42.0 and 55.0 MeV with the calculated values obtained using the hybrid model and found a good agreement. It has also been shown[1,52] that the GDH model was able to predict the excitation functions of the reaction ^{93}Nb (α,xnyp) for $x \leq 10$, $y \leq 6$ and for α-particle energies from 16 to 171 MeV.

References

1) M. Blann : Ann. Rev. Nucl. Sci. 25 (1975) 123.

2) J. Bisplinghoff : Phys. Rev. C33 (1986) 1569.

3) T. Tamura, T. Udagawa, D.H. Feng and K.K. Kan : Phys. Lett. B68 (1977) 109; T. Tamura and T. Udagawa, ibid. B78 (1978) 189.

4) D. Agassi, H.A. Weidenmuller, and G. Mantzouranis : Phys. Rep. C22 (1975) 145.

5) H. Feshbach, A. Kerman and S.E. Koonin : Ann. Phys.(N.Y.) 125 (1980) 429.

6) N. Bohr : Nature 137 (1936) 344.

7) J.B. Marrion and J.L. Fowler : Fast Neutron Physics, (Interscience Publishers, New York, 1963) Part II, 1525.

8) R.R. Roy and B.P. Nigam : Nucl. Phys. (John Wiley and Sons Inc., New York, 1967) 200.

9) P.E. Hodgson, Nuclear Reactions and Nuclear structure, (Calarendon Press, Oxford, 1971) 284.

10) V.F. Weisskopf and D.H. Ewing : Phys. Rev. 57 (1940) 472.

11) M. Afzal Ansari : Ph.D. Thesis, Aligarh Muslim University, Aligarh (1982).

12) E. Vogt : Advances in Nuclear Physics, (Plenum Press, New York, 1968) Vol. I, 261.

13) W. Hauser and H. Feshbach : Phys. Rev. 87 (1952) 366.

14) G. Michaud, L. Scherk and E. Vogt : Phys. Rev. C1 (1970) 864.

15) G. Michaud and W.A. Fowler : Phys. Rev. C2 (1970) 2041.

16) J.A. Holmes, S.E. Woosley, W.A. Fowler and B.A. Zimmerman : Atomic Data and Nucl. Data Tables 18 (1976) 305, Orange Aid Reprint OAR-422 (1975).

17) M. Blann and J. Bisplinghoff : ALICE/LIVERMORE-82, Lawrence Livermore Laboratory Report UCID-19614 (1982).

18) M. Blann : Phys. Rev. Lett. 27 (1971) 337; 27 (1971) 700(E); 27 (1971) 1550(E).

19) M. Blann : Phys. Rev. Lett. 28 (1972) 757.

20) R.K.Y. Singh : Ph.D. Thesis, Aligarh Muslim University, Aligarh (1985).

21) R. Serber : Phys. Rev. 72 (1947) 1114.

22) H.W. Bertini : Phys. Rev. 131 (1963) 1801.

23) K. Chen, G. Friedlander and J.M. Miller : Phys. Rev. 176 (1968) 1208.

24) K. Chen, G. Friedlander, G.D. Harp and J.M. Miller : Phys. Rev. C4 (1974) 2234.

25) K. Chen, Z. Fraenkel, G. Friedlander, J.R. Grover, J.M. Miller and Y. Shimamoto : Phys. Rev. 166 (1968) 949.

26) H.W. Bertini : Phys. Rev. C5 (1972) 2118; C6 (1973) 1045.

27) H.W. Bertini, G.D. Harp and F.E. Bertrand : Phys. Rev. C10 (1974) 2472.

28) G.D. Harp, J.M. Miller and B.J. Berne : Phys. Rev. 165 (1968) 1166.

29) G.D. Harp and J.M. Miller : Phys. Rev. C3 (1971) 1847.

30) J.J. Griffin : Phys. Rev. Lett. 17 (1966) 478.

31) M. Blann : Phys. Rev. Lett. 21 (1968) 1357.

32) E. Gadioli : Nukleonika 21 (1976) 385;
E. Gadioli, E. Gadioli-Erba, L. Sajo-Bohus and G. Tagliaferri : Nuo. Cim. Riv. 6 (1976) 1.

33) C. Kalbach-Cline : Nucl. Phys. A210 (1973) 590.

34) C. Kalbach : Z. Phys. A287 (1978) 319.

35) E. Gadioli, E. Gadioli Erba and P.G. Sona : Nucl. Phys. A217 (1973) 589.

36) C. Kalbach-Cline and M. Blann : Nucl. Phys. A172 (1971) 225.

37) C. Birattari, E. Gadioli, E. Gadioli Erba, A.M. Grassi Strini, G. Strini and G. Tagliaferri : Nucl. Phys. A201 (1973) 579.

38) I. Ribansky, P. Oblozinsky and E. Betak : Nucl. Phys. A205 (1973) 545.

39) T. Ericson : Adv. Phys. 9 (1960) 425.

40) F.C. Williams Jr : Nucl. Phys. A166 (1971) 231.

41) K.K. Gudima, S.G. Mashnik and V.D. Toneev : Nucl. Phys. A401 (1983) 329.

42) M. Blann : Lecture given in 'Workshop on Applied Nuclear Theory and Nuclear Model Calculations for Nuclear Technology Applications' 15 February – 18 March, 1988, ICTP, Trieste (Italy).

43) K. Kikuchi and M. Kawai, 'Nuclear Matter and Nuclear Interactions (North-Holland, Amsterdam, 1968).

44) M. Blann and A. Mignerey : Nucl. Phys. A186 (1972) 245.

45) F.D. Becchetti and G.W. Greenlees : Phys. Rev. 182 (1969) 1190.

46) M. Blann and H.K. Vonach : Phys. Rev. C28 (1983) 1475.

47) R. Hofstadter : Ann. Rev. Nucl. Sci. 7 (1957) 295.

48) R.D. Myers : Droplet Model of Atomic Nuclei (Plenum, New York, 1977).

49) A. Chevarier, N. Chevarier, A. Demeyer, G. Hollinger, P. Pertos and T.M. Duc : Phys. Rev. C8 (1973) 2115.

50) L.W. Swenson and C.R. Gruhn : Phys. Rev. 146 (1966) 886.

51) R.W. West : Phys. Rev. 141 (1966) 1033.

52) J. Ernst, R.I. Ibowski, H. Klampfl, H. Machner, T. Mayer-Kuckuk and R. Schanz : Z. Phys. A308 (1982) 301.

CHAPTER - III

NUCLEAR MODEL CODE

In order to describe and interpret the measurements, the advancement of experimental techniques has been taken into account with parallel advancement of nuclear theories and models as well. To meet the nuclear data requirements which are still difficult, impractical, or even impossible with present experimental techniques[1], the theoretical capability of the models has significant importance. Pre-equilibrium model codes are useful for prediction and calculations of reaction cross-sections and particle spectra for important practical applications[2].

Computer codes incorporating different nuclear models have been developed according to the data needs. Before using a code for mass data predictions, intensive testing of the code is required to verify its validity. In the present work the code 'ALICE/LIVERMORE-82[3] has been used for the study of excitation functions of α-particle induced reactions. The code 'ALICE/LIVERMORE-82', which is a revision of the ALICE[4] and OVERLAID ALICE[5] codes, has been formulated for performing pre-equilibrium, compound/statistical fission calculations in the general framework of the Weisskopf-Ewing evaporation model[6] the Bohr-wheeler transition state model for fission[7,8] and the hybrid/geometry dependent hybrid models for pre-equilibrium

decay[9,10].

3.1 Types of calculation available in code

This computer code can perform several types of calculations and combinations of the following types :

(1) A standard Weisskopf-Ewing calculation[6] with multiple particle emission may be done. Emitted particles may be either neutrons; n and p; n, p and α; or n,p,α and d. Excitation energies of the compound nucleus upto 200 MeV can be considered. The residual nuclei of a grid 11 mass units wide by 9 atomic numbers deep,may be calculated by this code. Particle spectra may be selected in the output, in addition to individual product yields and fission cross-sections.

The inverse reaction cross-sections as used in the present program, may either be read in from cards, computed with a classical sharp cutoff model, or by default are computed by an optical model subroutine. The evaporation cascade is computed with a bin width of 1 MeV.

(2) An s-wave approximation[11,12] may be selected, which gives an upper limit to the enhancement of γ-ray de-excitation due to angular momentum effects. In this option, the cross-section for emitting a particle at channel energy ϵ is evaluated for every partial wave in the entrance channel. It is assumed that the rotational energy for each partial wave is irrevocably

committed to rotational motion and therefore no energy is available for particle emission. The rotational energy versus J may be selected either as the rigid spherical rotor value, or from the equilibrium deformed rotating liquid drop model of Cohen et al.[13]. The transmission coefficients for the entrance channel partial waves to be used in the computation can be read in from cards or by default will be provided by the parabolic model[14] subroutine for projectiles of atomic number ≥ 2 or by the optical model subroutine for neutrons, protons and deuterons.

(3) The evaporation calculation can include fission competition according to the Bohr-Wheeler approach[7], using angular momentum dependent ground state and saddle point energies. These energies are taken from Cohen et al.[13] rotating liquid drop calculations. The calculations are performed for each partial wave; upper and lower limits on angular momentum may be selected. There is provision in the input to modify the liquid drop fission barriers by some multiplicative factor, as well as the ratio of ground state to saddle point level densities ($^{a}f/^{a}n$) (default = 1). There is an option in which it is assumed that nucleon emission reduces the daughter nucleus angular momentum by $1\hbar$ from that of the parent nucleus. There is also a provision in this code for pre-equilibrium emission via the hybrid/geometry dependent hybrid models.

3.2 Formulations

The cross-section for emitting a particle at channel energy ϵ may be written as[3,15]

$$\left(\frac{d\sigma}{d\epsilon}\right)_\nu = \pi\lambda\!\!\!^{-2} \sum_{I=o}^{\infty} (2I+1)T_I(2s_\nu+1) \sum_{l=o}^{\infty} T_\nu^l(\epsilon) \sum_{J=|I-l|}^{I+l} \rho(E,J)/D \quad \ldots \quad (3.1)$$

where $\lambda\!\!\!^{-}$ denotes the reduced de-Broglie wavelength of the incident ion, T_I is the transmission coefficient for the I^{th} partial wave of the incident ion, $\rho(E,J)$ is the spin-dependent level density for the residual nucleus, D is the integral of the numerator over all particles and emission energies and the remaining symbols are listed in Table - 3.1.

For simplification, assume that the level density $\rho(E,J)$ is replaced by $\rho(E,I)$ in Equation (3.1). Then

$$\left(\frac{d\sigma}{d\epsilon}\right)_\nu = \pi\lambda\!\!\!^{-2} \sum_{I=o}^{\infty} (2I+1)T_I(2s_\nu+1) \sum_{l=o}^{\infty} (2l+1)T_\nu^l(\epsilon)\rho(E,I)/D \quad \ldots \quad (3.2)$$

$$\sum_{l=o}^{\infty} (2l+1)T_\nu^l(\epsilon) = 2\sigma_\nu(\epsilon)m\epsilon/\pi\hbar^2 \quad \ldots \quad (3.3)$$

$$\left(\frac{d\sigma}{d\epsilon}\right)_\nu = \sum_{I=o}^{\infty} \sigma_I \cdot 2(2s_\nu+1)\sigma_\nu(\epsilon)m\epsilon\,\rho(E,I)/D' \quad \ldots \quad (3.4)$$

which has commonly been called the s-wave approximation. In this assumption, it has not been assumed that the emitted

Table - 3.1 Definition of Symbols

Γ_f	=	Fission width
Γ_ν	=	Particle-emission width
I	=	Emitting nucleus angular momentum
J_ν	=	Residual nucleus angular momentum
S	=	Intrinsic spin of particle ν (with ν = n,p,d, or α)
B_γ	=	Binding energy of particle ν (with ν = n,p,d, or α)
$T_\nu^l(\epsilon)$	=	Transmission coefficient for kinetic energy ϵ and orbital angular momentum l
ρ_f	=	Level density at fission saddle point
ρ_ν	=	Level density for particle emission
a_f	=	Single-particle level density at fission saddle point, used in ρ_f
a_ν	=	Single particle level density at equilibrium deformation used in ρ_ν
B(I)	=	Rotating-liquid-drop fission barrier at angular momentum I
B_f	=	Scaling parameter to adjust the fission barriers
$E_{min}(I)$	=	Rotational energy for a nucleus at angular momentum I and equilibrium deformation from RLDM
$E_{sp}(I)$	=	Rotational energy of a nucleus with angular momentum I at the saddle point deformation from RLDM
E	=	Excitation energy in the emitting (fissioning) nucleus

particles consist of only s-waves, but the initial angular momentum is preserved for each partial wave, i.e. it is implicitly assumed that the compound nucleus angular momentum reasonably represents the average residual nucleus angular momentum following particle evaporation. The above equations can further be simplified assuming that the nuclear moment of inertia is infinite. Then, the result of Weisskopf compound nucleus model[6] is obtained. Thus, if

$$\rho(E,I)\alpha(2I+1)\rho[E-E_{ROT}(I)] \quad \ldots \quad (3.5)$$

with

$$E_{ROT}(I) = 0 \quad \ldots \quad (3.6)$$

we obtain

$$\left(\frac{d\sigma}{d\epsilon}\right)_{\nu} = \sum_{I=0}^{\infty} \sigma_I(2s_{\nu}+1)\sigma_{\nu}(\epsilon)m\epsilon\rho(E)/D' \quad \ldots \quad (3.7)$$

the expression of Weisskopf.

Consider the physical meaning of these approximations in terms of the contour diagrams of Fig. 3.1. An infinite moment of inertia means that there is no level density cutoff at high spin; all populations above the particle binding energy can emit another particle. Assigning a finite moment of inertia reduces the phase space for emission from nuclei at high angular momentum, as is shown by the hatched region of Fig. 3.1.

Consider the E-J plane of Fig. 3.1, and the assumption of an infinite moment of inertia. In this case, since there

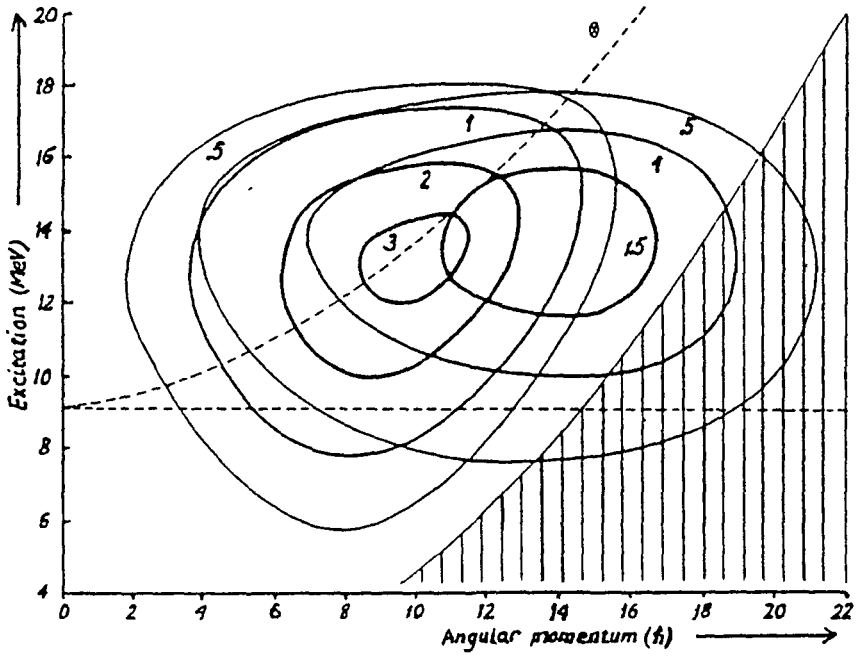

Fig. 3.1 E-J Contour diagram for compound nucleus particle evaporation. (Ref. 3)

is no energy associated to rotation - any nucleus with energy greater than the particle binding energy (horizontal dashed line in Fig. 3.1) can emit another particle, and population below the particle binding energy cannot emit further particles, de-exciting instead by γ-ray emission. The angular momentum of the nuclide does not play any important role, hence, is of no consequence in this particular mode.

Now consider the s-wave approximation as represented by Equation (3.2). An yrast line is defined implicitly and the phase space for particle emission is reduced as I increases. This can be seen from the level density approximation of Equation (3.5) where the level density spin dependence is simply entered as the energy available at each I above the yrast line. But the calculation now does not recognize the coupling of the orbital angular momentum of the out going particle. Therefore, the initial spin distributions are preserved. The emission of particle does not take place at each value of the angular momentum where the excitation energy equals the yrast energy plus the particle binding energy. This approximation may be seen to give enhanced γ-ray emission for higher angular momentum. It will give a broader excitation function for a particular product yield, and a shift to higher apparent threshold energies with increasing excitation and, therefore, higher angular momenta. These effects are mass dependent, as the yrast line reflects the nuclear moment of inertia.

The s-wave approximation cannot predict decay path characteristics which are sensitive to angular momentum and come from calculation of Equation (3.1). These details are mass, angular momentum and excitation energy dependent. The reasons for this can be seen in Fig. 3.1 by considering the range of residual angular momentum available for neutron, proton and alpha emission as a function of I and E of the emitting nucleus. To our knowledge, there is no easy way to accurately approximate these calculations, nor the changes between initial and final angular momentum without performing a calculation of the type represented by Equation (3.1). If it is desirous to predict, e.g., J-distributions of residual nuclei, such a calculation would be the best but definitely higher in terms of computer costs. If one wanted an estimate of product yields, it is rather to do simple s-wave and Weisskopf calculations.

The general expressions for the particle emission and fission widths, using saddle point and yrast energies based upon the RLDM are :

$$\Gamma_\nu \alpha (2s_\nu + 1) \sum_{l=0}^{\infty} \sum_{j=|I-l|}^{I+l} (2J+1) \int_0^{E-E_{min}(J)-B_\nu} \rho_\nu[E-E_{min}(J)-B_\nu-\epsilon] \cdot T_\nu^l(\epsilon)\, d\epsilon$$

$$\Gamma_f \alpha (2I+1) \int_0^{E-E_{sp}(I)} \rho_f[E-E_{sp}(I)-k]\, dk \; . \qquad \ldots \qquad (3.8)$$

The symbols appearing in Equation (3.8) are defined in Table - 3.1.

Now let us consider the logic of the computer code used to evaluate Equations (3.1) to (3.8). The core of the computer is divided into a chart of nuclides as shown in Fig. 3.2. There is a compound nucleus which is formed at some excitation energy and with some cross-section. The Weisskopf calculation is then used with a 1-MeV grid size to perform the evaporation of a neutron, proton, alpha or deuteron storing the residual nucleus population into the appropriate bin. If an s-wave calculation is selected, a suitable distribution of compound nucleus excitations is used as a starting point.

The logic or control, then moves over to the A-1 bin, the bin following neutron emission, after the neutron, proton, deuteron and alpha emission residual nucleus populations have been stored. The code uses the number of millibarns in the highest energy bin A-1 and redistributes that cross-section in the same manner. It then moves down to the next residual excitation bin, and so on, until it has redistributed all the cross-section and summed it in the appropriate bins of the residual nuclides. It repeats this logic, going across the A as far as requested by an input parameter (upto 11 mass units). Next it drops down in Z to the nucleus A-1, Z-1 and it repeats the process, etc.

Fission competition can also be computed for each nuclide, in which case the calculation is done for each partial wave in

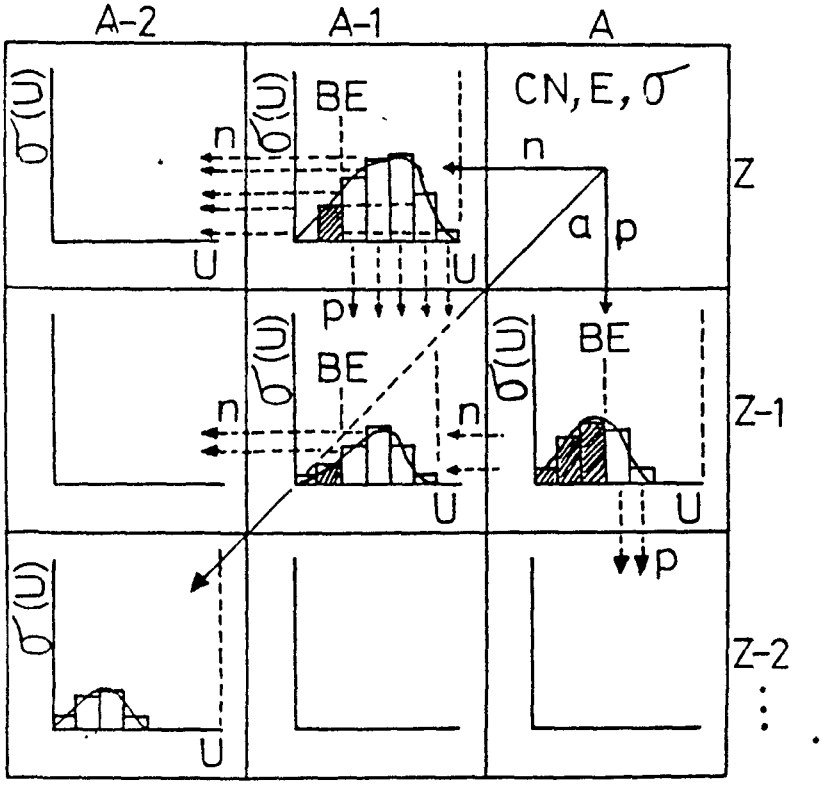

Fig. 3.2 Logic flow of the ALICE/ LIVERMORE-82 code. (Ref. 3)

the entrance channel assuming s-wave approximation or some other arbitrary assumption as to change in angular momentum in populating a given residual nuclide. This has not been included in the present calculation. Spin dependent codes ALERT I and ALERT II can be used if more rigorous calculations are needed. Although, this option has not been incorporated in the present work.

3.3 Code subroutines

There are several subroutines in this code.

3.3.1 LYMASS (BINDEN, MASS)

The LYMASS subroutine calculates the Q-value for formation of the compound nucleus and the neutron, proton, alpha and deuteron binding energies for all nuclides of interest in the evaporation chain. The calculation is done using the Myers-Swiatecki/Lysekil mass formula[16].

The option exists (MC≥ 10) of selecting experimental masses where known, using the mass formula only when experimental masses are not contained in the Table (MASS). When the option of experimental masses is selected[17], the Q-value and binding energies are both computed using experimental masses. The experimental nuclidic mass routines (BINDEN, MASS) are called-up by the LYMASS subroutine.

3.3.1.1 Pairing options

There are four basic pairing options available in the code through the input variable (Switch) MP, which may be MP = 0,1,2 or 3. The options are defined as follows :

MP = 0 Masses are calculated using a mass formula with the odd-even pairing term equal to zero for all nuclides. This option includes the odd-even effect, if any, on level densities.

MP = 1 Masses are calculated using either experimental masses or Lysekil masses with the pairing term $\delta = 11/\sqrt{A}$ taken as zero for even-even nuclides, $-\delta$ for odd-even and -2δ for odd-odd nuclides. This gives a back shifted level density/pairing treatment[18].

MP = 2 Pairing values may be fed for each nuclide in the A by Z array of interest defined by input parameters NA, NZ. Actually pairing values must be supplied for an array NA+2 by NZ+2.

MP = 3 All masses are calculated using either experimental masses or Lysekil masses with the pairing term $\delta = 11/\sqrt{A}$ taken as zero for odd-even nuclides, δ for even-even nuclides, and $-\delta$ for odd-odd nuclides. When effective excitations are computed for use in level densities, the thermodynamic energies are reduced by δ. The author of this code has recommended

the option, MP = 3.

3.3.1.2 Experimental masses

Lysekil masses are replaced by experimental masses for MC = 10.

3.3.2 OVER (TLJ)

These are optical model subroutines, used to calculate inverse reaction cross-sections for neutrons, protons, deuterons and alpha particles. They are also used to calculate reaction and partial reaction cross-sections when neutrons, protons or deuterons are projectiles. In these subroutines when they are used, the major part of computational time is ordinarily spent.

3.3.3 SIGI

This is a subroutine which uses classical sharp-cutoff algorithms to compute inverse reaction cross-sections. This subroutine requires less than 1% of the time of the optical model routine OVER.

3.3.4 PARAP

In subroutine PARAP, all reaction cross-sections and partial reaction cross-sections other than for incident neutrons, protons or deuterons, or unless read in as input, are

calculated using the parabolic model.

3.3.5 FISROT

In this subroutine, angular momentum dependent liquid drop fission barriers, saddle point and ground state energies are calculated using the rotating liquid drop model of Cohen, Plasil and Swiatecki[13].

3.3.6 HYBRID (MFP, NUCMFP)

This subroutine calculates pre-compound decay using the hybrid[9] and geometry-dependent hybrid models[10]. The present code version will select most pre-compound parameters through built in default options. The MFP subroutine supplies intranuclear transition rates using the nuclear optical model[19] whereas NUCMFP uses Pauli corrected nucleon-nucleon scattering cross-sections for this purpose[20]. These intranuclear transition rates, and their role in pre-compound decay are discussed in Ref. 21.

3.3.7 PLT/PLEX

These subroutines can be used to plot excitation functions on the output device for printed output.

3.3.8 SHAFT

This subroutine is used for many of the print statements

for cross-sections and spectra.

3.4 Use of the Code

The present version of the code uses a stored table of level densities pow (2000) represented by the following formula

$$\rho(U) = (U - \delta)^{-5/4} \exp(2\sqrt{a(U-\delta)})$$

where the default value of 'a' is A/9. The mass number used for all cases is that of the compound nucleus instead of the residual nuclei. It would be useful to replace pow (IB) by $(IB/10)^{-5/4} \exp 2(\sqrt{a_{res} \cdot IB/10})$, where 'flot of IB' is the residual excitation times ten, were a_{res} represents the mass number of the residual nucleus divided by PLD (default = 9). This provides space savings by removing pow (2000) array and give more accurate results. There would be some increases in CPU time for most applications if this were done.

In the present code, another point of accuracy involves the use of a 1 MeV bin size instead of 0.5 MeV which has been used in the earliest code. Summations for product yields are over bins of excitation 1 MeV wide-up to the binding energy of the least tightly bound particle plus energies for which charged particle inverse cross-sections are zero. There is no interpolation of cross-section within a bin, so the summation is performed to the nearest integer bin. Since particle binding energies are roughly 5 MeV, this represents a binning uncertainty

of the order of 20% which is less than the other total uncertainties in the calculations. However, that if one calculates e.g. excitation functions using input every 1 MeV in the laboratory system, the conversion into the CM system will cause jumps in the number of bins integrated for product yields, imposing a slight sawtooth effect into individual product yields.

Another compromise involves in the calculation of the inverse reaction cross-sections. When the optical model subroutines are used the inverse reaction cross-sections are calculated only for the (A,Z) of the compound nucleus. When the classical sharp-cutoff routine is used, the inverse reaction cross-sections are recalculated each time the Z of the emitting nuclei changes; the mass assumed is taken to be the compound nucleus mass less $2\Delta Z$, where ΔZ is the difference between original compound nucleus Z and emitting nucleus Z.

The present code has been modified so that input subroutines can easily be removed from the code and used separately to provide input files. This would result in very large program core size reductions.

References

1) P.G. Young, E.D. Arthur and D.G. Madland : Proc. Int. Symp. on Nucl. Data for Technology, Knoxville, Tennese (1979) p. 639.

2) Summary Rept., Nucl. Theory in Neutron Nucl. Data Evaluation, Vol. I, IAEA - 190 (1975) p. 14.

3) M. Blann and J. Bisplinghoff : 'ALICE/LIVERMORE-82' Lawrence Livermore Laboratory Report UCID-19614 (1982).

4) M. Blann and F. Plasil : University of Rochester Report COO-3494-10 (1973) (unpublished).

5) M. Blann : University of Rochester Report COO-3494-29 (1975) (unpublished).

6) V.F. Weisskopf and D.H. Ewing : Phys. Rev. 57 (1940) 472.

7) N. Bohr and J.A. Wheeler : Phys. Rev. 56 (1939) 426.

8) R. Vandenbosch and J.R. Huizenga : 'Nuclear Fission' (Academic Press, N.Y., 1973).

9) M. Blann : Phys. Rev. Lett. 27 (1971) 337.

10) M. Blann : Phys. Rev. Lett. 28 (1972) 757.

11) T. Ericson : Adv. Phys. 9 (1960) 425.

12) M. Blann and G. Merkel : Phys. Rev. B137 (1965) 367.

13) S. Cohen, F. Plasil and W.J. Swiatecki : Ann. of Phys. (N.Y.) 82 (1974) 557.

14) T.D. Thomas : Phys. Rev. 116 (1959) 703.

15) M. Blann and M. Beckerman : Nukleonika 23 (1978) 1.

16) W.D. Myers and W.J. Swiatecki : Ark. Fys. 36 (1967) 343.

17) J.H.E. Mattauch, W. Thiele and A.H. Wapstra : Nucl. Phys. 67 (1965) 1.

18) J.R. Huizenga, H.K. Vonach, A.A. Katsanos, A.S. Gorski and C.J. Stephan : Phys. Rev. 182 (1969) 1149.

19) F.D. Becchetti and G.W. Greenlees : Phys. Rev. 182 (1969) 1190.

20) K. Kikuchi and M. Kawai : 'Nuclear Matter and Nuclear Reactions' North Holland Publishing Co. (1968).

21) M. Blann : Nucl. Phys. A213 (1973) 570.

CHAPTER - IV

EXPERIMENTAL TECHNIQUE AND MEASUREMENTS

A nuclear reaction is a process that occurs when a nuclear particle (nucleon or nucleus) gets into close contact with another. Most of the known nuclear reactions are produced by exposing different materials to a beam of accelerated nuclear particles from a particle accelerator, a reactor, a radioactive source or cosmic radiation. Usually a strong energy and momentum exchange takes place and the final products of the reactions are one, two or more nuclear particles leaving the point of close contact in various directions. The strength of a particular nuclear reaction is usually expressed in terms of a parameter called 'Cross-section' measured in Units of 10^{-24} cm^2, which as defined as equal to 'barn' and abbreviated as b.

The two important techniques which are usually employed in the measurement of alpha particle induced reaction cross-sections are :

1. In-beam or on-line studies
2. Off-beam or off-line studies

1. <u>In-beam studies</u>

In this technique the detection of radiations is done simultaneously with the irradiation of the target. The reaction cross-sections for a particular reaction can be studied by

analysing the emitted particles or prompt gamma ray spectra associated with the reaction. In this technique, the decay scheme of the residual nuclei should be well known. The gamma ray spectra are generally complex and sometimes γ-γ coincidences are necessary for the proper identification of gamma rays. The gamma ray detector should be well shielded from the neutrons coming from background, emitted in the reaction.

2. Off-beam studies

In this technique the detection of radiation and irradiation of the target are done separately. The principle of this technique is to analyze the activity of residual nucleus obtained from a particular reaction. Therefore, we may call it the 'activation technique'. The beta or gamma activities associated with the residual nucleus can be studied by using the appropriate detectors. Although this technique has several advantages, but is limited to those isotopes which are stable and whose product nuclides are un-stable and have convenient half-lives. Moreover, the decay scheme of the product nuclei should be well established. The high sensitivity with which this induced activity can be detected and the individually characteristic modes of decay of each radioisotope, leads to the many advantages inherent in this technique. Among these particular advantages are ; extremely high sensitivity; selectivity and the possibility of non-destructive analysis. Cross-sections $\sim$ 1μb have been measured[1] using the activation

technique. In the present measurements, the off-line studies have been done. Following are the details of formulation :

4.1 Formulation

Let us consider the decay rate equation governing the nuclear transformation and decay of the activated product, when a target is irradiated to a constant flux ϕ of projectiles, the rate of production of any activity, R_p can be written as[2,3]

$$R_p = \sigma \phi N_o \qquad \ldots \qquad (4.1)$$

where N_o $(= mNf/A_o)$ is the number of target nuclei of the isotope under investigation present in the sample, m is the mass of the element in grams, N is the Avogadros number, f is the abundance of the isotope in the target, A_o is the atomic weight of the element and σ is the activation cross-section.

Let t be the time of irradiation of a target by a constant alpha beam with flux ϕ, which yield a certain radioactive reaction product X. The equation which governs the growth of X-type activity during irradiation can be written as

$$\frac{dX}{dt} = \sigma \phi N_o - X\lambda \qquad \ldots \qquad (4.2)$$

where λ is the decay constant of X-type of activated nuclei and X is the number of radioactive atoms present. If the irradiation is carried out for time t_1, then the activity of X-type nuclei in the specimen at the instant when the irradiation of

the sample was just stopped, will be given by

$$W = X_o\lambda = \sigma \Phi N_o [1 - \exp(-\lambda t_1)] \quad \ldots \quad (4.3)$$

where $[1-\exp(-\lambda t_1)]$ is called the saturation factor.

If the activity of the radioactive nucleus X is measured after a time t' from the stop of irradiation, the activity at that moment will be given by

$$\frac{dX}{dt'} = W \exp(-\lambda t') = X_o \lambda \exp(-\lambda t')$$

$$\text{or} \quad \frac{dX}{dt'} = \sigma \Phi N_o [1-\exp(-\lambda t_1)] \exp(-\lambda t')$$

$$\text{or} \quad dX = \sigma \Phi N_o [1-\exp(-\lambda t_1)] \exp(-\lambda t')dt' \quad \ldots \quad (4.4)$$

Let us suppose that C be the actual number of disintegrations of the sample during a time period t_3 starting after a time t_2 from the stop of the irradiation. Then the number of disintegrations C, can be obtained by integrating Equation (4.4) in the time interval t_2 and $t_2 + t_3$ as

$$C = \int dX = \sigma \Phi N_o [1-\exp(-\lambda t_1)] \int_{t_2}^{t_2+t_3} \exp(-\lambda t')dt'$$

$$\text{or} \quad C = \frac{\sigma \Phi N_o [1-\exp(-\lambda t_1)] [1-\exp(-\lambda t_3)]}{\lambda \exp \lambda t_2} \quad \ldots \quad (4.5)$$

Now, if A is the number of counts observed during the time interval t_3 by the counting device, ϵ is the detector efficiency of the detector, G is the geometry factor, Θ is the absolute intensity of a particular gamma ray and K is the correction

factor for gamma self-absorption in the disc shaped target given as [5]

$$K = [1-\exp(-\mu d)]/\mu d$$

where μ is the gamma ray absorption coefficient taken from reference 6 and d is the thickness of the disc shaped target under investigation, then the actual number of disintegration C will be given as

$$C = \frac{A}{\epsilon . G . \Theta . K} \quad \ldots \quad (4.6)$$

From Equations (4.5) and (4.6) we can write,

$$\sigma = \frac{A . \lambda . \exp \lambda t_2}{\Phi . N_o . (\epsilon . G) . \Theta . K [1-\exp(-\lambda t_1)][1-\exp(-\lambda t_3)]} \quad \ldots \quad (4.7)$$

We have used Equation (4.7) in the determination of activation cross-sections.

In the measurement, the experimental cross-section value for a given reaction has been taken as the weighted average of these individual cross-sections. The averaging of the data has been done using the following method [7].

If suppose $x_1 \pm \Delta x_1$, $x_2 \pm \Delta x_2$, $x_3 \pm \Delta x_3$ ..... are the different measured values of the same quantity, then the weighted average

$$\bar{X} = \frac{\Sigma W_i x_i}{\Sigma W_i} \quad \ldots \quad (4.8)$$

where

$$W_i = \frac{1}{(\Delta x_i)^2}$$

and

$$\text{The internal error} = [\Sigma W_i]^{-1/2} \quad \ldots \quad (4.9)$$

$$\text{The external error} = \left[\frac{\Sigma W_i (\bar{x}-x_i)^2}{n(n-1)\Sigma W_i}\right]^{1/2} \quad \ldots \quad (4.10)$$

Using Equations (4.7) to (4.10), a computer programme has been made to calculate cross-sections at various energies.

4.2 Calibration and Detector Efficiency

The word 'Calibration' means 'in accordance with' i.e., if the gamma rays expected to appear in the spectrum are well known in advance, the corresponding peaks can be readily indentified by inspection. On the other hand, the energy of any unknown gamma ray can be determined from calibration curve. Precise calibration of the pulse height interms of absolute gamma ray energy is very important for proper identification of the photopeaks in a gamma ray spectrum[8,9]. Accurate calibration requires standard sources having gamma energies that are not different from those to be measured. To account for these non-linearities over the whole energy range, it is useful to have multiple calibration peaks at various points along the measured energy range. In the present measurement, the energy calibration of the gamma ray spectrometer has been done using standard gamma ray sources ^{22}Na, ^{54}Mn, ^{57}Co,

^{60}Co, ^{133}Ba, ^{137}Cs and ^{152}Eu. The energy calibration curve (energy versus channel number) has been obtained by fitting the data to a straight line using a standard computer programme. Gamma rays of interest in the spectrum of irradiated samples have been identified using this energy calibration.

The efficiency of a detector is a measure of how many pulses occur for a given number of gamma rays. It's knowledge is essential in the study of excitation functions. The use of individual standard sources in the determination of detection efficiencies may introduce some errors due to non-reproducibility of geometry. These errors may be removed by using a single multiple standard source. In the present work, a standard source of ^{152}Eu has been taken for the determination of detector efficiencies. ^{152}Eu has a number of major gamma rays whose energy covers a range from 122 KeV to 1408 KeV.

The intrinsic photopeak detection efficiency, for a point source at different gamma energies can be determined by using the following relation :

$$\epsilon = \frac{C \exp(\lambda t)}{S_o . \theta . G} \qquad \ldots \qquad (4.11)$$

where C is the number of events recorded in one second under the photopeak, λ is the decay constant of the radioactive nuclei, t is the time lapsed between start of counting and the date of fabrication of standard γ-ray source, S_o is the actual number of radiation quanta emitted by the standard source per second at

the time of its fabrication, Θ is the absolute intensity of relevant gamma-ray and G is the geometry factor given by, $G = \Omega/4\pi$, where Ω is the solid angle in steradians subtended by the detector surface facing the source. By measuring the photopeak area over a fixed period of time under the various gamma peaks and by determining the detector solid angle from its di-mensions and source-detector distance, we can calculate the photopeak efficiency of the corresponding gamma rays. The source-detector distance is very critical factor which sould be measured accurately to minimize the errors in the reproducibility of the geometry. The probable error in the determination of the geometry factor has been avoided by determining the relative detection efficiencies as :

$$\epsilon . G = \frac{C \exp(\lambda t)}{S_o . \Theta} \qquad \ldots \qquad (4.12)$$

Experimentally, C has been determined for each photopeak for a time period of about 30 minutes, keeping the ^{152}Eu source at the desired geometry. The value of S_o is taken from the data supplied by the manufacturer and the values of 'Θ' and $T_{1/2}$ ($\lambda = 0.693/T_{1/2}$) are taken from reference 10. The geometry dependent efficiencies ($\epsilon . G$) have been determined at distances of 0.8 cm, 2.8 cm and 6.3 cm from the detector surface, geometries used in the counting of gamma activities induced by the alpha particles. A typical geometry dependent efficiency curve of the 100 cc ORTEC Ge(Li) detector obtained at a distance of 0.8 cm from the detector surface is shown in Fig. 4.1.

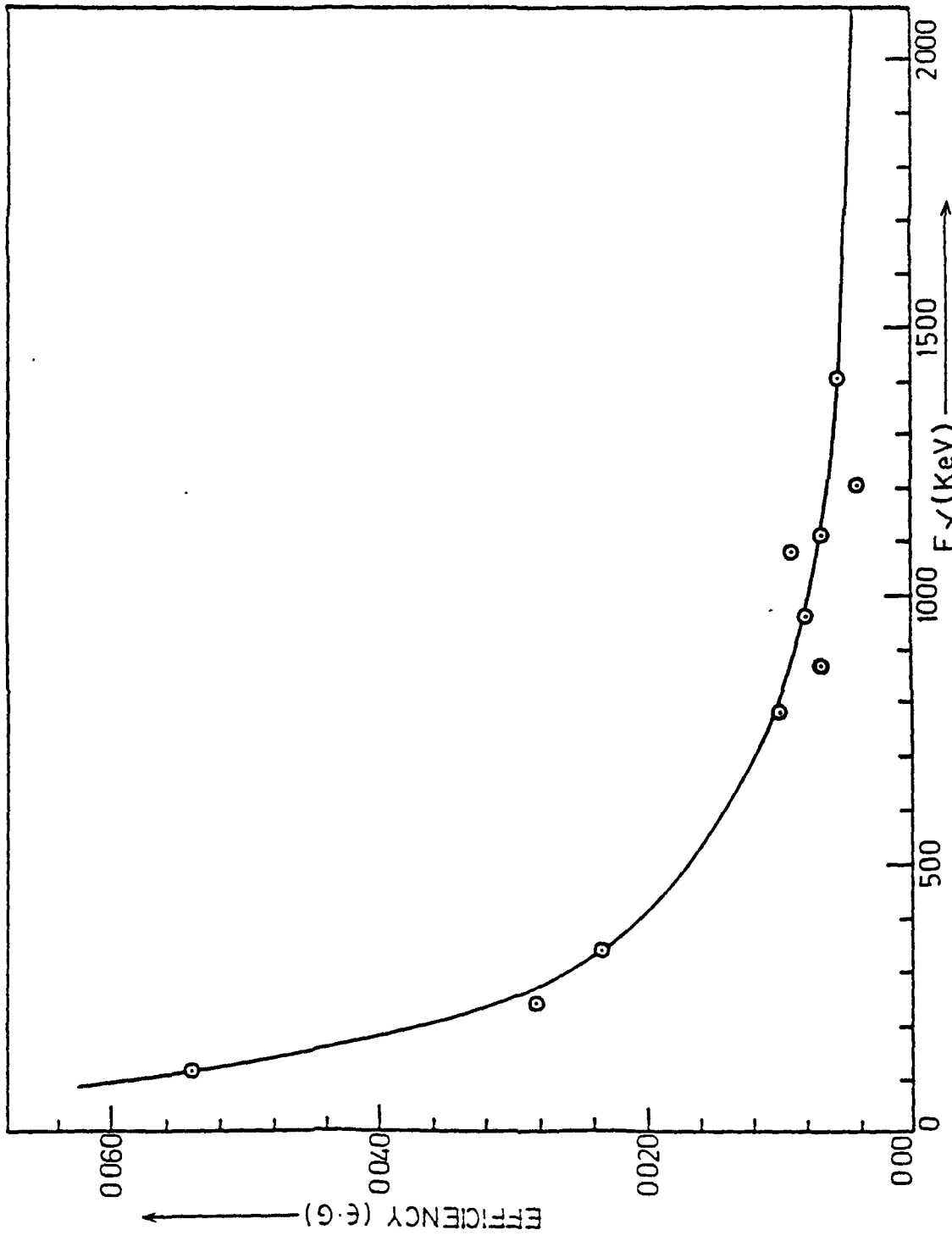

Fig. 4.1 Geometry dependent efficiency curve for 100 cc Ge(Li) detector.

4.3 Irradiations

The stacked foil technique is generally used for the study of charged particle reaction cross-sections[11-16]. In this technique, a number of target foils are arranged to form a stack. Energy degrader foils can be used in between the target foils to obtain the desired projectile energies. In a single run, a number of target foils can be irradiated to different projectile energies by using this technique. Thus the reaction cross-sections can be studied at different energies with a single irradiation of the target stack to the projectile beam.

The targets for irradiations were prepared from spectrographically pure (SPECPURE) natural samples of purity better than 99.99%. In cases of ^{55}Mn, $^{69,71}Ga$ and ^{209}Bi, targets were prepared by vacuum evaporation technique at the Target Division of the Variable Energy Cyclotron Centre (VECC), Calcutta (India). The thickness of deposition for these targets were $\simeq$ 1-4 mg/cm^2. However, in the case of copper ($^{63,65}Cu$), thin metallic foils of thickness 10.68 mg/cm^2 were used. All the target and degrader foils were cut into pieces of size 1.5 X 1.5 cm^2 and accurately weighed so that the thickness of each foil was accurately known. The target foils were fixed with a solution of zapon in acetone on brass or aluminium target holders having a circular hole of diameter 1.2 cm in its centre. When the acetone evaporated the zapon held the target foils to the target holders. Energy degrader aluminium foils of different thickness were sandwiched between the target foils, so as to get the desired α-particle

energy incident on each foil. Two blank target holders were kept, one each in the beginning and the end of the stacks at the time of irradiation in order to check any background activity produced in the target holders.

The stacks comprising of the targets and aluminium degrader foils are shown in Fig. 4.2. The irradiations of the stacks have been carried out using ≃ 60 MeV diffused α-beam of diameter 8 mm at the Variable Energy Cyclotron Centre (VECC), Calcutta (India). Beam energy was determined from a curve that related the cyclotron RF with energy, constructed from experimental data on elastic scattering. The energy of alpha particles striking different target foils has been calculated using the foil thickness and the relevant alpha particles stopping power. The stopping powers of Northcliffe and Schilling[17] have been adopted in the calculations. No consideration of straggling for increase in the path length of the incident beam in the stopping material has been made for the estimation of energy loss in target thickness because of its negligibly small effects for alpha particles[13].

The target stacks were clamped in a water cooled aluminium 'Faraday Cup'. The 'Faraday cup' was insulated from rest of the system to measure the beam current of the alpha particles striking the target foils. The 'Faraday cup' was also connected to a calibrated current integrator, in order to measure the total charge collected during a particular irradiation. A typical experimental set-up for stack irradiation is shown in Fig. 4.3.

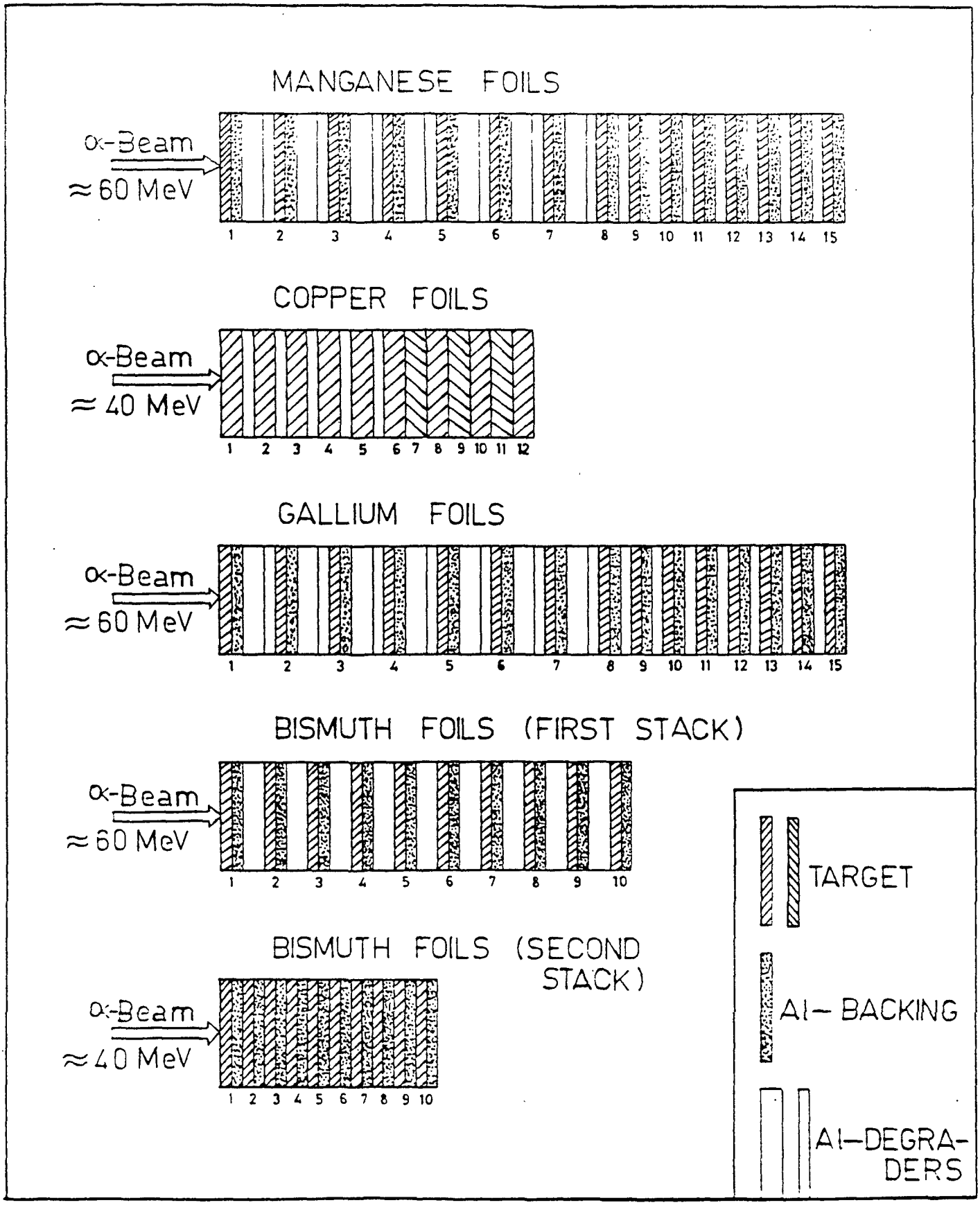

Fig. 4.2 Arrangement of different target stacks.

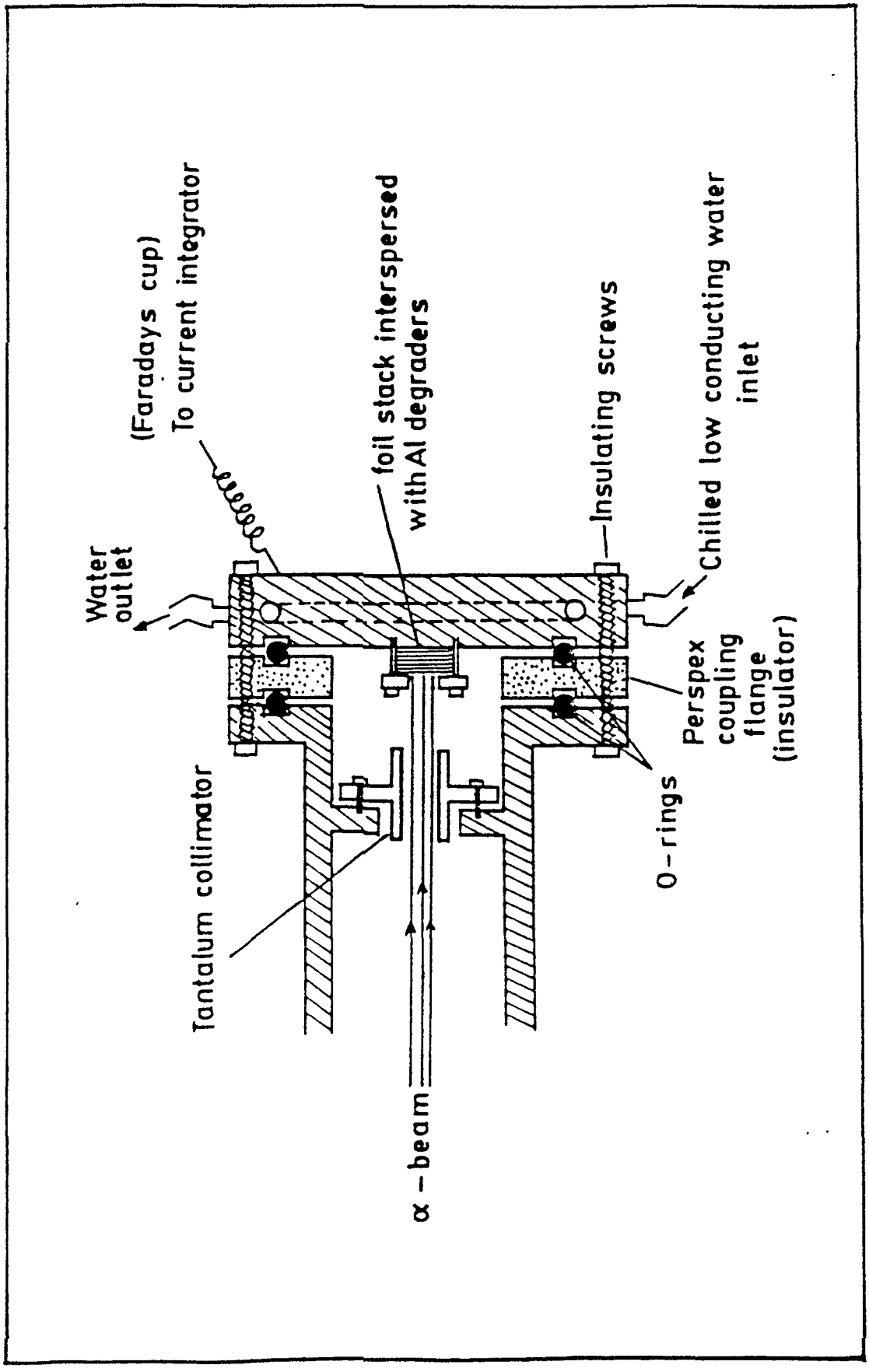

Fig. 4.3 An experimental set-up for stack foil irradiation with α-particle beam.

The beam currents used in the present investigation were between 100 nA to 200 nA. The target stacks were irradiated for time periods ranging from 30 minutes to 60 minutes. Since there have been little fluctuations in the beam current during the irradiations, the average incident flux has been calculated with the knowledge of total charge collected in the 'Faraday cup'. The incident average flux for different irradiations was of the order of 10^{11} α-particles/cm^2. sec. In the present measurements the uncertainty in the initial beam energy was $\pm$ 0.5 MeV.

4.4 Counting

The important and the major step of the experiment is the determination of the induced activity in the target foils. The most precise method for this measurement is the use of high resolution gamma ray spectroscopy. The good resolution helps not only to separate closely spaced peaks but also assists in the detection of weak gamma rays of discrete energies when superimposed on a broad continuum. Germanium detectors are preferred for the analysis of complex gamma ray spectra involving many energies. A 100 cc ORTEC Ge(Li) detector having a resolution of2 keV at 1.33 MeV has been used to detect the characteristic gamma-lines. The foils were detached from the 'Faraday cup' after irradiation and were kept one by one in the desired geometry near the detector for counting the gamma activities. The choice of the counting geometry for a particular observation was made such that the count rate is appreciable and at the same time the

dead time of the detector is low.

The gamma ray spectra have been analysed using pre-calibrated CANBERRA-80 and CANBERRA-88 multichannel analysers. Before starting the counting of the induced gamma activities, a background spectrum was recorded to check the presence of any background gamma peak coming due to contamination of the detector surroundings. Any contaminating activity from the target holder was also checked by recording the background spectrum with the blank target holder. The spectra were then recorded for time periods ranging from 300 seconds to 700 seconds depending on the intensities of the induced activities so as to get good counting statistics. The recording time was corrected for the dead time of the analyser.

The reaction product nuclei were identified by characteristic gamma-transitions following their decay. The counts under the photopeaks were estimated from the total counts in the respective peak after making the corrections for background counts.

4.5 Measurements

In the present work, an attempt has been made to measure the alpha induced reaction cross-sections for ^{55}Mn, $^{63,65}Cu$, $^{69,71}Ga$ and ^{209}Bi targets between excitation energies $\lesssim$ 7-60 MeV. The various type of reactions induced by alpha particles on ^{55}Mn, $^{63,65}Cu$, $^{69,71}Ga$ and ^{209}Bi have been observed by detecting the characteristic gamma lines obtained from the decay of the residua. nuclei. The reaction channels (residual nucleus unstable) for

^{55}Mn, $^{63,65}Cu$, $^{69,71}Ga$ and ^{209}Bi which are possible in the energy range considered in the present measurements are listed in Tables 4.1 - 4.4.

The other details viz. residual nucleus, Q-value, Half-life gamma-ray energies and corresponding absolute intensities are also given in the Tables 4.1 - 4.4. The Q-values of the different reactions have been taken from Ref. 19 and 20 and the other decay data from Ref. 10. In the list very week gamma rays are not included whenever strong gamma rays are available for the same emitting nuclide. Gamma rays having higher energies are also not included in the list. We have considered only those reactions which gave appreciable activities for the meaningful excitation studies. A computer program based on Equations (4.7 - 4.10) have been used to calculate the alpha induced reaction cross-sections at different energies. The errors quoted in the measured cross-section values are internal or external (whichever was greater). The details of the measurements are described individually for each target and for each reaction.

4.5.1 Target Nucleus : ^{55}Mn

Natural specpure manganese has been used for the preparation of the target foils in the present investigation. Manganese of thickness 1 mg/cm^2 was deposited onto aluminium backing of thickness 6.75 mg/cm^2, by vacuum evaporation technique. The stack was composed of 15 (Fifteen) manganese foils sandwiched between aluminium degraders of thickness 20.387 mg/cm^2 and 6.75 mg/cm^2.

Table - 4.1

Nuclear spectroscopic data used for the evaluation of cross-sections in ^{55}Mn target

Reaction	Q-value (MeV)	Half-life ($T_{1/2}$)	E_γ (MeV)	Absolute γ-intensity θ_γ(%)
$^{55}Mn(\alpha,n)^{58g}Co$	-03.51	70.78d	0.811	99.9
$^{55}Mn(\alpha,n)^{58m}Co$	-03.51	9.15h	0.025	0.03
$^{55}Mn(\alpha,2n)^{57}Co$	-12.08	271.65d	0.014	9.8
			0.122	85.6
			0.136	11.1
$^{55}Mn(\alpha,3n)^{56}Co$	-23.46	78.76d	0.847	99.9
			1.038	13.9
			1.238	67.6
			1.360	4.3
			1.771	15.7
			2.015	3.1
			2.035	7.9
$^{55}Mn(\alpha,4n)^{55}Co$	-33.56	17.54h	0.092	2.7
			0.411	1.0
			0.477	20.3
			0.804	2.1
			0.932	75.0
			1.317	7.1
			1.370	3.0
			1.409	16.5

Contd.....

Contd..... (Table - 4.1)

$^{55}Mn(\alpha,\alpha n)^{54}Mn$	-10.20	312.20d	0.835	100.0
$^{55}Mn(\alpha,2p3n)^{54}Mn$	-38.50	312.20d	0.835	100.0
$^{55}Mn(\alpha,\alpha 3n)^{52g}Mn$	-31.22	5.59d	0.744	90.0
			0.848	3.3
			0.936	94.5
			1.246	4.2
			1.334	5.1
			1.434	100.0
$^{55}Mn(\alpha,\alpha 3n)^{52m}Mn$	-31.22	21.40m	1.434	98.2

Table - 4.2

Nuclear spectroscopic data used for the evaluation of cross-sections in $^{63,65}Cu$ target

Reaction	Q-value (MeV)	Half-life ($T_{1/2}$)	E_γ (MeV)	Absolute γ-intensity θ_γ(%)
$^{63}Cu(\alpha,n)^{66}Ga$	-07.51	9.45h	0.834	6.1
			1.039	38.0
			1.232	1.2
			1.333	1.3
			1.919	2.1
$^{63}Cu(\alpha,2n)^{65}Ga$	-16.65	15.20m	0.053	4.9
			0.061	11.5

Contd.....

Contd..... (Table - 4.2)

			0.115	54.6
			0.153	8.9
			0.207	2.6
			0.768	1.3
			0.932	1.8
$^{63}Cu(\alpha,pn)^{65}Zn$	-12.59	244.02d	1.116	50.8
$^{65}Cu(\alpha,n)^{68}Ga$	-05.83	68.33m	1.077	3.0
$^{65}Cu(\alpha,2n)^{67}Ga$	-14.12	78.26h	0.093	38.0
			0.185	23.6
			0.209	2.7
			0.300	19.0
			0.393	5.3
$^{65}Cu(\alpha,3n)^{66}Ga$	-25.33	9.45h	0.834	6.1
			1.039	38.0
			1.232	1.2
			1.333	1.3
			1.919	2.1
$^{65}Cu(\alpha,p3n)^{65}Zn$	-30.41	244.02d	1.116	50.8

Table - 4.3

Nuclear spectroscopic data used for the evaluation of cross-sections in $^{69,71}Ga$ target

Reaction	Q-value (MeV)	Half-life ($T_{1/2}$)	E_γ (MeV)	Absolute γ-intensity θ_γ(%)
$^{69}Ga(\alpha,n)^{72}As$	-06.74	26.0h	0.630	7.9
			0.834	83.4
			1.050	1.0
			1.464	1.1
$^{69}Ga(\alpha,2n)^{71}As$	-15.15	61.0h	0.175	83.7
			0.327	2.7
			0.500	2.8
			1.096	4.2
$^{69}Ga(\alpha,3n)^{70}As$	-26.77	53.0m	0.252	2.5
			0.497	2.5
			0.595	16.3
			0.607	3.9
			0.668	21.2
			0.745	20.8
			0.889	3.1
			0.893	2.0
			0.906	12.2
			1.040	81.7
			1.099	4.4

Contd.....

Contd..... (Table - 4.3)

			1.114	21.2
			1.118	3.2
			1.339	8.9
			1.413	8.6
			1.523	5.1
			1.708	17.9
			1.781	3.9
			2.008	2.9
			2.020	16.7
$^{69}Ga(\alpha,p3n)^{69}Ge$	-32.04	39.05h	0.318	1.4
			0.574	11.6
			0.872	10.3
			1.106	27.0
$^{69}Ga(\alpha,\alpha3n)^{66}Ga$	-29.71	9.46h	0.834	6.1
			1.039	38.0
			1.232	1.2
			1.333	1.3
			1.919	2.1
$^{71}Ga(\alpha,n)^{74}As$	-04.93	17.79d	0.596	60.0
			0.601	5.6
$^{71}Ga(\alpha,2pn)^{72}Ga$	-21.78	14.12h	0.630	24.4
			0.834	95.6
			0.894	9.8
			1.051	6.9
			1.597	4.2

Contd.....

Contd..... (Table - 4.3)

			1.861	5.2
$^{71}Ga(\alpha,4n)^{71}As$	-32.10	61.0h	0.175	83.7
			0.327	2.7
			0.500	2.8
			1.096	4.2

Table - 4.4

Nuclear spectroscopic data used for the evaluation of cross-sections in ^{209}Bi target

Reaction	Q-value (MeV)	Half-life ($T_{1/2}$)	E_γ (MeV)	Absolute γ-intensity Θ_γ(%)
$^{209}Bi(\alpha,3n)^{210}At$	-27.98	8.3h	0.245	79.4
			0.527	1.1
			0.817	1.7
			0.852	1.4
			0.955	1.8
			1.181	99.3
			1.436	29.0
			1.483	46.5
			1.599	13.4

Contd.....

Contd..... (Table - 4.4)

$^{209}Bi(\alpha,4n)^{209}At$	-35.24	5.40h	0.104	2.1
			0.195	22.8
			0.233	1.0
			0.239	12.7
			0.545	94.4
			0.551	5.1
			0.666	1.9
			0.781	86.6
			0.790	65.9
			0.864	2.1
			0.903	3.8
			1.103	5.6
			1.114	1.4
			1.170	3.1
			1.175	2.0
			1.217	1.1
			1.263	2.0
			1.582	1.8

The composition of the stack is shown in Fig. 4.2. The target stack was irradiated with a 60 MeV diffused α-beam of diameter 8 mm. After passing through all the target foils, beam was made to fall on the 'Faraday cup' for measuring the beam current and the total charge collected during irradiation. The irradiation of the

stack was performed with a beam current of ~ 200 nA for a time period of 1.0 hour. The gamma activities of each foil were measured by keeping the foils one by one in the desired geometry. The cross-sections for the (α,xn), x = 1-4, $(\alpha,\alpha n)$, $(\alpha,2p3n)$ and $(\alpha,\alpha 3n)$ reactions have been measured at fifteen different incident α-particle energies viz., 6.8 ± 2.7 MeV, 12.2 ± 1.8 MeV, 16.2 ± 1.5 MeV, 19.6 ± 1.3 MeV, 22.5 ± 1.2 MeV, 25.2 ± 1.2 MeV, 27.8 ± 1.1 MeV, 30.2 ± 1.0 MeV, 35.5 ± 0.9 MeV, 40.3 ± 0.8 MeV, 44.7 ± 0.7 MeV, 48.9 ± 0.7 MeV, 52.8 ± 0.7 MeV, 56.5 ± 0.6 MeV and 59.95 ± 0.6 MeV. A typical gamma ray spectrum obtained from the activation of manganese target foil by 44.7 MeV α-particles and taken after about 38.0 hours from the stop of the irradiation is shown in Fig. 4.4.

4.5.1.1 $^{55}Mn(\alpha,n)$ Reaction

The (α,n) reaction on ^{55}Mn produces two isomers of ^{58}Co. Both the isomers are unstable. The half-life of the ground state is 70.78 days and the metastable state is 9.15 hours. The ground state decays mainly by electron capture (85%) and β^+(15%) to the excited states of ^{58}Fe (stable isotope). The metastable state of ^{58}Co decays to the ground state with isomeric-transition. The half-life of the metastable state is much shorter than that of the ground state. Therefore, the cross-sections for the ground state producing reaction is almost the total cross-section for the production of ^{58}Co isomers. The Q-value of this reaction is -3.51 MeV. The gamma rays obtained from the decay of these isomers are given in Table 4.1. The reaction producing the ground

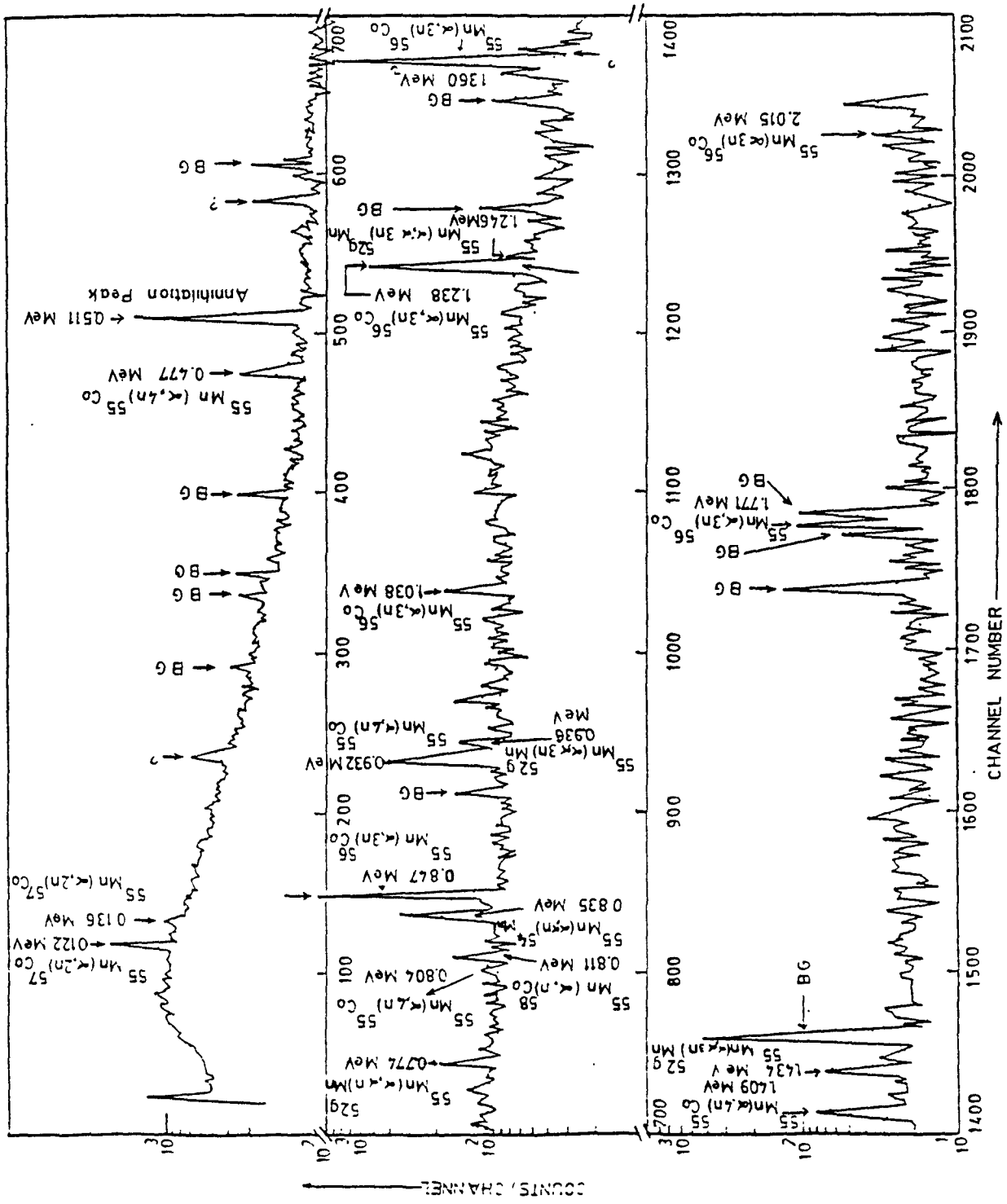

Fig. 4.4 Typical gamma ray spectrum obtained from the activation of ^{55}Mn target by 44.7 MeV α-particles.

state isomer has been studied by considering the 0.811 MeV gamma ray at twelve alpha particle energies. The decay scheme of the residual nucleus is shown in Fig. 4.5(a). Values of the parameters such as half-life of product nucleus, incident flux, number of target nuclei, absolute gamma ray intensity, detection efficiency of the gamma rays, γ-self absorption factor, irradiation time, time lapse, recording time, the counts under the photopeak and the projectile energy etc. are given in Table - 4.5. The cross-sections obtained with the gamma ray of 0.811 MeV are tabulated in Table - 4.6.

Table - 4.5

Experimental data for $^{55}Mn(\alpha,n)^{58g}Co$ reaction

Half-life of product nucleus = 6115392 sec.

Time of irradiation, t_1 = 3600 sec.

Incident flux, Φ = 1.2326×10^{12} α-particles/cm^2-sec.

Number of target nuclei, N_o = 5.5012×10^{18}

Project. Energy E_α (MeV)	Gamma-Energy E_γ (MeV)	Absol. γ-intens. Θ_γ (%)	Geometry dependent efficien. $\epsilon.G$	γ-self absorp. factor K	Time lapse t_2 (sec)	Record. time t_3 (sec)	Photo peak count (A)
6.8±2.7	0.811	99.9	0.00980	0.99993	152580	700	2383
12.2±1.8	0.811	99.9	0.00980	0.99993	151380	700	12349
16.2±1.5	0.811	99.9	0.00980	0.99993	149160	700	10120
19.6±1.3	0.811	99.9	0.00980	0.99993	147960	700	5194

Contd.....

Contd..... (Table - 4.5)

22.5±1.2	0.811	99.9	0.00980	0.99993	146820	700	2138
25.2±1.2	0.811	99.9	0.00980	0.99993	145740	700	1228
27.8±1.1	0.811	99.9	0.00980	0.99993	144660	700	1010
30.2±1.0	0.811	99.9	0.00980	0.99993	143640	700	761
35.5±0.9	0.811	99.9	0.00980	0.99993	142560	700	304
40.3±0.8	0.811	99.9	0.00980	0.99993	141480	700	233
44.7±0.7	0.811	99.9	0.00980	0.99993	135600	700	191
48.9±0.7	0.811	99.9	0.00980	0.99993	134460	700	152

Table - 4.6

Activation cross-sections for the $^{55}Mn(\alpha,n)^{58g}Co$ reaction

E_α (MeV)	Cross-sections (mb) with gamma ray of 0.811 MeV
6.8±2.7	127.95±3.17
12.2±1.8	662.96±6.39
16.2±1.5	543.16±5.90
19.6±1.3	278.73±4.40
22.5±1.2	114.72±3.05
25.2±1.2	65.88±2.58
27.8±1.1	54.18±2.47
30.2±1.0	40.82±2.31
35.5±0.9	16.30±2.25
40.3±0.8	12.49±2.47
44.7±0.7	10.24±2.73
48.9±0.7	8.14±3.00

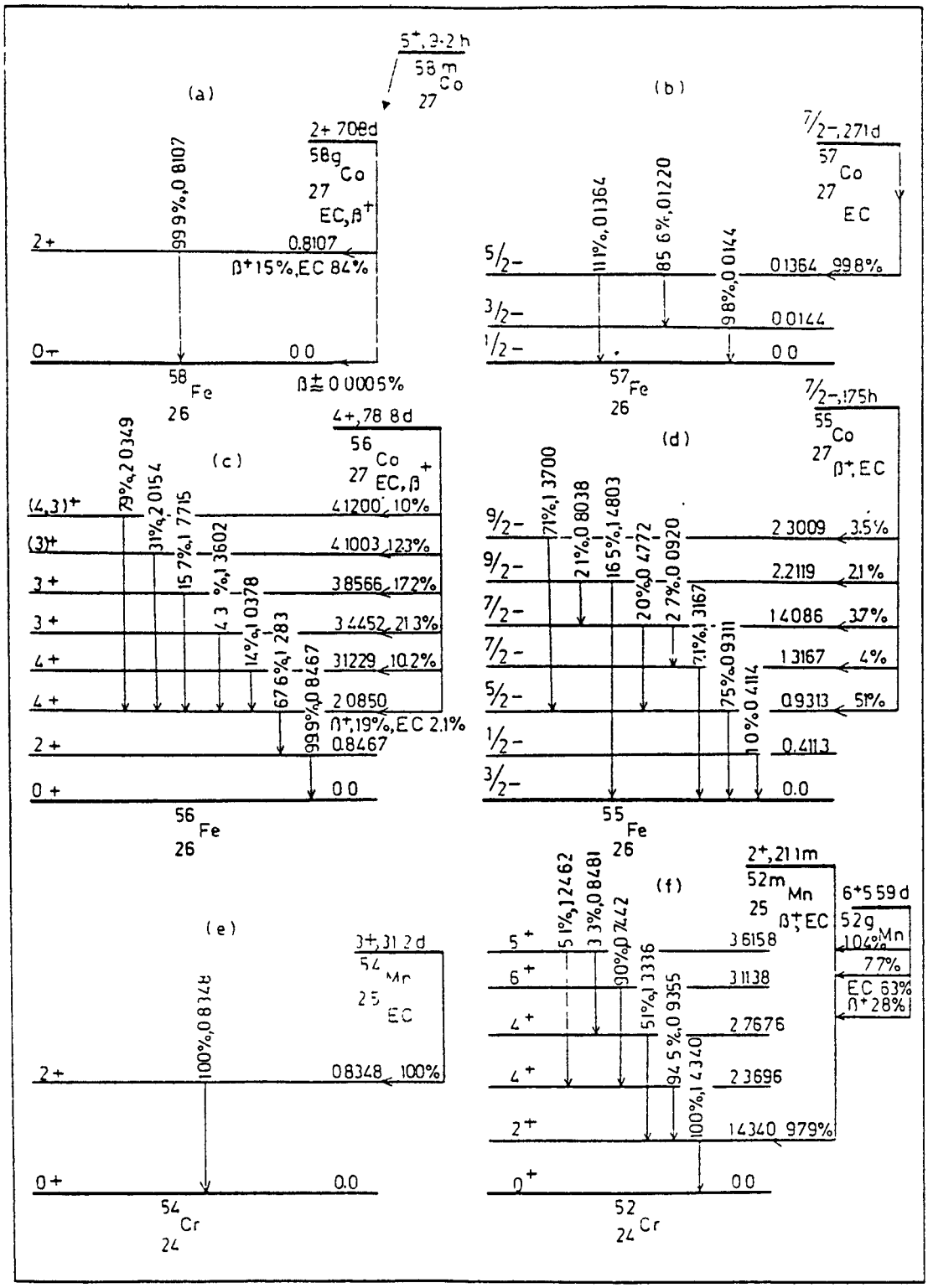

Fig. 4.5 Partial decay schemes for isotopes ^{58}Co, ^{57}Co, ^{56}Co, ^{55}Co, ^{54}Mn and ^{52}Mn formed in alpha induced reactions on ^{55}Mn.

4.5.1.2 $^{55}Mn(\alpha,2n)$ Reaction

The Q-value for $(\alpha,2n)$ reaction on ^{55}Mn is -12.08 MeV. This reaction produces ^{57}Co residual nucleus, being unstable and which decays mainly by electron capture with half-life of 271.65 days to the excited states of ^{57}Fe (stable isotope). The gamma rays emitted from the product nucleus are enlisted in Table - 4.1. The reaction has been studied at fourteen incident alpha-particle energies by considering the 0.122 MeV and 0.136 MeV gamma rays obtained from the decay of their residual nucleus. In the analysis of experimental data, the intense, i.e. 0.122 MeV gamma ray is preferable at alpha particle energies having low cross-sections whereas the less intense 0.136 MeV gamma ray is preferable at energies associated with high cross-sections. The decay scheme of ^{57}Co is shown in Fig. 4.5(b). The values of the parameters used in the calculation of cross-sections are given in Table - 4.7 and the cross-sections obtained with the different gamma rays are tabulated in Table - 4.8.

4.5.1.3 $^{55}Mn(\alpha,3n)$ Reaction

The Q-value of $(\alpha,3n)$ reaction on ^{55}Mn is -23.46 MeV. This reaction produces unstable ^{56}Co residual nucleus which decays mainly by electron capture (81%) and β^+(19%) with a half-life of 78.8 days to the excited states of ^{56}Fe (stable isotope). The gamma rays obtained from the decay of their product nucleus are given in Table - 4.1. The reaction has been studied considering the four major gamma rays viz., 0.847 MeV, 1.038 MeV, 1.238 MeV

Table - 4.7

Experimental data for $^{55}Mn(\alpha,2n)^{57}Co$ reaction

Half-life of product nucleus = 23470560 sec.

Time of irradiation, t_1 = 3600 sec.

Incident flux, Φ = 1.2326×10^{12} α-particles/cm^2-sec.

Number of target nuclei, N_o = 5.5012×10^{18}

Project. Energy E_α (MeV)	Gamma-Energy E_γ (MeV)	Absol. γ-intens. Θ_γ (%)	Geometry dependent efficien. $\epsilon.G$	γ-self absorp. factor K	Time lapse t_2 (sec)	Record. time t_3 (sec)	Photo peak count (A)
12.2±1.8	0.122	85.6	0.05440	0.99988	151380	700	851
	0.136	11.1	0.05100	0.99989	151380	700	-
16.2±1.5	0.122	85.6	0.05440	0.99988	149160	700	13657
	0.136	11.1	0.05100	0.99989	149160	700	1652
19.6±1.3	0.122	85.6	0.05440	0.99988	147960	700	23703
	0.136	11.1	0.05100	0.99989	147960	700	2947
22.5±1.2	0.122	85.6	0.05440	0.99988	146820	700	22492
	0.136	11.1	0.05100	0.99989	146820	700	2600
25.2±1.2	0.122	85.6	0.05440	0.99988	145740	700	20378
	0.136	11.1	0.05100	0.99989	145740	700	2495
27.8±1.1	0.122	85.6	0.05440	0.99988	144660	700	20381
	0.136	11.1	0.05100	0.99989	144660	700	2454
30.2±1.0	0.122	85.6	0.05440	0.99988	143640	700	16008
	0.136	11.1	0.05100	0.99989	143640	700	1926
35.5±0.9	0.122	85.6	0.05440	0.99988	142560	700	4695
	0.136	11.1	0.05100	0.99989	142560	700	522
40.3±0.8	0.122	85.6	0.05440	0.99988	141480	700	4095
	0.136	11.1	0.05100	0.99989	141480	700	472
44.7±0.7	0.122	85.6	0.05440	0.99988	135600	700	2753
	0.136	11.1	0.05100	0.99989	135600	700	384
48.9±0.7	0.122	85.6	0.05440	0.99988	134460	700	1414
	0.136	11.1	0.05100	0.99989	134460	700	-

Contd.....

Contd..... (Table - 4.7)

52.8±0.7	0.122	85.6	0.05440	0.99988	130440	700	1097
	0.136	11.1	0.05100	0.99989	130440	700	-
56.5±0.6	0.122	85.6	0.05440	0.99988	129240	700	937
	0.136	11.1	0.05100	0.99989	129240	700	-
59.95±0.6	0.122	85.6	0.05440	0.99988	126840	700	809
	0.136	11.1	0.05100	0.99989	126840	700	-

Table - 4.8

Activation cross-sections for the $^{55}Mn(\alpha,2n)^{57}Co$ reaction

E_α (MeV)	Cross-sections (mb) obtained with gamma-rays of		Weighted average cross-section(mb
	0.122 MeV	0.136 MeV	
12.2±1.8	36.37±7.22	-	36.37±7.22
16.2±1.5	583.56±8.89	580.73±44.64	583.45±8.71
19.6±1.3	1012.78±8.59	1035.93±47.46	1013.52±8.45
22.5±1.2	961.01±9.78	913.92±44.64	958.85±9.56
25.2±1.2	870.66±9.57	876.99±44.29	870.94±9.36
27.8±1.1	870.76±9.40	862.55±39.72	870.32±9.15
30.2±1.0	683.90±8.97	676.94±49.56	683.68±8.83
35.5±0.9	200.58±7.56	183.46±39.36	199.97±7.43
40.3±0.8	174.94±7.52	165.89±39.71	174.63±7.39
44.7±0.7	117.59±7.35	134.93±40.41	118.14±7.22
48.9±0.7	60.39±7.35	-	60.39±7.35
52.8±0.7	46.85±7.69	-	46.85±7.69
56.5±0.6	40.01±6.66	-	40.01±6.66
59.95±0.6	34.55±8.71	-	34.55±8.71

and 1.771 MeV at ten incident α-particle energies. The 0.847 MeV photopeak cannot be used in the analysis at energies above the threshold of $^{55}Mn(\alpha,\alpha 3n)^{54}Mn$ reaction, for the gamma ray is also associated with this reaction. The decay scheme of ^{56}Co is shown in Fig. 4.5(c). The experimental data for this reaction are given in Table - 4.9 and the cross-sections obtained with different gamma rays are tabulated in Table - 4.10.

Table - 4.9

Experimental data for $^{55}Mn(\alpha,3n)^{56}Co$ reaction

Half-life of product nucleus = 6804864 sec.

Time of irradiation, t_1 = 3600 sec.

Incident flux, $\bar{\Phi}$ = 1.2326×10^{12} α-particles/cm^2-sec.

Number of target nuclei, N_o = 5.5012×10^{18}

Project. Energy E_α (MeV)	Gamma-Energy E_γ (MeV)	Absol. γ-intens. Θ_γ (%)	Geometry dependent efficien. $\epsilon.G$	γ-self absorp. factor K	Time lapse t_2 (sec)	Record. time t_3 (sec)	Photo peak count (A)
25.2±1.2	0.847	99.9	0.00930	0.99993	145740	700	49
	1.038	13.9	0.00720	0.99995	145740	700	-
	1.238	67.6	0.00580	0.99995	145740	700	39
	1.771	15.7	0.00470	0.99996	145740	700	-
27.8±1.1	0.847	99.9	0.00930	0.99993	144660	700	346
	1.038	13.9	0.00720	0.99995	144660	700	65
	1.238	67.6	0.00580	0.99995	144660	700	215
	1.771	15.7	0.00470	0.99996	144660	700	33

Contd.....

Contd..... (Table - 4.9)

30.2±1.0	0.847	99.9	0.00930	0.99993	143640	700	919
	1.038	13.9	0.00720	0.99995	143640	700	103
	1.238	67.6	0.00580	0.99995	143640	700	400
	1.771	15.7	0.00470	0.99996	143640	700	69
35.5±0.9	0.847	99.9	0.00930	0.99993	142560	700	-
	1.038	13.9	0.00720	0.99995	142560	700	173
	1.238	67.6	0.00580	0.99995	142560	700	675
	1.771	15.7	0.00470	0.99996	142560	700	109
40.3±0.8	0.847	99.9	0.00930	0.99993	141480	700	-
	1.038	13.9	0.00720	0.99995	141480	700	322
	1.238	67.6	0.00580	0.99995	141480	700	1327
	1.771	15.7	0.00470	0.99996	141480	700	209
44.7±0.7	0.847	99.9	0.00930	0.99993	135600	700	-
	1.038	13.9	0.00720	0.99995	135600	700	317
	1.238	67.6	0.00580	0.99995	135600	700	1398
	1.771	15.7	0.00470	0.99996	135600	700	181
48.9±0.7	0.847	99.9	0.00930	0.99993	134460	700	-
	1.038	13.9	0.00720	0.99995	134460	700	158
	1.238	67.6	0.00580	0.99995	134460	700	664
	1.771	15.7	0.00470	0.99996	134460	700	99
52.8±0.7	0.847	99.9	0.00930	0.99993	130440	700	-
	1.038	13.9	0.00720	0.99995	130440	700	141
	1.238	67.6	0.00580	0.99995	130440	700	402
	1.771	15.7	0.00470	0.99996	130440	700	79
56.5±0.6	0.847	99.9	0.00930	0.99993	129240	700	-
	1.038	13.9	0.00720	0.99995	129240	700	-
	1.238	67.6	0.00580	0.99995	129240	700	314
	1.771	15.7	0.00470	0.99996	129240	700	64
59.95±0.6	0.847	99.9	0.00930	0.99993	126840	700	-
	1.038	13.9	0.00720	0.99995	126840	700	-
	1.238	67.6	0.00580	0.99995	126840	700	296
	1.771	15.7	0.00470	0.99996	126840	700	-

Table - 4.10

Activation cross-sections for the $^{55}Mn(\alpha,3n)^{56}Co$ reaction

E_α (MeV)	Cross-sections (mb) with gamma rays of				Weighted average cross-section(mb)
	0.847 MeV	1.038 MeV	1.238 MeV	1.771 MeV	
25.2±1.2	3.08±1.32	-	5.80±3.57	-	3.04±1.24
27.8±1.1	21.71±2.32	37.88±15.15	31.97±4.46	26.00±07.91	24.28±1.98
30.2±1.0	57.67±2.82	60.02±26.22	59.47±5.35	54.54±12.65	57.95±2.44
35.5±0.9	-	100.80±18.64	100.35±5.95	86.15±15.02	98.62±5.30
40.3±0.8	-	187.59±24.47	197.26±7.43	165.17±16.60	191.59±6.54
44.7±0.7	-	184.57±28.53	207.69±8.02	142.96±18.96	197.02±9.28
48.9±0.7	-	91.98±25.62	98.63±8.02	78.18±18.16	95.04±7.05
52.8±0.7	-	82.05±38.41	59.69±7.72	62.36±22.89	60.74±7.19
56.5±0.6	-	-	46.62±9.06	50.52±27.63	46.99±8.61
59.95±0.6	-	-	43.94±11.13	-	43.94±11.13

4.5.1.4 $^{55}Mn(\alpha,4n)$ Reaction

This reaction on manganese having a Q-value of -33.56 MeV, produces unstable ^{55}Co residual nucleus which decays mainly by β^+(77%) and electron capture (23%) with a half-life of 17.74 hours to the excited states of ^{55}Fe (unstable isotope) which itself de-excite with a half-life of 2.7 years by its characteristic gamma rays. The cross-sections for this reaction have been measured at six incident α-particle energies considering the most intense gamma rays viz., 0.477 MeV, 0.932 MeV and 1.409 MeV. The decay scheme of ^{55}Co is shown in Fig. 4.5 (d). The values of the parameters used in the calculation of

cross-sections are given in Table - 4.11. The cross-sections obtained using these parameters are given in Table - 4.12.

Table - 4.11

Experimental data for $^{55}Mn(\alpha,4n)^{55}Co$ reaction

Half-life of product nucleus = 63144 sec.

Time of irradiation, t_1 = 3600 sec.

Incident flux, ϕ = 1.2326×10^{12} α-particles/cm^2-sec.

Number of target nuclei, N_o = 5.5012×10^{18}

Project. Energy E_α (MeV)	Gamma-Energy E_γ (MeV)	Absol. γ-intens. Θ_γ (%)	Geometry dependent efficien. $\epsilon.G$	γ-self absorp. factor K	Time lapse t_2 (sec)	Record. time t_3 (sec)	Photo peak count (A)
40.3±0.8	0.477	20.3	0.01830	0.99992	141480	700	160
	0.932	75.0	0.00820	0.99994	141480	700	227
	1.409	16.5	0.00530	0.99995	141480	700	53
44.7±0.7	0.477	20.3	0.01830	0.99992	135600	700	637
	0.932	75.0	0.00820	0.99994	135600	700	894
	1.409	16.5	0.00530	0.99995	135600	700	133
48.9±0.7	0.477	20.3	0.01830	0.99992	134460	700	1010
	0.932	75.0	0.00820	0.99994	134460	700	1601
	1.409	16.5	0.00530	0.99995	134460	700	234
52.8±0.7	0.477	20.3	0.01830	0.99992	130440	700	1206
	0.932	75.0	0.00820	0.99994	130440	700	1932
	1.409	16.5	0.00530	0.99995	130440	700	310
56.5±0.6	0.477	20.3	0.01830	0.99992	129240	700	1419
	0.932	75.0	0.00820	0.99994	129240	700	2378
	1.409	16.5	0.00530	0.99995	129240	700	350
59.95±0.6	0.477	20.3	0.01830	0.99992	126840	700	1704
	0.932	75.0	0.00820	0.99994	126840	700	2784
	1.409	16.5	0.00530	0.99995	126840	700	389

Table - 4.12

Activation cross-sections for the $^{55}Mn(\alpha,4n)^{55}Co$ reaction

E_α (MeV)	Cross-sections(mb) with gamma rays of			Weighted average cross-section(mb)
	0.477 MeV	0.932 MeV	1.409 MeV	
40.3±0.8	1.11±0.36	0.95±0.12	1.56±0.62	0.99±0.11
44.7±0.7	4.15±0.50	3.52±0.18	3.68±0.80	3.59±0.17
48.9±0.7	6.49±0.57	6.22±0.23	6.39±0.96	6.26±0.21
52.8±0.7	7.42±0.51	7.18±0.29	8.09±1.12	7.28±0.25
56.5±0.6	8.61±0.81	8.72±0.34	9.02±1.16	8.73±0.30
59.95±0.6	10.07±0.61	9.95±0.39	9.76±1.43	9.97±0.32

4.5.1.5 $^{55}Mn(\alpha,\alpha n)$ Reaction

The Q-value for $(\alpha,\alpha n)$ reaction on ^{55}Mn is -10.2 MeV. This reaction produces ^{54}Mn residual nucleus, being unstable and which decays mainly by electron capture with a half-life of 312.2 days to the excited states of ^{54}Cr (stable isotope). This residual nucleus is also produced by $(\alpha,2p3n)$ reaction, the Q-value of this reaction being -38.50 MeV. The experimental cross-sections are solely for the $(\alpha,\alpha n)$ reaction below, the threshold for the $(\alpha,2p3n)$ reaction i.e., 41.3 MeV. The cross-sections for the $(\alpha,\alpha n)$ reaction have been measured at seven incident α-particle energies using the 0.835 MeV gamma ray. The decay scheme of ^{54}Mn is shown in Fig. 4.5(e). The experimental data for this reaction are given in Table - 4.13 and the cross-sections obtained with the gamma ray of 0.835 MeV are tabulated in Table - 4.14.

Table - 4.13

Experimental data for $^{55}Mn(\alpha,\alpha n)^{54}Mn$ reaction

Half-life of product nucleus = 26974080 sec.

Time of irradiation, t_1 = 3600 sec.

Incident flux, ϕ = 1.2326×10^{12} α-particles/cm^2-sec.

Number of target nuclei, N_o = 5.5012×10^{18}

Project. Energy E_α (MeV)	Gamma-Energy E_γ (MeV)	Absol. γ-intens. Θ_γ (%)	Geometry dependent efficien. $\epsilon.G$	γ-self absorp. factor K	Time lapse t_2 (sec)	Record. time t_3 (sec)	Photo peak count (A)
19.6±1.3	0.835	100	0.00950	0.99993	147960	700	93
22.5±1.2	0.835	100	0.00950	0.99993	146820	700	400
25.2±1.2	0.835	100	0.00950	0.99993	145740	700	522
27.8±1.1	0.835	100	0.00950	0.99993	144660	700	749
30.2±1.0	0.835	100	0.00950	0.99993	143640	700	883
35.5±0.9	0.835	100	0.00950	0.99993	142560	700	689
40.3±0.8	0.835	100	0.00950	0.99993	141480	700	706

Table - 4.14

Activation cross-sections for the $^{55}Mn(\alpha,\alpha n)^{54}Mn$ reaction

E_α (MeV)	Cross-sections (mb) with gamma ray of 0.835 MeV
19.6±1.3	22.37±12.99
22.5±1.2	96.20±16.35
25.2±1.2	125.54±12.99
27.8±1.1	180.12±13.95
30.2±1.0	212.34±14.43
35.5±0.9	165.69±13.71
40.3±0.8	169.77±13.95

4.5.1.6 $^{55}Mn(\alpha,2p3n)$ Reaction

The Q-value of $(\alpha,2p3n)$ reaction on ^{55}Mn is -38.50 MeV. This reaction also produces the same ^{54}Mn residual nucleus as produced by $(\alpha,\alpha n)$ reaction. Below the threshold for the $(\alpha,2p3n)$ reaction i.e. 41.3 MeV, the cross-sections are solely for the $(\alpha,\alpha n)$ reaction and above the threshold of $(\alpha,2p3n)$ reaction the cross-sections obtained are the sum of both reactions. The composite cross-section for $(\alpha,\alpha n)$ + $(\alpha,2p3n)$ reactions have been measured at five incident α-particle energies using the 0.835 MeV gamma ray. The decay scheme of ^{54}Mn is shown in Fig. 4.5(e). The experimental data for these reactions are given in Table - 4.15 and the composite cross-sections obtained with the gamma ray of 0.835 MeV are tabulated in Table - 4.16.

4.5.1.7 $^{55}Mn(\alpha,\alpha 3n)$ Reaction

This reaction on manganese having a Q-value of -31.22 MeV, produces two isomers of ^{52}Mn having half-lives of 21.1 minutes and 5.59 days, the latter being the ground state. The metastable state decays independently through (98.25%) with β^+ + EC to the excited states of ^{52}Cr (stable isotope). The ground state also decays through electron capture (72%) and β^+(28%) to the excited states of ^{52}Cr (stable isotope). In the present work, only the cross-sections of the ground state producing reaction have been measured at five incident α-particle energies. The gamma rays of 0.744 MeV, 0.935 MeV and 1.434 MeV obtained

Table - 4.15

Experimental data for $^{55}Mn(\alpha,\alpha n)^{54}Mn$ + $^{55}Mn(\alpha,2p3n)^{54}Mn$ reactions

Half-life of product nucleus = 26974080 sec.

Time of irradiation, t_1 = 3600 sec.

Incident flux, Φ = 1.2326×10^{12} α-particles/cm^2-sec.

Number of target nuclei, N_o = 5.5012×10^{18}

Project. Energy E_α (MeV)	Gamma-Energy E_γ (MeV)	Absol. γ-intens. Θ_γ (%)	Geometry dependent efficien. $\epsilon \cdot G$	γ-self absorp. factor K	Time lapse t_2 (sec)	Record. time t_3 (sec)	Photo peak count (A)
44.7±0.7	0.835	100	0.00950	0.99993	135600	700	596
48.9±0.7	0.835	100	0.00950	0.99993	134460	700	298
52.8±0.7	0.835	100	0.00950	0.99993	130440	700	443
56.5±0.6	0.835	100	0.00950	0.99993	129240	700	495
59.95±0.6	0.835	100	0.00950	0.99993	126840	700	517

Table - 4.16

Activation cross-sections for $^{55}Mn(\alpha,\alpha n)^{54}Mn$ + $^{55}Mn(\alpha,2p3n)^{54}Mn$ reactions

E_α (MeV)	Cross-section(mb) with gamma ray of 0.835 MeV
44.7±0.7	143.30±15.87
48.9±0.7	71.65±14.67
52.8±0.7	106.50±17.31
56.5±0.6	118.99±23.80
59.95±0.6	124.27±24.04

from the decay of ^{52}Mn ground state have been used in the analysis of this reaction. The 0.847 MeV gamma ray emitted from the ground state isomer is common with that of (α,3n) reaction as can be seen from Table - 4.1. The cross-sections for the metastable isomer have not been measured because the half-life of this is very small (21.1 m),while the counting was started after about 35.0 hours. The decay scheme of ^{52}Mn is shown in Fig. 4.5(f). The experimental data for ^{55}Mn(α,α3n) ^{52g}Mn reaction are given in Table - 4.17 and the cross-sections obtained with different gamma rays are tabulated in Table - 4.18.

Table - 4.17

Experimental data for ^{55}Mn(α,α3n)^{52g}Mn reaction

Half-life of product nucleus = 482976 sec.

Time of irradiation, t_1 = 3600 sec.

Incident flux, Φ = 1.2326×10^{12} α-particles/cm^2-sec.

Number of target nuclei, N_o = 5.5012×10^{18}

Project. Energy E_α (MeV)	Gamma-Energy E_γ (MeV)	Absol. γ-intens. Θ_γ (%)	Geometry dependent efficien. ϵ.G	γ-self absorp. factor K	Time lapse t_2 (sec)	Record. time t_3 (sec)	Photo peak count (A)
44.7±0.7	0.744	90.0	0.01120	0.99993	135600	700	277
	0.936	94.5	0.00820	0.99994	135600	700	176
	1.434	100.0	0.00520	0.99995	135600	700	138
48.9±0.7	0.744	90.0	0.01120	0.99993	134460	700	1831
	0.936	94.5	0.00820	0.99994	134460	700	1628
	1.434	100.0	0.00520	0.99995	134460	700	1166

Contd.....

Contd..... (Table - 4.17)

52.8±0.7	0.744	90.0	0.01120	0.99993	130440	700	4286
	0.936	94.5	0.00820	0.99994	130440	700	3458
	1.434	100.0	0.00520	0.99995	130440	700	2643
56.5±0.6	0.744	90.0	0.01120	0.99993	129240	700	7113
	0.936	94.5	0.00820	0.99994	129240	700	6300
	1.434	100.0	0.00520	0.99995	129240	700	4178
59.95±0.6	0.744	90.0	0.01120	0.99993	126840	700	8730
	0.936	94.5	0.00820	0.99994	126840	700	7684
	1.434	100.0	0.00520	0.99995	126840	700	5469

Table - 4.18

Activation cross-sections for the $^{55}Mn(\alpha,\alpha 3n)^{52g}Mn$ reaction

E_α (MeV)	Cross-sections(mb) with gamma rays of			Weighted average cross-section(mb)
	0.477 MeV	0.938 MeV	1.434 MeV	
44.7±0.7	1.37±0.28	1.13±0.33	1.32±0.29	1.28±0.17
48.9±0.7	9.01±0.39	10.42±0.43	11.12±0.47	10.05±0.36
52.8±0.7	20.97±0.51	22.01±0.56	26.07±0.65	22.35±0.67
56.5±0.6	34.74±0.64	40.02±0.74	39.55±0.83	37.67±1.03
59.95±0.6	42.50±0.74	48.65±0.85	51.60±0.95	46.76±1.58

4.5.2. Target Nucleus : $^{63,65}Cu$

Natural copper (abundance, ^{63}Cu = 69.2% and ^{65}Cu = 30.8%) metallic foils of thickness 10.68 mg/cm^2 have been used in the present studies. The stack was made of 12(twelve) copper foils sandwiched between aluminium degraders of thickness 6.75 mg/cm^2. The composition of stack is shown in Fig. 4.2. The target stack was irradiated with a 40 MeV diffused α-beam of diameter 8 mm. The irradiation of the stack was done for 40 minutes with a beam current of ~150 nA. The beam current and total charge collected during irradiation were monitered with the help of the 'Faraday cup' as described in the case of manganese target. The gamma activities of each foil was measured by keeping the foils one by one in the desired geometry. The cross-sections for $^{63}Cu(\alpha,xn)$, x = 1,2 and (α,pn) and $^{65}Cu(\alpha,xn)$, x = 1-3 and $(\alpha,p3n)$ reactions have been measured at twelve incident α-particle energies viz., 16.8 ± 1.6 MeV, 18.8 ± 1.5 MeV, 20.7 ± 1.4 MeV, 22.5 ± 1.3 MeV, 24.3 ± 1.3 MeV, 25.9 ± 1.2 MeV, 27.5 ± 1.2 MeV, 30.1 ± 1.1 MeV, 32.7 ± 1.0 MeV, 35.0 ± 1.0 MeV, 37.3 ± 0.9 MeV and 39.4 ± 0.9 MeV. A typical gamma ray spectrum obtained from the activation of the copper target foil by 18.8 MeV α-particle and taken after about 6 hours from the stop of the irradiation, is shown in Fig. 4.6.

4.5.2.1 $^{63}Cu(\alpha,n)$ Reaction

The Q-value of (α,n) reaction on ^{63}Cu is -7.51 MeV. This reaction produces the ^{66}Ga residual nucleus, which is unstable and decays by β^+(56.5%) and electron capture (43.5%) with a

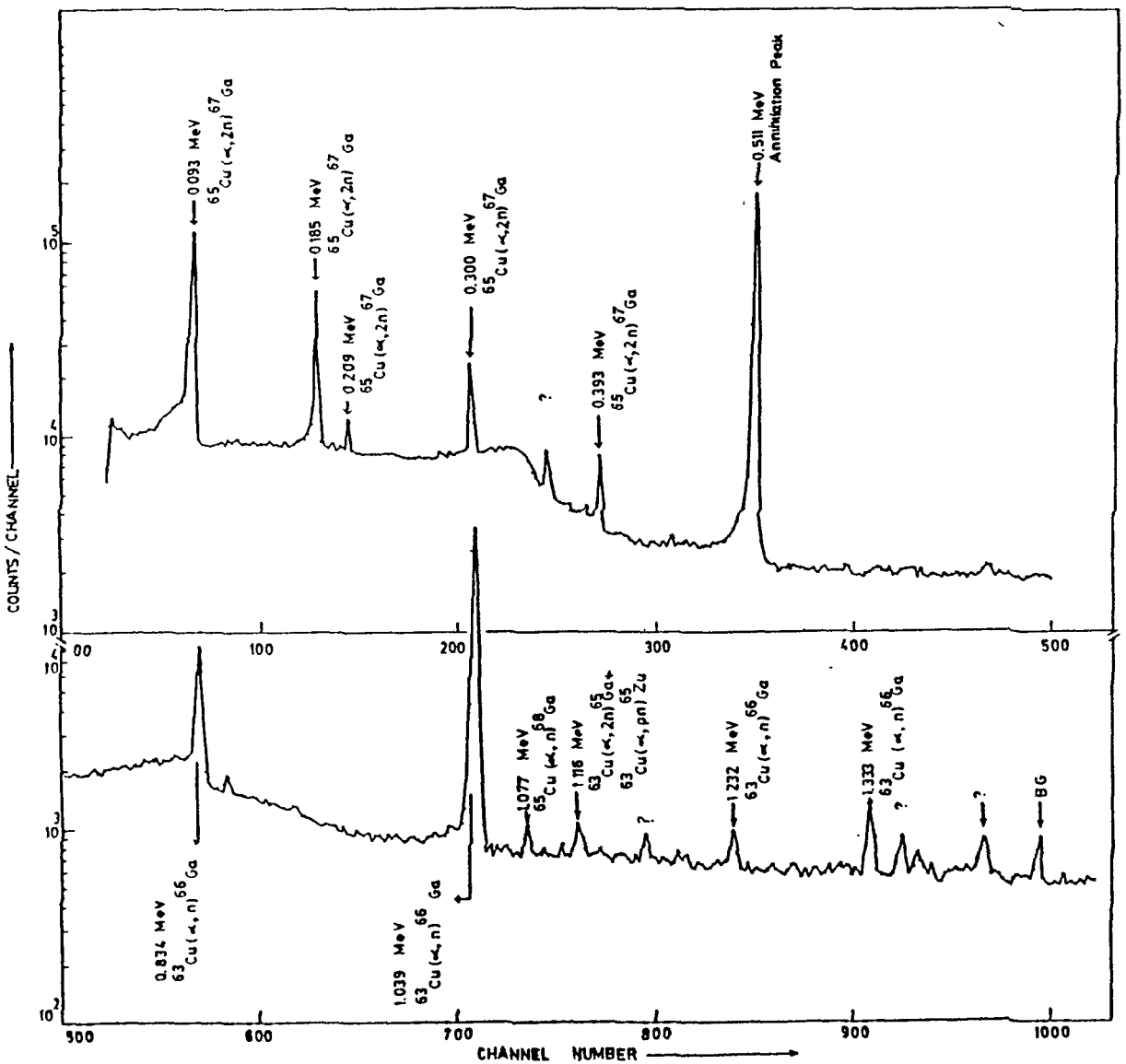

Fig. 4.6 Typical gamma ray spectrum obtained from the activation of $^{63,65}Cu$ target by 18.8 MeV α-particles.

half-life of 9.45 hours to the excited states of ^{66}Zn (stable isotope). Since the target foil was natural copper, the same residual nucleus ^{66}Ga is also produced by $^{65}Cu(\alpha,3n)$ reaction. Thus, the cross-sections are solely for the $^{63}Cu(\alpha,n)$ reaction below the threshold energy of the $^{65}Cu(\alpha,3n)$ reaction. The reaction cross-sections have been studied by considering the gamma rays of 0.834 MeV and 1.039 MeV obtained from the decay of ^{66}Ga. The cross-sections below the threshold of $^{65}Cu(\alpha,3n)$ reaction have been measured at seven incident α-particle energies. The decay scheme of ^{66}Ga is shown in Fig. 4.7(a). The experimental data required for the calculation of the cross-sections are given in Table - 4.19. The cross-sections obtained using these values are given in Table - 4.20.

Above the threshold energy of $^{65}Cu(\alpha,3n)$ reaction the cross-sections obtained are the sum of $^{63}Cu(\alpha,n)$ and $^{65}Cu(\alpha,3n)$ reactions. The composite cross-sections for (α,n) and $(\alpha,3n)$ reactions have been measured at five alpha particle energies. The experimental data for these reactions are given in Table - 4.21 and the cross-sections obtained with different gamma rays are given in Table - 4.22.

The contributions of (α,n) and $(\alpha,3n)$ reactions have been separated in such a manner that the measured cross-sections for (α,n) reaction below $(\alpha,3n)$ reaction threshold energy have been reproduced from theoretical calculations. The theoretical (α,n) cross-sections were further extrapolated and its contribution was subtracted to get the counts for the $(\alpha,3n)$ reaction. The

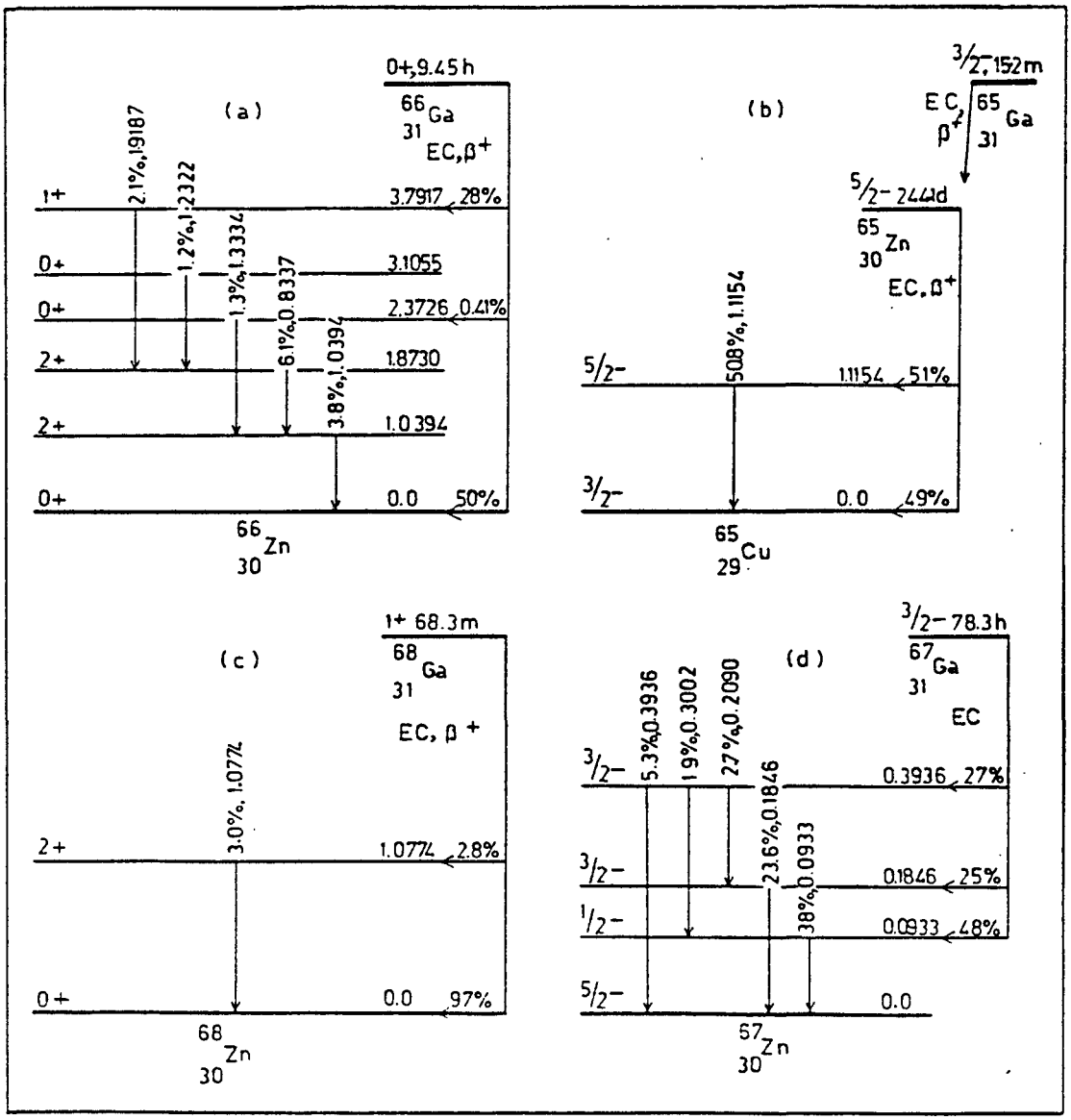

Fig. 4.7 Partial decay schemes for isotopes ^{66}Ga, ^{65}Ga, ^{68}Ga and ^{67}Ga formed in alpha induced reactions on $^{63,65}Cu$.

separated counts of (α,n) reaction above the threshold of (α,3n) reaction alongwith the other experimental data are given in Table - 4.23 and the cross-sections obtained with different gamma rays are tabulated in Table - 4.24.

Table - 4.19

Experimental data for $^{63}Cu(\alpha,n)^{66}Ga$ reaction

Half-life of product nucleus = 34020 sec.
Time of irradiation, t_1 = 1800 sec.
Incident flux, Φ = 8.3143×10^{11} α-particles/cm^2-sec.
Number of target nuclei, N_o = 3.5497×10^{19}

Project. Energy - E_α (MeV)	Gamma-Energy E_γ (MeV)	Absol. γ-intens. Θ_γ (%)	Geometry dependent efficien. $\epsilon.G$	γ-self absorp. factor K	Time lapse t_2 (sec)	Record. time t_3 (sec)	Photo peak count (A)
16.8±1.6	0.834	6.1	0.00815	0.99962	20820	500	60640
	1.039	38.0	0.00611	0.99968	20820	500	263876
18.8±1.5	0.834	6.1	0.00815	0.99962	22980	500	33772
	1.039	38.0	0.00611	0.99968	22980	500	147700
20.7±1.4	0.834	6.1	0.00815	0.99962	24420	500	35328
	1.039	38.0	0.00611	0.99968	24420	500	154567
22.5±1.3	0.834	6.1	0.00815	0.99962	25860	500	23348
	1.039	38.0	0.00611	0.99968	25860	500	101468
24.3±1.3	0.834	6.1	0.00815	0.99962	27180	500	13680
	1.039	38.0	0.00611	0.99968	27180	500	58820
25.9±1.2	0.834	6.1	0.00815	0.99962	28440	500	7742
	1.039	38.0	0.00611	0.99968	28440	500	36138
27.5±1.2	0.834	6.1	0.00815	0.99962	29700	500	5351
	1.039	38.0	0.00611	0.99968	29700	500	23824

Table - 4.20

Activation cross-sections for the $^{63}Cu(\alpha,n)^{66}Ga$ reaction

E_α (MeV)	Cross-sections (mb) obtained with gamma-rays of		Weighted average cross-section(mb)
	0.834 MeV	1.039 MeV	
16.8±1.6	352.78±3.50	328.70±0.83	329.97±3.80
18.8±1.5	205.31±2.69	192.26±0.58	192.84±1.90
20.7±1.4	221.16±2.84	207.19±0.57	207.72±1.90
22.5±1.3	150.52±2.39	140.06±0.52	140.54±1.54
24.3±1.3	90.59±1.87	83.41±0.41	83.73±1.06
25.9±1.2	52.60±1.52	52.57±0.33	52.58±0.33
27.5±1.2	37.30±1.28	35.56±0.28	35.64±0.27

Table - 4.21

Experimental data for $^{63}Cu(\alpha,n)^{66}Ga$+$^{65}Cu(\alpha,3n)^{66}Ga$ reactions

Half-life of product nucleus= 34020 sec.

Time of irradiation, t_1 = 1800 sec

Incident flux, ϕ = 8.3143×10^{11} α-part./cm^2-sec.

Number of target nuclei, N_o = 1.5313×10^{19}

Project. Energy E_α (MeV)	Gamma-Energy E_γ (MeV)	Absol. γ-intens. θ_γ (%)	Geometry dependent efficien. ϵ.G	γ-self absorp. factor K	Time lapse t_2 (sec)	Record. time t_3 (sec)	Photo peak count (A)
30.1±1.1	0.834	6.1	0.00815	0.99962	30900	500	3164
	1.039	38.0	0.00611	0.99968	30900	500	14970
32.7±1.0	0.834	6.1	0.00815	0.99962	32220	500	4803
	1.039	38.0	0.00611	0.99968	32220	500	19747
35.0±1.0	0.834	6.1	0.00815	0.99962	33660	500	7184
	1.039	38.0	0.00611	0.99968	33660	500	30434
37.3±0.9	0.834	6.1	0.00815	0.99962	34980	500	10087
	1.039	38.0	0.00611	0.99968	34980	500	44062
39.4±0.9	0.834	6.1	0.00815	0.99962	36180	500	12005
	1.039	38.0	0.00611	0.99968	36180	500	52803

Table - 4.22

Activation cross-sections for $^{63}Cu(\alpha,n)^{66}Ga$ + $^{65}Cu(\alpha,3n)^{66}Ga$ reactions

E_α (MeV)	Cross-sections (mb) obtained with gamma-rays of		Weighted average cross-section(mb)
	0.834 MeV	1.039 MeV	
30.1±1.1	52.39±2.50	53.08±2.50	53.05±0.52
32.7±1.0	81.70±2.82	71.91±0.62	72.36±1.45
35.0±1.0	125.84±3.63	114.15±0.80	114.69±1.73
37.3±0.9	181.51±4.41	169.77±0.97	170.32±1.75
39.4±0.9	221.37±4.92	208.49±1.09	209.80±1.92

Table - 4.23

Experimental data for $^{63}Cu(\alpha,n)^{66}Ga$ reaction (Above 30.1 MeV)

Half-life of product nucleus = 34020 sec.
Time of irradiation, t_1 = 1800 sec.
Incident flux, Φ = 8.3143×10^{11} α-part./cm^2-sec
Number of target nuclei, N_o = 3.5497×10^{19}

Project. Energy E_α (MeV)	Gamma-Energy E_γ (MeV)	Absol. γ-intens. Θ_γ (%)	Geometry dependent efficien. ϵ.G	γ-self absorp. factor K	Time lapse t_2 (sec)	Record. time t_3 (sec)	Photo peak count (A)
30.1±1.1	0.834	6.1	0.00815	0.99962	30900	500	3008
	1.039	38.0	0.00611	0.99968	30900	500	14028
32.7±1.0	0.834	6.1	0.00815	0.99962	32220	500	2014
	1.039	38.0	0.00611	0.99968	32220	500	9395
35.0±1.0	0.834	6.1	0.00815	0.99962	33660	500	1484
	1.039	38.0	0.00611	0.99968	33660	500	6922
37.3±0.9	0.834	6.1	0.00815	0.99962	34980	500	1116
	1.039	38.0	0.00611	0.99968	34980	500	5207
39.4±0.9	0.834	6.1	0.00815	0.99962	36180	500	859
	1.039	38.0	0.00611	0.99968	36180	500	4005

Table - 4.24

Activation cross-sections for the $^{63}Cu(\alpha,n)^{66}Ga$ reaction (Above 30.1 MeV)

E_α (MeV)	Cross-sections (mb) with gamma-rays of		Weighted average cross-section (mb)
	0.834 MeV	1.039 MeV	
30.1±1.1	21.49±1.03	21.46±0.22	21.46±0.21
32.7±1.0	14.78±0.51	14.76±0.13	14.76±0.12
35.0±1.0	11.21±0.32	11.20±0.08	11.20±0.08
37.3±0.9	8.66±0.21	8.65±0.05	8.66±0.05
39.4±0.9	6.83±0.15	6.82±0.04	6.82±0.04

4.5.2.2 $^{63}Cu(\alpha,2n)$ and $^{63}Cu(\alpha,pn)$ Reactions

The Q-values for $(\alpha,2n)$ and (α,pn) reactions on ^{63}Cu are -16.65 MeV and -12.59 MeV respectively. The $(\alpha,2n)$ reaction produces an unstable ^{65}Ga residual nucleus, which decays by β^+(86%) and electron capture (14%) with a half-life of 15.2 minutes to the excited states of ^{65}Zn (unstable isotope) which itself de-excite with a half-life of 244.02 days by its characteristic gamma rays. In the present measurements, there was a time gap of about 6.0 hours between the stop of irradiation and the start of counting. Thus, the 15.2 minutes half-life due to $(\alpha,2n)$ reaction could not be observed. The half-life of 244.02 days was followed and therefore, the measured cross-sections are the cumulative sum of both the reactions. The cross-sections have been studied by considering the gamma ray of

1.116 MeV obtained from the decay of ^{65}Zn. The cross-sections have been measured at twelve incident α-particle energies. The decay scheme of ^{65}Ga and ^{65}Zn are given in Fig. 4.7(b). The experimental data required in the calculation of the cross-sections are given in Table - 4.25. The cross-sections obtained using these values are given in Table - 4.26.

Table - 4.25

Experimental data for $^{63}Cu(\alpha,2n)^{65}Ga + ^{63}Cu(\alpha,pn)^{65}Zn$ reactions

Half-life of product nucleus = 21083328 sec.

Time of irradiation, t_1 = 1800 sec.

Incident flux, Φ = 8.3143×10^{11} α-particles/cm^2-sec.

Number of target nuclei, N_o = 3.5497×10^{19}

Project. Energy E_α (MeV)	Gamma-Energy E_γ (MeV)	Absol. γ-intens. Θ_γ (%)	Geometry dependent efficien. $\epsilon.G$	γ-self absorp. factor K	Time lapse t_2 (sec)	Record. time t_3 (sec)	Photo peak count (A)
16.8±1.6	1.116	50.8	0.00542	0.99968	20820	500	552
18.8±1.5	1.116	50.8	0.00542	0.99968	22980	500	600
20.7±1.4	1.116	50.8	0.00542	0.99968	24420	500	874
22.5±1.3	1.116	50.8	0.00542	0.99968	25860	500	1242
24.3±1.3	1.116	50.8	0.00542	0.99968	27180	500	2242
25.9±1.2	1.116	50.8	0.00542	0.99968	28840	500	2642
27.5±1.2	1.116	50.8	0.00542	0.99968	29700	500	2168
30.1±1.1	1.116	50.8	0.00542	0.99968	30900	500	1838
32.7±1.0	1.116	50.8	0.00542	0.99968	32200	500	1596
35.0±1.0	1.116	50.8	0.00542	0.99968	33660	500	-
37.3±0.9	1.116	50.8	0.00542	0.99968	34980	500	-
39.4±0.9	1.116	50.8	0.00542	0.99968	36180	500	1284

Table - 4.26

Activation cross-sections for $^{63}Cu(\alpha,2n)^{65}Ga$ + $^{63}Cu(\alpha,pn)^{65}Zn$ reactions

E_α (MeV)	Cross-section(mb) with gamma ray of 1.116 MeV
16.8±1.6	229.56±83.17
18.8±1.5	249.53±63.22
20.7±1.4	363.50±63.63
22.5±1.3	516.58±54.07
24.3±1.3	932.54±78.61
25.9±1.2	1098.97±62.39
27.5±1.2	901.84±54.08
30.1±1.1	764.60±45.76
32.7±1.0	663.95±50.34
35.0±1.0	-
37.3±0.9	-
39.4±0.9	534.23±74.39

4.5.2.3 $^{65}Cu(\alpha,n)$ Reaction

The Q-value of this reaction is -5.83 MeV. This reaction produces ^{68}Ga residual nucleus (unstable) which decays by β^+(90%) and electron capture (10%) with a half-life of 68.33 minutes to the excited states of ^{68}Zn (stable isotope). The reaction has been studied by considering the intense gamma ray of 1.077 MeV. The cross-sections have been measured at four α-particle energies. The decay scheme of ^{68}Ga is shown in Fig. 4.7(c). The values of the parameters used in the calculation of cross-sections

are given in Table - 4.27. The cross-sections obtained using these parameters are given in Table - 4.28.

Table - 4.27

Experimental data for $^{65}Cu(\alpha,n)^{68}Ga$ reactions

Half-life of product nucleus = 4099 sec.

Time of irradiation, t_1 = 1800 sec.

Incident flux, Φ = 8.3143×10^{11} α-particles/cm^2-sec.

Number of target nuclei, N_o = 1.5313×10^{19}

Project. Energy E_α (MeV)	Gamma-Energy E_γ (MeV)	Absol. γ-intens. Θ_γ (%)	Geometry dependent efficien. ϵ.G	γ-self absorp. factor K	Time lapse t_2 (sec)	Record. time t_3 (sec)	Photo peak count (A)
16.8±1.6	1.077	3.0	0.00560	0.99968	20820	500	4429
18.8±1.5	1.077	3.0	0.00560	0.99968	22980	500	1807
20.7±1.4	1.077	3.0	0.00560	0.99968	24420	500	1124
22.5±1.3	1.077	3.0	0.00560	0.99968	25860	500	743

Table - 4.28

Activation cross-sections for the $^{65}Cu(\alpha,n)^{68}Ga$ reaction

E_α (MeV)	Cross-sections(mb) with gamma ray of 1.077 MeV
16.6±1.6	556.27±43.08
18.8±1.5	326.99±44.15
20.7±1.4	256.46±58.40
22.5±1.3	218.79±59.77

4.5.2.4 $^{65}Cu(\alpha,2n)$ Reaction

This reaction on ^{65}Cu having a Q-value of -14.12 MeV, produces unstable ^{67}Ga residual nucleus, and which decays mainly by electron capture with a half-life of 78.26 hours to the excited states of ^{66}Zn (stable isotope). The gamma rays of 0.093 MeV, 0.185 MeV and 0.300 MeV obtained from the decay of ^{67}Ga have been considered in the analysis of $(\alpha,2n)$ reaction cross-sections. The cross-sections for this reaction have been measured at twelve incident α-particle energies. The decay scheme of ^{67}Ga is shown in Fig. 4.7(d). The experimental data required in the calculation of cross-sections are given in Table - 4.29. The cross-sections obtained using these values are given in Table - 4.30.

Table - 4.29

Experimental data for $^{65}Cu(\alpha,2n)^{67}Ga$ reaction

Half-life of product nucleus = 281736 sec.

Time of irradiation, t_1 = 1800 sec.

Incident flux, ϕ = 8.3143×10^{11} α-particles/cm^2-sec.

Number of target nuclei, N_o = 1.5313×10^{19}

Project. Energy E_α (MeV)	Gamma-Energy E_γ (MeV)	Absol. γ-intens. θ_γ (%)	Geometry dependent efficien. $\epsilon.G$	γ-self absorp. factor K	Time lapse t_2 (sec)	Record. time t_3 (sec)	Photo peak count (A)
16.8±1.6	0.093	38.0	0.03970	0.99838	20820	500	23260
	0.185	23.6	0.02900	0.99915	20820	500	10215
	0.300	19.0	0.02170	0.99945	20820	500	7523

Contd.....

Contd..... (Table - 4.29)

18.6±1.5	0.093	38.0	0.03970	0.99838	22980	500	84740
	0.185	23.6	0.02900	0.99915	22980	500	41476
	0.300	19.0	0.02170	0.99945	22980	500	26358
20.7±1.4	0.093	38.0	0.03970	0.99838	24420	500	165024
	0.185	23.6	0.02900	0.99915	24420	500	80637
	0.300	19.0	0.02170	0.99945	24420	500	51244
22.5±1.3	0.093	38.0	0.03970	0.99838	25860	500	202022
	0.185	23.6	0.02900	0.99915	25860	500	98716
	0.300	19.0	0.02170	0.99945	25860	500	62733
24.3±1.3	0.093	38.0	0.03970	0.99838	27180	500	211424
	0.185	23.6	0.02900	0.99915	27180	500	103310
	0.300	19.0	0.02170	0.99945	27180	500	65653
25.9±1.2	0.093	38.0	0.03970	0.99838	28440	500	223922
	0.185	23.6	0.02900	0.99915	28440	500	109417
	0.300	19.0	0.02170	0.99945	28440	500	69534
27.5±1.2	0.093	38.0	0.03970	0.99838	29700	500	221383
	0.185	23.6	0.02900	0.99915	29700	500	108176
	0.300	19.0	0.02170	0.99945	29700	500	68745
30.1±1.1	0.093	38.0	0.03970	0.99838	30900	500	203300
	0.185	23.6	0.02900	0.99915	20900	500	99340
	0.300	19.0	0.02170	0.99945	30900	500	63129
32.7±1.0	0.093	38.0	0.03970	0.99838	32220	500	183234
	0.185	23.6	0.02900	0.99915	32220	500	82673
	0.300	19.0	0.02170	0.99945	32220	500	52538
35.0±1.0	0.093	38.0	0.03970	0.99838	33660	500	125711
	0.185	23.6	0.02900	0.99915	33660	500	61427
	0.300	19.0	0.02170	0.99945	33660	500	39036
37.3±0.9	0.093	38.0	0.03970	0.99838	34980	500	102557
	0.185	23.6	0.02900	0.99915	34980	500	50113
	0.300	19.0	0.02170	0.99945	34980	500	31846
39.4±0.9	0.093	38.0	0.03970	0.99838	36180	500	72305
	0.185	23.6	0.02900	0.99915	36180	500	35331
	0.300	19.0	0.02170	0.99945	36180	500	22453

Table - 4.30

Activation cross-sections for the $^{65}Cu(\alpha,2n)^{67}Ga$ reaction

E_α (MeV)	Cross-sections(mb) with gamma rays of			Weighted average cross-section(mb)
	0.093 MeV	0.185 MeV	0.300 MeV	
16.8±1.6	37.83±2.13	55.94±4.69	68.40±6.62	58.37±1.86
18.8±1.5	211.82±2.44	228.35±5.13	240.82±7.42	216.97±3.83
20.7±1.4	413.97±3.03	445.53±6.23	469.86±9.09	424.18±7.44
22.5±1.3	508.57±2.48	547.35±5.35	577.24±7.78	520.22±8.90
24.3±1.3	533.97±2.05	574.69±4.52	606.08±6.59	545.76±9.21
25.9±1.2	567.29±1.80	610.55±4.06	643.90±5.94	579.33±9.64
27.5±1.2	562.60±1.64	605.50±3.76	638.57±6.04	573.48±9.08
30.1±1.1	518.18±1.50	557.68±3.47	588.13±5.10	528.71±8.66
32.7±1.0	468.55±1.55	465.63±3.50	491.06±5.12	469.70±2.44
35.0±1.0	322.60±1.71	347.19±3.74	366.15±6.24	329.14±5.26
37.3±0.9	264.04±1.89	284.17±4.07	299.68±5.90	270.13±4.63
39.4±0.9	186.70±2.03	200.94±4.29	211.91±6.22	191.11±3.30

4.5.2.5 $^{65}Cu(\alpha,3n)$ Reaction

The Q-value for $(\alpha,3n)$ reaction on ^{65}Cu is -25.33 MeV. This reaction also produces the same residual nucleus ^{66}Ga as was produced by $^{63}Cu(\alpha,n)$ reaction. The decay scheme of ^{66}Ga is shown in Fig. 4.7(a). The separated counts of $(\alpha,3n)$ reaction alongwith the other experimental data are given in Table - 4.31. The cross-sections obtained with different gamma rays at five α-particle energies are tabulated in Table - 4.32.

Table - 4.31

Experimental data for $^{65}Cu(\alpha,3n)^{66}Ga$ reaction

Half-life of product nucleus = 34020 sec.

Time of irradiation, t_1 = 1800 sec.

Incident flux, $\bar{\Phi}$ = 8.3143×10^{11} α-particles/cm^2-sec.

Number of target nuclei N_o = 1.5313×10^{19}

Project. Energy E_α (MeV)	Gamma-Energy E_γ (MeV)	Absol. γ-intens. Θ_γ (%)	Geometry dependent efficien. $\epsilon.G$	γ-self absorp. factor K	Time lapse t_2 (sec)	Record. time t_3 (sec)	Photo peak count (A)
30.1±1.1	0.834	6.1	0.00815	0.99962	30900	500	156
	1.039	38.0	0.00611	0.99968	30900	500	942
32.7±1.0	0.834	6.1	0.00815	0.99962	32220	500	2789
	1.039	38.0	0.00611	0.99968	32220	500	10348
35.0±1.0	0.834	6.1	0.00815	0.99962	33660	500	5700
	1.039	38.0	0.00611	0.99968	33660	500	23512
37.3±0.9	0.834	6.1	0.00815	0.99962	34980	500	8971
	1.039	38.0	0.00611	0.99968	34980	500	38855
39.4±0.9	0.834	6.1	0.00815	0.99962	36180	500	11146
	1.039	38.0	0.00611	0.99968	36180	500	48798

Table - 4.32

Activation cross-sections for the $^{65}Cu(\alpha,3n)^{66}Ga$ reaction

E_α (MeV)	Cross-sections(mb) with gamma rays		Weighted average cross-section (mb)
	0.834 MeV	1.039 MeV	
30.1±1.1	2.58±0.12	3.34±0.04	3.28±0.15
32.7±1.0	47.44±1.63	37.69±0.32	38.06±1.32
35.0±1.0	99.85±2.87	88.19±0.62	88.70±1.69
37.3±0.9	161.43±3.92	149.71±0.86	150.25±1.73
39.4±0.9	205.53±4.57	192.67±1.00	193.26±1.90

4.5.3 Target Nucleus : $^{69,71}Ga$

Natural specpure gallium oxide (natural abundance, ^{69}Ga = 60.1% and ^{71}Ga = 39.9%) has been used for the preparation of target foils. Gallium oxide of thickness 0.9 mg/cm^2 was deposited onto aluminium backing of thickness 6.75 mg/cm^2 by vacuum evaporation technique. The stack was made of fiteen (15) target foils sandwiched between aluminium degraders of thickness 20.87 mg/cm^2 and 6.75 mg/cm^2 is shown in Fig. 4.2. The target stack was irradiated to 60 MeV α-particle beam diffused to 8 mm diameter. The irradiation of the stack was done for 45 minutes. The α-beam current was $\backsim$ 100 nA. The beam current was monitored by 'Faraday-cup' by charge collection method, kept just behind the target foils. The cross-sections for the $^{69}Ga(\alpha,xn)$, x = 1-3 and $(\alpha,p3n)$ and $^{71}Ga(\alpha,n)$ and $^{71}Ga(\alpha,4n)$ reactions have been measured at fourteen different incident α-particle energies viz., 9.7 ± 2.0 MeV, 14.1 ± 1.6 MeV, 17.8 ± 1.3 MeV, 21.1 ± 1.2 MeV, 24.0 ± 1.1 MeV, 26.7 ± 1.0 MeV, 29.2 ± 0.9 MeV, 34.6 ± 0.8 MeV, 39.5 ± 0.8 MeV, 44.0 ± 0.7 MeV, 48.2 ± 0.7 MeV, 52.2 ± 0.6 MeV, 55.9 ± 0.6 MeV and 59.5 ± 0.6 MeV. A typical gamma ray spectrum obtained from the activation of gallium target foil by 24.0 MeV α-particles taken after about 13.0 hours from the stop of the irradiation is shown in Fig. 4.8.

4.5.3.1 $^{69}Ga(\alpha,n)$ Reaction

The Q-value for (α,n) reaction on ^{69}Ga is -6.74 MeV. This reaction produces ^{72}As residual nucleus, which is unstable

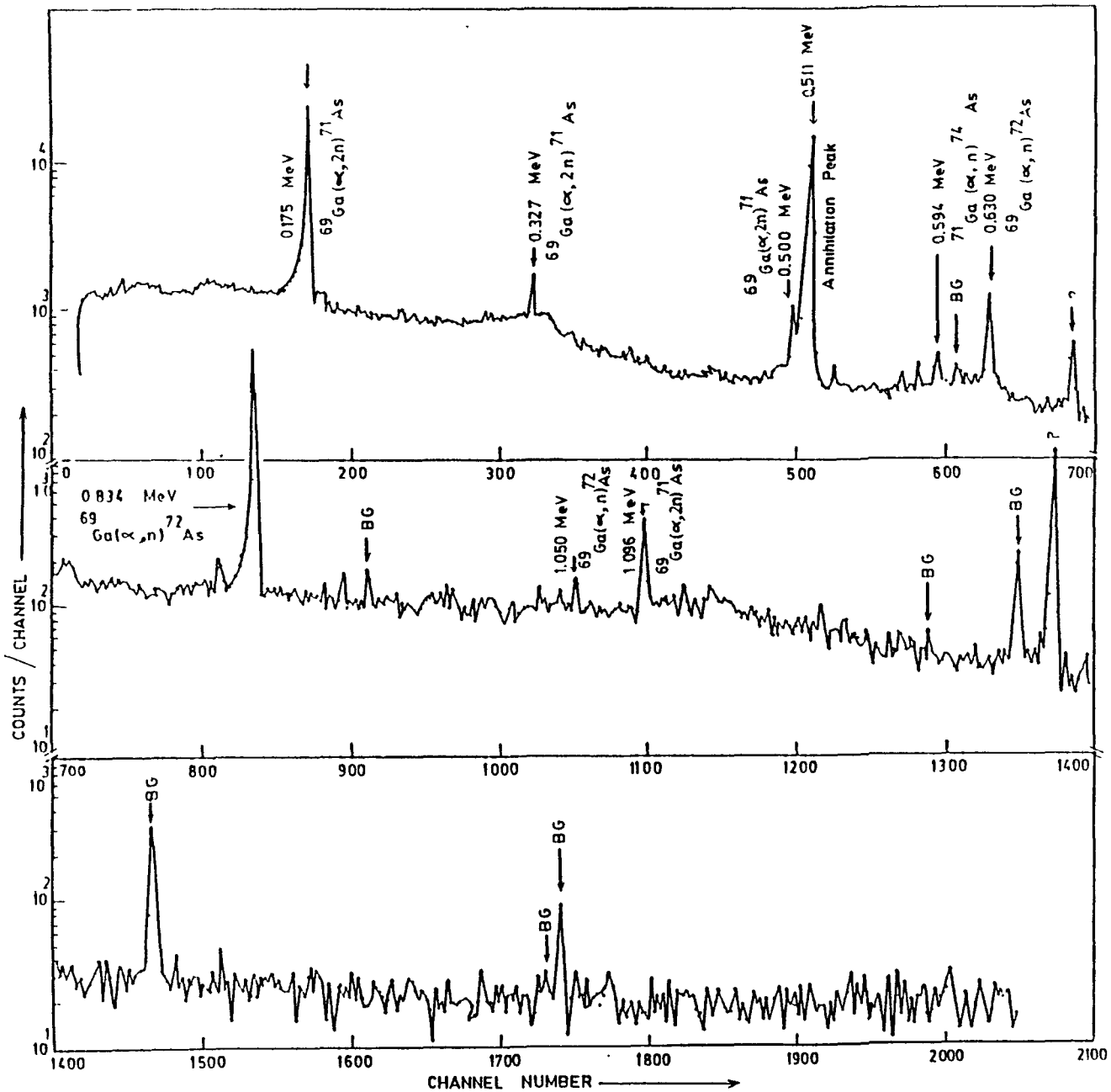

Fig. 4.8 Typical gamma ray spectrum obtained from the activation of ^{69,71}Ga target by 24.0 MeV α-particles.

and decays by β^+(77%) and electron capture (23%) with a half-life of 26.0 hours to the excited states of ^{72}Ge (stable isotope). The decay scheme of ^{72}As is shown in Fig. 4.9(a). The cross-sections for this reaction have been studied only upto 21.1 MeV α-particle energy because above this energy three more reactions i.e., ^{69}Ga(α,α3n), ^{71}Ga(α,3n) and ^{71}Ga(α,2pn) are occuring at the same time and decays with the same gamma rays i.e., 0.630 MeV and 0.834 MeV as was obtained in the ^{69}Ga(α,n) reaction. The details of gamma rays and Q-values etc. are given in Table - 4.3. Thus, the cross-sections for (α,n) reaction have been measured at four incident α-particle energies using 0.630 MeV and 0.834 MeV gamma rays from threshold to 21.1 MeV. The experimental data for this reaction are given in Table - 4.33 and the cross-sections obtained with the different gamma rays are tabulated in Table - 4.34.

4.5.3.2 ^{69}Ga(α,2n) Reaction

The Q-value of (α,2n) reaction on ^{69}Ga is -15.15 MeV. This reaction produces the ^{71}As residual nucleus, which is unstable and decays by electron capture (68%) and β^+(32%) with a half-life of 61.0 hours to the excited states of ^{71}Ge (unstable isotope) which itself deexcite with a half-life of 11.2 days by its characteristic gamma rays. The decay scheme of ^{71}As is shown in Fig. 4.9(b). Since the target foil was natural gallium, the same residual nucleus ^{71}As is also produced by ^{71}Ga(α,4n) reaction. Therefore, the cross-sections are solely for the

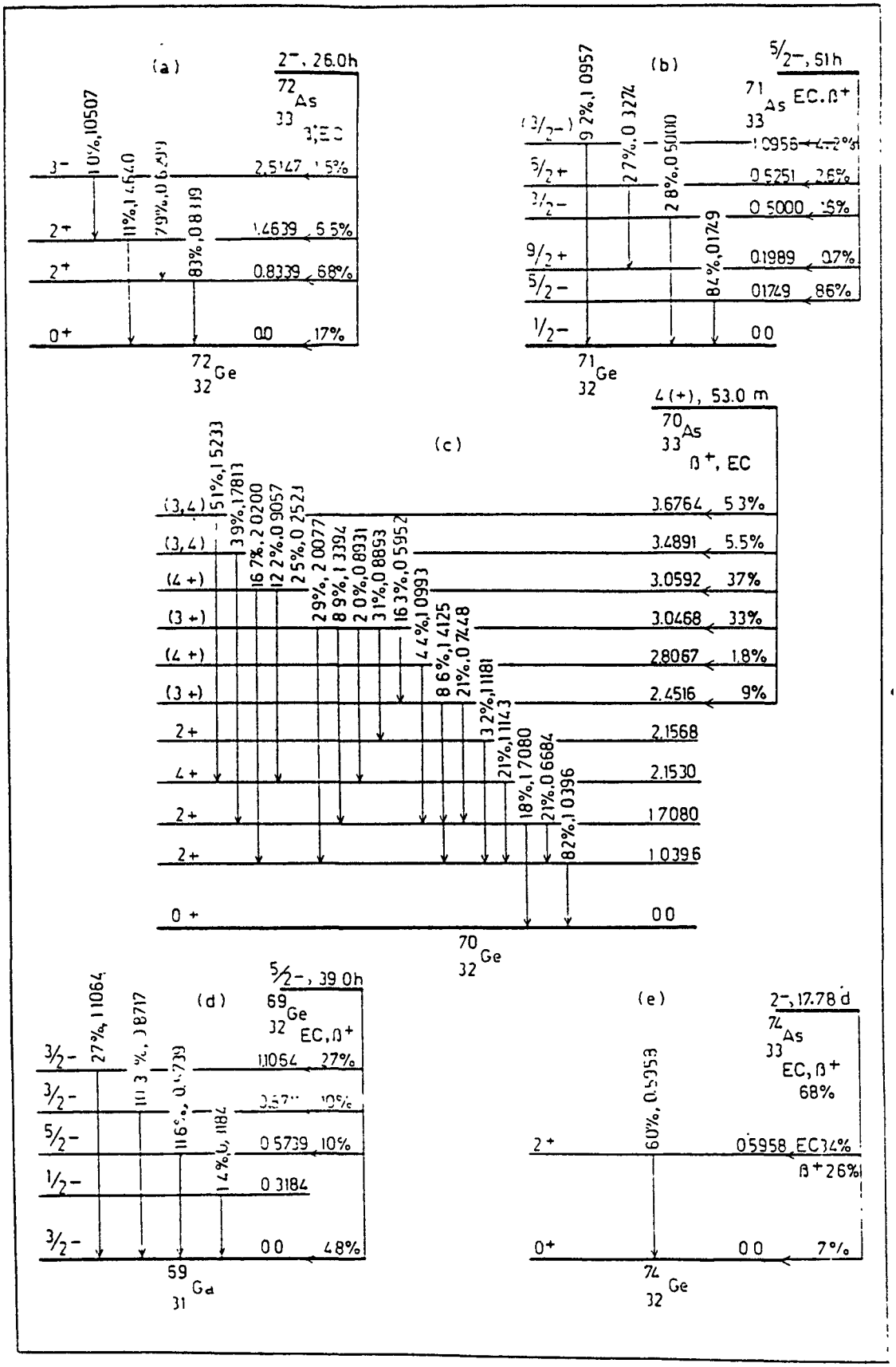

Fig. 4.9 Partial decay schemes for isotopes ^{72}As, ^{71}As, ^{70}As, ^{69}Ge and ^{74}As formed in alpha induced reactions on $^{69,71}Ga$.

Table - 4.33

Experimental data for $^{69}Ga(\alpha,n)^{72}As$ reaction

Half-life of product nucleus = 93636 sec.

Time of irradiation, t_1 = 2700 sec.

Incident flux, Φ = 5.9667×10^{11} α-particles/cm^2-sec.

Number of target nuclei, N_o = 1.7648×10^{18}

Project. Energy E_α (MeV)	Gamma-Energy E_γ (MeV)	Absol. γ-intens. Θ_γ (%)	Geometry dependent efficien. $\epsilon \cdot G$	γ-self absorp. factor K	Time lapse t_2 (sec)	Record. time t_3 (sec)	Photo peak count (A)
9.7±2.0	0.630	7.9	0.01400	0.99993	59400	500	217
	0.834	80.0	0.00950	0.99994	59400	500	1108
14.1±1.6	0.630	7.9	0.01400	0.99993	57180	500	3284
	0.834	80.0	0.00950	0.99994	57180	500	22637
17.8±1.3	0.630	7.9	0.01400	0.99993	55020	500	5383
	0.834	80.0	0.00950	0.99994	55020	500	38848
21.1±1.2	0.630	7.9	0.01400	0.99993	52680	500	4077
	0.834	80.0	0.00950	0.99994	52680	500	30961

Table - 4.34

Activation cross-sections for the $^{69}Ga(\alpha,n)^{72}As$ reaction

E_α (MeV)	Cross-sections(mb) with gamma rays of		weighted average cross-section (mb)
	0.630 MeV	0.834 MeV	
9.7±2.0	29.29±6.21	21.77±1.02	21.96±1.01
14.1±1.6	435.98±15.00	437.55±3.52	437.47±3.43
17.8±1.3	709.31±19.73	738.98±4.49	737.22±5.46
21.1±1.2	523.53±17.34	578.84±3.87	576.21±8.32

(α,2n) reaction below the threshold energy of (α,4n) reaction. Below the threshold of (α,4n) reaction, cross-sections have been measured at six α-particle energies by considering the gamma rays of 0.175 MeV and 1.096 MeV. The values of parameters used in the calculation of cross-sections are given in Table - 4.35. The cross-sections obtained using these parameters are shown in Table - 4.36.

Above the threshold energy of (α,4n) reaction the cross-sections obtained are the sum of (α,2n) and (α,4n) reactions. The composite cross-sections for (α,2n) and (α,4n) reactions have been measured at six α-particle incident energies. Values of the parameters required in the calculation of the cross-sections are given in Table - 4.37. The cross-sections obtained using these values are given in Table - 4.38.

The contributions of (α,2n) and (α,4n) reactions have been separated as was done in the case of $^{63}Cu(\alpha,n)$ and $^{65}Cu(\alpha,3n)$ reactions. The separated counts of (α,2n) reaction above the threshold of (α,4n) reaction alongwith the other experimental data are given in Table - 4.39 and the cross-sections obtained using these values are tabulated in Table - 4.40.

4.5.3.3 $^{69}Ga(\alpha,3n)$ Reaction

This reaction on ^{69}Ga, Q-value of -26.77 MeV, produces ^{70}As residual nucleus, which is unstable and decays by β^+(84%) and electron capture (16%) with a half-life of 53.0 minutes to

Table - 4.35

Experimental data for $^{69}Ga(\alpha,2n)^{71}As$ reaction(Below 39.5 MeV)

Half-life of product nucleus = 219600 sec.

Time of irradiation, t_1 = 2700 sec.

Incident flux, ϕ = 5.9667×10^{11} α-particles/cm^2-sec.

Number of target nuclei, N_o = 1.7648×10^{18}

Project. Energy E_α (MeV)	Gamma-Energy E_γ (MeV)	Absol. γ-intens. Θ_γ (%)	Geometry dependent efficien. $\epsilon.G$	γ-self absorp. factor K	Time lapse t_2 (sec)	Record. time t_3 (sec)	Photo peak count (A)
17.8±1.3	0.175	83.7	0.04220	0.99988	55020	500	1736
	1.096	4.2	0.00670	0.99995	55020	500	-
21.1±1.2	0.175	83.7	0.04220	0.99988	52680	500	35522
	1.096	4.2	0.00670	0.99995	52680	500	295
24.0±1.1	0.175	83.7	0.04220	0.99988	47700	500	90050
	1.096	4.2	0.00670	0.99995	47700	500	731
26.7±1.0	0.175	83.7	0.04220	0.99988	30300	501	129444
	1.096	4.2	0.00670	0.99995	30300	501	995
29.2±0.9	0.175	83.7	0.04220	0.99988	28080	500	111283
	1.096	4.2	0.00670	0.99995	28080	500	820
34.6±0.8	0.175	83.7	0.04220	0.99988	25860	504	95562
	1.096	4.2	0.00670	0.99995	25860	504	760

Table - 4.36

Activation cross-sections for the $^{69}Ga(\alpha,2n)^{71}As$ reaction

E_α (MeV)	Cross-sections(mb) with gamma rays of		Weighted average cross-section (mb)
	0.175 MeV	1.096 MeV	
17.8±1.3	13.10±1.19	-	13.10±1.19
21.1±1.2	266.12±2.24	277.33±47.44	266.15±2.23
24.0±1.1	664.12±2.44	676.49±43.50	664.16±2.43
26.7±1.0	901.83±2.70	869.87±50.71	901.74±2.69
29.2±0.9	771.44±2.51	713.30±47.84	771.28±3.18
34.6±0.8	652.60±2.44	651.27±52.27	652.59±2.44

Table - 4.37

Experimental data for $^{69}Ga(\alpha,2n)^{71}As$ + $^{71}Ga(\alpha,4n)^{71}As$ reactions

(above 39.5 MeV)

Half-life of product nucleus = 219600 sec.

Time of irradiation, t_1 = 2700 sec.

Incident flux, Φ = 5.9667×10^{11} α-particles/cm^2-sec.

Number of target nuclei, N_o = 1.7648×10^{18}

Project. Energy E_α (MeV)	Gamma-Energy E_γ (MeV)	Absol. γ-intens. Θ_γ (%)	Geometry dependent efficien. $\epsilon.G$	γ-self absorp. factor K	Time lapse t_2 (sec)	Record. time t_3 (sec)	Photo peak count (A)
39.5±0.8	0.175	83.7	0.04220	0.99988	23760	511	40577
44.0±0.7	0.175	83.7	0.04220	0.99988	21000	500	31880
48.2±0.7	0.175	83.7	0.04220	0.99988	19080	501	28209
52.2±0.6	0.175	83.7	0.04220	0.99988	16620	501	31886
55.9±0.6	0.175	83.7	0.04220	0.99988	14340	501	34241
59.5±0.6	0.175	83.7	0.04220	0.99988	10560	506	28638

Table - 4.38

Activation cross-sections for the $^{69}Ga(\alpha,2n)^{71}As$ + $^{71}Ga(\alpha,4n)^{71}As$ reactions(above 39.5 MeV)

E_α (MeV)	Cross-sections (mb) with gamma ray of 0.175 MeV
39.5±0.8	271.51±1.77
44.0±0.7	216.12±1.86
48.2±0.7	189.69±1.78
52.2±0.7	212.76±2.19
55.9±0.6	226.84±2.23
59.5±0.6	185.61±3.06

Table - 4.39

Experimental data for $^{69}Ga(\alpha,2n)^{71}As$ reaction(above 39.5 MeV)

Half-life of product nucleus = 219600 sec.

Time of irradiation, t_1 = 2700 sec.

Incident flux, Φ = 5.9667×10^{11} α-particles/cm^2-sec.

Number of target nuclei, N_o = 1.7648×10^{18}

Project. Energy E_α (MeV)	Gamma-Energy E_γ (MeV)	Absol. γ-intens. Θ_γ (%)	Geometry dependent ϵ .G	γ-self absorp. factor K	Time lapse t_2 (sec)	Record. time t_3 (sec)	Photo peak count (A)
39.5±0.8	0.175	83.7	0.04220	0.99988	23760	511	16441
44.0±0.7	0.175	83.7	0.04220	0.99988	21000	500	9819
48.2±0.7	0.175	83.7	0.04220	0.99988	19080	501	8923
52.2±0.6	0.175	83.7	0.04220	0.99988	16620	501	7495
55.9±0.6	0.175	83.7	0.04220	0.99988	14340	501	5736
59.5±0.6	0.175	83.7	0.04220	0.99988	10560	506	4320

Table - 4.40

Activation cross-sections for the $^{69}Ga(\alpha,2n)^{71}As$ reaction(Above 39.5 MeV)

E_α (MeV)	Cross-sections(mb) with gamma ray of 0.175 MeV
39.5±0.8	110.01±0.72
44.0±0.7	66.56±0.57
48.2±0.7	60.00±0.56
52.2±0.6	50.01±0.51
55.9±0.6	38.00±0.37
59.5±0.6	28.00±0.46

the excited states of ^{70}Ge(stable isotope). The decay scheme of ^{70}As is shown in Fig. 4.9(c). The reaction has been studied by considering the seven major gamma rays viz., 0.668 MeV, 0.745 MeV, 0.906 MeV, 1.114 MeV, 1.413 MeV, 1.708 MeV and 2.020 MeV at seven incident α-particle energies. The 0.595 MeV and 1.040 MeV photopeaks cannot be used in the analysis at energies above the threshold of $^{71}Ga(\alpha,n)$ and $^{69}Ga(\alpha, 3n)$ reactions, as the gamma rays are also associated with these reactions. The experimental data for this reaction are given in Table - 4.41 and the cross-sections obtained with different gamma rays are tabulated in Table - 4.42.

Table - 4.41

Experimental data for $^{69}Ga(\alpha,3n)^{70}As$ reaction

Half-life of product nucleus = 3180 sec.

Time of irradiation, t_1 = 2700 sec.

Incident flux, Φ = 5.9667×10^{11} α-particles/cm^2-sec.

Number of target nuclei, N_o = 1.7648×10^{18}

Project. Energy E_α (MeV)	Gamma-Energy E_γ (MeV)	Absol. γ-intens. Θ_γ (%)	Geometry dependent efficien. $\epsilon \cdot G$	γ-self absorp. factor K	Time lapse t_2 (sec)	Record. time t_3 (sec)	Photo peak count (A)
34.6±0.8	0.668	21.2	0.01290	0.99993	25860	504	124
	0.745	20.8	0.01120	0.99994	25860	504	114
	0.906	12.2	0.00860	0.99994	25860	504	55
	1.114	21.2	0.00660	0.99995	25860	504	-
	1.413	8.6	0.00530	0.99995	25860	504	-
	1.708	17.9	0.00500	0.99996	25860	504	-
	2.020	16.7	0.00490	0.99997	25860	504	-
39.5±0.8	0.668	21.2	0.01290	0.99993	23760	511	525
	0.745	20.8	0.01120	0.99994	23760	511	406
	0.906	12.2	0.00860	0.99994	23760	511	230
	1.114	21.2	0.00660	0.99995	23760	511	244
	1.413	8.6	0.00530	0.99995	23760	511	77
	1.708	17.9	0.00500	0.99996	23760	511	177
	2.020	16.7	0.00490	0.99997	23760	511	180
44.0±0.7	0.668	21.2	0.01290	0.99993	21000	500	1319
	0.745	20.8	0.01120	0.99994	21000	500	1168
	0.906	12.2	0.00860	0.99994	21000	500	507
	1.114	21.2	0.00660	0.99995	21000	500	620
	1.413	8.6	0.00530	0.99995	21000	500	236
	1.708	17.9	0.00500	0.99996	21000	500	487
	2.020	16.7	0.00490	0.99997	21000	500	416

Contd.....

Contd..... (Table - 4.41)

48.2±0.7	0.668	21.2	0.01290	0.99993	19080	501	1486
	0.745	20.8	0.01120	0.99994	19080	501	1319
	0.906	12.2	0.00860	0.99994	19080	501	557
	1.114	21.2	0.00660	0.99995	19080	501	698
	1.413	8.6	0.00530	0.99995	19080	501	291
	1.708	17.9	0.00500	0.99996	19080	501	572
	2.020	16.7	0.00490	0.99997	19080	501	477
52.2±0.6	0.668	21.2	0.01290	0.99993	16620	501	1603
	0.745	20.8	0.01120	0.99994	16620	501	1436
	0.906	12.2	0.00860	0.99994	16620	501	606
	1.114	21.2	0.00660	0.99995	16620	501	810
	1.413	8.6	0.00530	0.99995	16620	501	281
	1.708	17.9	0.00500	0.99996	16620	501	555
	2.020	16.7	0.00490	0.99997	16620	501	490
55.9±0.6	0.668	21.2	0.01290	0.99993	14340	501	1882
	0.745	20.8	0.01120	0.99994	14340	501	1785
	0.906	12.2	0.00860	0.99994	14340	501	716
	1.114	21.2	0.00660	0.99995	14340	501	1197
	1.413	8.6	0.00530	0.99995	14340	501	355
	1.708	17.9	0.00500	0.99996	14340	501	684
	2.020	16.7	0.00490	0.99997	14340	501	597
59.5±0.6	0.668	21.2	0.01290	0.99993	10560	506	2101
	0.745	20.8	0.01120	0.99994	10560	506	2144
	0.906	12.2	0.00860	0.99994	10560	506	891
	1.114	21.2	0.00660	0.99995	10560	506	1285
	1.413	8.6	0.00530	0.99995	10560	506	458
	1.708	17.9	0.00500	0.99996	10560	506	709
	2.020	16.7	0.00490	0.99997	10560	506	882

Table - 4.42

Activation cross-sections for the $^{69}Ga(\alpha,3n)^{70}As$ reaction

E_α (MeV)	Cross-sections (mb) with gamma rays of							Weighted average cross-section (mb)
	0.668 MeV	0.745 MeV	0.896 MeV	1.114 MeV	1.413 MeV	1.708 MeV	2.090 MeV	
34.6±0.8	56.86±28.89	61.36±30.14	65.24±53.38	-	-	-	-	60.94±19.43
39.5±0.8	150.36±26.35	136.48±25.55	171.58±44.76	136.51±36.36	132.32±56.71	154.66±28.84	172.31±27.76	151.34±11.92
44.7±0.7	211.32±19.71	219.64±17.86	211.58±35.06	194.04±22.85	226.87±42.30	238.05±21.02	222.76±19.31	217.95±08.51
48.2±0.7	156.38±10.21	162.92±12.23	152.68±21.93	143.49±15.21	183.75±31.57	183.65±14.13	167.78±15.19	162.26±05.49
52.2±0.6	98.69±07.45	103.77±06.79	97.18±14.43	97.41±12.87	103.80±19.95	104.25±09.39	100.83±11.32	101.29±03.72
55.9±0.6	70.50±04.98	78.48±05.80	69.86±11.22	87.59±11.27	79.79±17.98	78.17±08.69	74.74±09.77	75.31±02.98
59.5±0.6	34.21±03.27	40.98±03.50	37.79±05.94	40.87±05.53	44.75±10.26	35.22±05.51	48.00±04.90	39.14±01.77

4.5.3.4 $^{69}Ga(\alpha,p3n)$ Reaction

The Q-value for $(\alpha,p3n)$ reaction on ^{69}Ga is -32.04 MeV. This reaction produces ^{69}Ge residual nucleus (unstable) which decays by electron capture (64%) and β^+(36%) with half-life of 39.0 hours to the excited states of ^{69}Ga (stable isotope). The decay scheme of ^{69}Ge is shown in Fig. 4.9(d). The gamma rays of 0.574 MeV, 0.872 MeV and 1.106 MeV obtained from the decay of ^{69}Ge were used in the analysis of this reaction. The cross-sections for this reaction have been measured at five incident α-particle energies. The experimental data for this reaction required in the calculations of cross-sections are given in Table - 4.43. The cross-sections obtained using these values are given in Table - 4.44.

Table - 4.43

Experimental data for $^{69}Ga(\alpha,p3n)^{69}Ge$ reaction

Half-life of product nucleus = 140580 sec.
Time of irradiation, t_1 = 2700 sec.
Incident flux, ϕ = 5.9667×10^{11} α-particles/cm^2-sec.
Number of target nuclei, N_o = 1.7648×10^{18}

Project. Energy E_α (MeV)	Gamma-Energy E_γ (MeV)	Absol. γ-intens. Θ_γ (%)	Geometry dependent efficien. $\epsilon.G$	γ-self absorp-factor K	Time lapse t_2 (sec)	Record. time t_3 (sec)	Photo peak count (A)
44.0±0.7	0.574	11.6	0.01550	0.99993	21000	500	451
	0.872	10.3	0.00900	0.99994	21000	500	240
	1.106	27.0	0.00660	0.99995	21000	500	475

Contd.....

Contd..... (Table - 4.43)

48.2±0.7	0.574	11.6	0.01550	0.99993	19080	501	1355
	0.872	10.3	0.00900	0.99994	19080	501	765
	1.106	27.0	0.00660	0.99995	19080	501	1426
52.2±0.6	0.574	11.6	0.01550	0.99993	16620	501	2350
	0.872	10.3	0.00900	0.99994	16620	501	1382
	1.106	27.0	0.00660	0.99995	16620	501	2481
55.9±0.6	0.574	11.6	0.01550	0.99993	14340	501	4221
	0.872	10.3	0.00900	0.99994	14340	501	2115
	1.106	27.0	0.00660	0.99995	14340	501	3908
59.5±0.6	0.574	11.6	0.01550	0.99993	10560	506	3624
	0.872	10.3	0.00900	0.99994	10560	506	1986
	1.106	27.3	0.00660	0.99995	10560	506	3914

Table - 4.44

Activation cross-sections for the $^{69}Ga(\alpha,p3n)^{69}Ge$ reaction

E_α (MeV)	Cross-sections (mb) with gamma rays of			Weighted average cross-section(mb)
	0.574 MeV	0.872 MeV	1.106 MeV	
44.0±0.7	39.99±10.29	41.28±15.13	42.52±06.44	41.75±05.14
48.2±0.7	118.79±10.52	130.07±14.79	126.18±07.34	124.66±05.58
52.2±0.6	203.54±11.17	232.14±15.96	216.89±09.27	214.89±06.51
56.9±0.6	361.50±14.99	351.29±21.43	337.82±11.84	347.62±08.53
59.5±0.6	301.64±17.56	320.58±26.31	328.82±15.29	317.66±10.50

4.5.3.5 $^{71}Ga(\alpha,n)$ Reaction

The (α,n) reaction on ^{71}Ga produces ^{74}As residual nucleus, which is unstable and decays by electron capture (37%) and β^{-}(31%) with a half-life of 17.78 days to the excited states of ^{74}Ge (stable isotope). The Q-value of this reaction is -4.93 MeV. The decay scheme of ^{74}As is shown in Fig. 4.9(e). The cross-sections for this reaction have been measured at seven incident α-particle energies using the 0.595 MeV gamma ray. Values of parameters required in the calculation of cross-sections are given in Table - 4.45. The cross-sections obtained using these values are given in Table - 4.46.

Table - 4.45

Experimental data for $^{71}Ga(\alpha,n)^{74}As$ reaction

Half-life of product nucleus = 1537056 sec.

Time of irradiation, t_1 = 2700 sec.

Incident flux, Φ = 5.9667×10^{11} α-particles/cm^2-sec.

Number of target nuclei, N_o = 1.1386×10^{18}

Project. Energy E_α (MeV)	Gamma-Energy E_γ (MeV)	Absol. γ-intens. Θ_γ (%)	Geometry dependent efficien. $\epsilon \cdot G$	γ-self absorp. factor K	Time lapse t_2 (sec)	Record. time t_3 (sec)	Photo peak count (A)
9.7±2.0	0.595	60.0	0.01500	0.99992	59400	500	158
14.1±1.6	0.595	60.0	0.01500	0.99992	57180	500	2084
17.8±1.3	0.595	60.0	0.01500	0.99992	55020	500	2152
21.1±1.2	0.595	60.0	0.01500	0.99992	52680	500	927
24.0±1.1	0.595	60.0	0.01500	0.99992	47700	500	490
26.7±1.0	0.595	60.0	0.01500	0.99992	30300	501	238
29.2±0.9	0.595	60.0	0.01500	0.99992	28080	500	174

Table - 4.46

Activation cross-sections for the $^{71}Ga(\alpha,n)^{74}As$ reaction

E_α (MeV)	Cross-sections(mb) with gamma-ray of 0.595 MeV
9.7±2.0	43.61±09.94
14.1±1.6	574.69±30.06
17.8±1.3	592.86±37.74
21.1±1.2	255.11±34.40
24.0±1.1	134.55±24.44
26.7±1.0	64.72±17.40
29.2±0.9	47.36±14.70

4.5.3.6 $^{71}Ga(\alpha,4n)$ Reaction

The Q-value for $(\alpha,4n)$ reaction on ^{71}Ga is -32.10 MeV. This reaction produces the same residual nucleus ^{71}As as was produced by ^{69}Ga $(\alpha,2n)$ reaction. The decay scheme of ^{71}As is shown in Fig. 4.9(b). The separated counts of $(\alpha,4n)$ reaction alongwith other experimental data are given in Table - 4.47 and the cross-sections obtained with the gamma ray of 0.175 MeV are tabulated in Table - 4.48.

Table - 4.47

Experimental data for $^{71}Ga(\alpha,4n)^{71}As$ reaction

Half-life of product nucleus = 219600 sec.
Time of irradiation, t_1 = 2700 sec.
Incident flux, Φ = 5.9667×10^{11} α-particles/cm^2-sec.
Number of target nuclei, N_o = 1.1386×10^{18}

Project. Energy E_α (MeV)	Gamma-Energy E_γ (MeV)	Absol. γ-intens. θ_γ (%)	Geometry dependent efficien. $\epsilon.G$	γ-self absorp. factor K	Time lapse t_2 (sec)	Record. time t_3 (sec)	Photo peak count (A)
48.2±0.7	0.175	83.7	0.04220	0.99988	19080	501	19286
52.2±0.6	0.175	83.7	0.04220	0.99988	16620	501	24391
55.9±0.6	0.175	83.7	0.04220	0.99988	14340	501	28505
59.5±0.6	0.175	83.7	0.04220	0.99988	10560	506	24318

Table - 4.48

Activation cross-sections for the $^{71}Ga(\alpha,4n)^{71}As$ reaction

E_α (MeV)	Cross-section((mb) with gamma-ray of 0.175 MeV
48.2±0.7	201.01±1.88
52.2±0.6	252.25±2.60
55.9±0.6	292.69±2.89
59.5±0.6	244.29±4.03

4.5.4 Target Nucleus : ^{209}Bi

Specpure bismuth metal was used for target preparation. Bismuth metal of thickness 3.56 mg/cm^2 was deposited onto aluminium backing of thickness 6.75 mg/cm^2, by vacuum evaporation technique. The irradiation of the target foils were made in two different stacks. The first stack was made of 10 (ten) bismuth foils sandwiched between aluminium degraders of thickness 20.387 mg/cm^2. The second stack was made of 10 (ten) bismuth foils without any aluminium degrader foil. The stacks arrangement are shown in Fig. 4.2. The α-particle energy incident on the first stack was $\lesssim$ 60 MeV while on the second stack it was $\lesssim$ 40 MeV. The two independent α-irradiations were performed to cover the entire energy range, using the diffused α-beam of 8 mm diameter. The beam current was kept $\sim$ 100 nA and the irradiation time was 1.0 hour in both irradiations.

The α-particle flux and the total charge collected on these target stacks were monitored by charge collection method using a 'Farady-cup', which was kept closely behind the target and coupled to a calibrated charge integrator.

The alpha particle energies obtained in the first stack were 26.8 ± 0.9 MeV, 31.5 ± 0.9 MeV, 35.9 ± 0.8 MeV, 40.0 ± 0.8 MeV, 43.8 ± 0.7 MeV, 47.4 ± 0.7 MeV, 50.7 ± 0.6 MeV, 53.9 ± 0.6 MeV, 57.0 ± 0.6 MeV and 59.9 ± 0.6 MeV whereas α-particle energies of 26.8 ± 0.8 MeV, 28.3 ± 0.7 MeV, 29.8 ± 0.7 MeV, 31.2 ± 0.7 MeV, 32.6 ± 0.7 MeV, 33.9 ± 0.6 MeV, 35.2 ± 0.6 MeV, 36.4 ± 0.6 MeV, 37.7 ± 0.6 MeV and 38.9 ± 0.6 MeV were obtained in second stack.

The cross-sections for the (α,3n) and (α,4n) reactions on ^{209}Bi have been measured at the above energies. A typical gamma ray spectrum obtained from the activation of the bismuth target foil by 59.9 MeV α-particle energy taken after about 42.0 hours from the stop of irradiation is shown in Fig. 4.10.

4.5.4.1 $^{209}Bi(\alpha,3n)$ Reaction

The Q-value for (α,3n) reaction on ^{209}Bi is -27.98 MeV. This reaction produces ^{210}At residual nucleus, which is unstable and decays mainly by EC + β^+ (99.82%) with a half-life of 8.3 hours to the excited states of ^{210}Po which itself de-excite with the half-life of 138.38 days by its characteristic gamma rays. The decay scheme of ^{210}At is shown in Fig. 4.11(a). The reaction has been studied by considering the five major gamma rays viz., 0.245 MeV, 1.181 MeV, 1.437 MeV, 1.483 MeV and 1.599 MeV. The cross-sections of the reaction have been measured at sixteen α-particle energies considering the above mentioned gamma rays. The experimental data for this reaction are given in Tables - 4.49 and - 4.50. The cross-sections obtained with the different gamma rays are tabulated in Table - 4.51.

4.5.4.2 $^{209}Bi(\alpha,4n)$ Reaction

The Q-value of (α,4n) reaction on ^{209}Bi is -35.24 MeV. This reaction produces unstable ^{209}At residual nucleus which

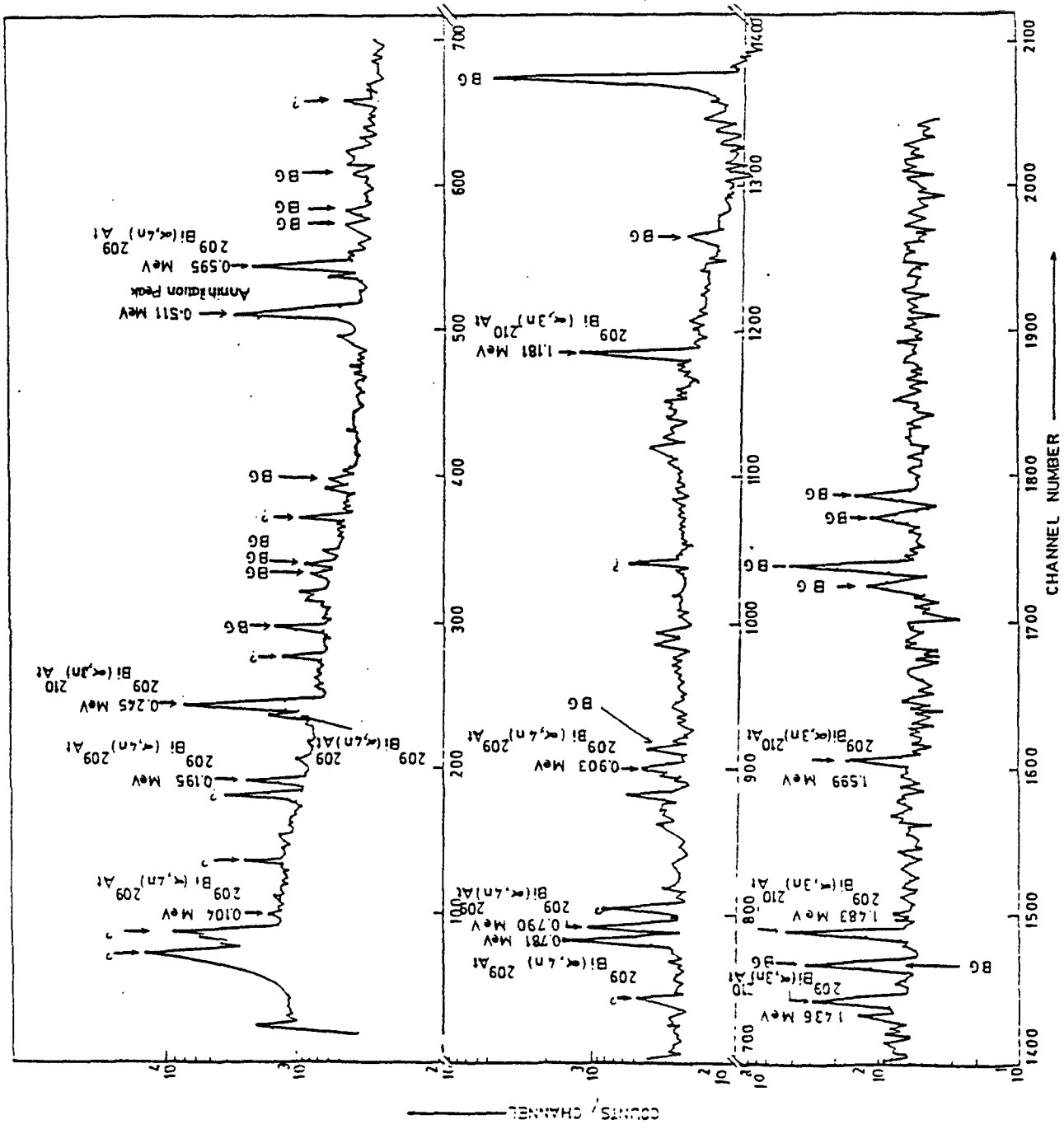

Fig. 4.10 Typical gamma ray spectrum obtained from the activation of 209Bi target of 59.9 MeV α-particles.

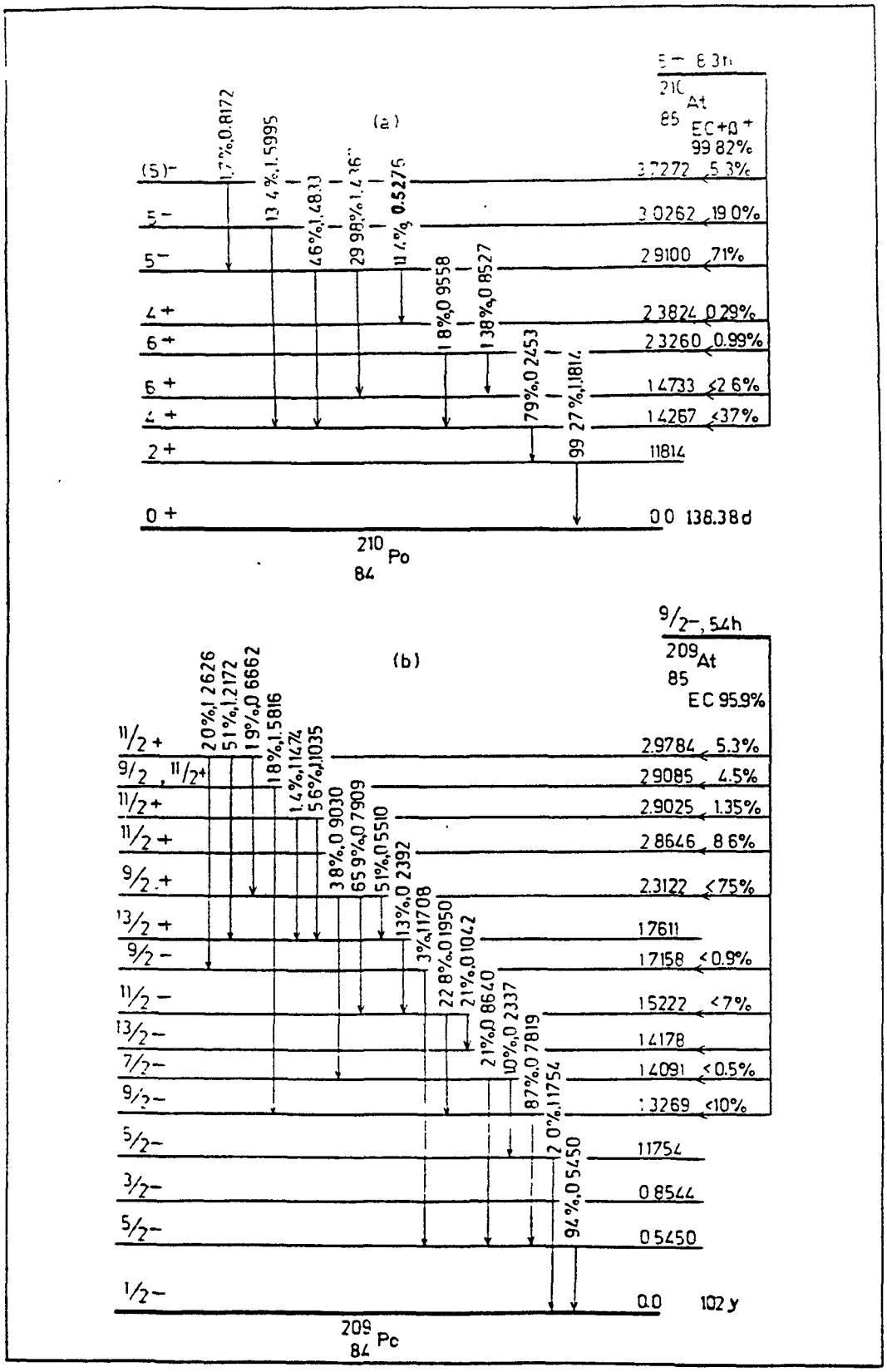

Fig. 4.11 Partial decay schemes for isotopes ^{210}At and ^{209}At formed in alpha induced reactions on ^{209}Bi.

Table - 4.49

Experimental data for $^{209}Bi(\alpha,3n)^{210}At$ reaction (First stack)

Half-life of product nucleus = 29880 sec.
Time of irradiation, t_1 = 3600 sec.
Incident flux, $\bar{\Phi}$ = 5.7847×10^{11} α-particles/cm^2-sec.
Number of target nuclei= 5.1536×10^{18}

Project. Energy E_α (MeV)	Gamma-Energy E_γ (MeV)	Absol. γ-intens. Θ_γ (%)	Geometry dependent efficien. ϵ.G	γ-self absorp. factor K	Time lapse t_2 (sec)	Record. time t_3 (sec)	Photo peak count (A)
29.8±0.7	0.245	79.4	0.01010	0.99891	13020	300	6515
	1.181	99.3	0.00240	0.99988	13020	300	1969
	1.436	28.9	0.00200	0.99989	13020	300	480
	1.483	46.5	0.00195	0.99989	13020	300	740
	1.599	13.4	0.00190	0.99990	13020	300	-
31.2±0.7	0.245	79.4	0.01010	0.99891	15900	300	8129
	1.181	99.3	0.00240	0.99988	15900	300	2413
	1.436	28.9	0.00200	0.99989	15900	300	556
	1.483	46.5	0.00195	0.99989	15900	300	920
	1.599	13.4	0.00190	0.99990	15900	300	-
32.6±0.7	0.245	79.4	0.01010	0.99891	21600	300	108956
	1.181	99.3	0.00240	0.99988	21600	300	31828
	1.436	28.9	0.00200	0.99989	21600	300	7740
	1.483	46.5	0.00195	0.99989	21600	300	12185
	1.599	13.4	0.00190	0.99990	21600	300	-
33.9±0.7	0.245	79.4	0.01010	0.99891	22380	300	222586
	1.181	99.3	0.00240	0.99988	22380	300	63248
	1.436	28.9	0.00200	0.99989	22380	300	15381
	1.483	46.5	0.00195	0.99989	22380	300	24408
	1.599	13.4	0.00190	0.99990	22380	300	-

Contd.....

Contd..... (Table - 4.49)

35.2±0.6	0.245	79.4	0.01010	0.99891	24600	300	259585
	1.181	99.3	0.00240	0.99988	24600	300	73704
	1.436	28.9	0.00200	0.99989	24600	300	17646
	1.483	46.5	0.00195	0.99989	24600	300	28462
	1.599	13.4	0.00190	0.99990	24600	300	-
36.4±0.6	0.245	79.4	0.01010	0.99891	26700	300	350684
	1.181	99.3	0.00240	0.99988	26700	300	99119
	1.436	28.9	0.00200	0.99989	26700	300	24088
	1.483	46.5	0.00195	0.99989	26700	300	38669
	1.599	13.4	0.00190	0.99990	26700	300	-
37.7±0.6	0.245	79.4	0.01010	0.99891	30960	300	366847
	1.181	99.3	0.00240	0.99988	30960	300	104008
	1.436	28.3	0.00200	0.99989	30960	300	25178
	1.483	46.5	0.00195	0.99989	30960	300	40445
	1.599	13.4	0.00190	0.99990	30960	300	-
38.9±0.6	0.245	79.4	0.01010	0.99891	33300	300	309898
	1.181	99.3	0.00240	0.99988	33300	300	86189
	1.436	28.3	0.00200	0.99989	33300	300	21646
	1.483	46.5	0.00195	0.99989	33300	300	33673
	1.599	13.4	0.00190	0.99990	33300	300	-

Table - 4.50

Experimental data for $^{209}Bi(\alpha,3n)^{210}At$ reaction (Second stack)

Half-life of product nucleus = 29880 sec.

Time of irradiation, t_1 = 3600 sec.

Incident flux, ϕ = 5.6524×10^{11} α-particles/cm^2-sec.

Number of target nuclei, N_o = 5.1536×10^{18}

Project. Energy E_α (MeV)	Gamma-Energy E_γ (MeV)	Absol. γ-intens. Θ_γ (%)	Geometry dependent efficien. ϵ.G	γ-self absorp. factor K	Time lapse t_2 (sec)	Record. time t_3 (sec)	Photo peak count (A)
31.5±0.9	0.245	79.4	0.03340	0.99891	164820	270	2153
	1.181	99.3	0.00620	0.99988	164820	270	487
	1.436	28.9	0.00520	0.99989	164820	270	119
	1.483	46.5	0.00510	0.99989	164820	270	186
	1.599	13.4	0.00495	0.99990	164820	270	-
35.9±0.8	0.245	79.4	0.03340	0.99891	163320	271	38028
	1.181	99.3	0.00620	0.99988	163320	271	9084
	1.436	28.9	0.00520	0.99989	163320	271	2204
	1.483	46.5	0.00510	0.99989	163320	271	3478
	1.599	13.4	0.00495	0.99990	163320	271	957
40.0±0.8	0.245	79.4	0.03340	0.99891	161640	272	25629
	1.181	99.3	0.00620	0.99988	161640	272	6015
	1.436	28.9	0.00520	0.99989	161640	272	1473
	1.483	46.5	0.00510	0.99989	161640	272	2183
	1.599	13.4	0.00495	0.99990	161640	272	701
43.8±0.7	0.245	79.4	0.03340	0.99891	160140	270	14641
	1.181	99.3	0.00620	0.99988	160140	270	3431
	1.436	28.9	0.00520	0.99989	160140	270	804
	1.483	46.5	0.00510	0.99989	160140	270	1162
	1.599	13.4	0.00495	0.99990	160140	270	408

Contd.....

Contd..... (Table - 4.50)

47.4±0.7	0.245	79.4	0.03340	0.99891	159420	270	14571
	1.181	99.3	0.00620	0.99988	159420	270	3410
	1.436	28.9	0.00520	0.99989	159420	270	878
	1.483	46.5	0.00510	0.99989	159420	270	1185
	1.599	13.4	0.00495	0.99990	159420	270	414
50.7±0.6	0.245	79.4	0.03340	0.99891	158220	270	13800
	1.181	99.3	0.00620	0.99988	158220	270	3209
	1.436	28.9	0.00520	0.99989	158220	270	723
	1.483	46.5	0.00510	0.99989	158220	270	1199
	1.599	13.4	0.00495	0.99990	158220	270	299
53.9±0.6	0.245	79.4	0.03340	0.99891	156960	271	12027
	1.181	99.3	0.00620	0.99988	156960	271	2575
	1.436	28.9	0.00520	0.99989	156960	271	630
	1.483	46.5	0.00510	0.99989	156960	271	954
	1.599	13.4	0.00495	0.99990	156960	271	213
59.9±0.6	0.245	79.4	0.03340	0.99891	150360	450	14461
	1.181	99.3	0.00620	0.99988	150360	450	3433
	1.436	28.9	0.00520	0.99989	150360	450	838
	1.483	46.5	0.00510	0.99989	150360	450	1049
	1.599	13.4	0.00495	0.99990	150360	450	280

Table - 4.51

Activation cross-sections for the $^{209}Bi(\alpha,3n)^{210}At$ reaction

E_α (MeV)	Cross-sections (mb) with gamma rays of					Weighted average cross-section (mb)
	0.245 MeV	1.181 MeV	1.436 MeV	1.483 MeV	1.599 MeV	
29.8±0.7	15.41±0.27	15.65±00.41	15.73±00.85	15.55±00.61	-	15.61±0.21
31.2±0.7	20.55±0.34	20.51±00.49	19.48±01.02	19.48±01.02	-	20.47±0.25
31.5±0.9	59.17±1.73	57.59±04.02	57.65±07.27	57.11±05.53	-	58.74±1.49
32.6±0.7	314.41±1.13	308.74±02.01	309.52±04.04	310.67±03.06	-	312.65±0.91
33.9±0.6	654.02±1.50	624.71±02.84	626.32±05.66	633.67±04.36	-	646.49±3.67
36.2±0.6	803.04±1.69	766.45±03.18	756.52±06.43	777.96±09.89	-	791.81±4.86
35.9±0.8	1005.65±6.16	1033.72±13.66	1027.36±27.04	1027.53±19.20	1011.01±41.20	1012.32±5.29
36.4±0.6	1139.00±2.06	1082.19±03.94	1084.24±07.83	1109.70±06.03	-	1123.81±6.91
37.7±0.6	1315.23±2.35	1253.50±04.47	1250.99±08.94	1281.20±06.81	-	1297.81±7.65
38.9±0.6	1173.62±2.77	1106.85±04.25	1135.48±08.50	1126.17±06.56	-	1154.60±7.93
40.0±0.8	649.47±5.07	655.91±10.69	657.95±18.76	618.02±11.89	709.65±30.37	647.00±4.17
43.8±0.7	360.98±5.52	364.01±09.65	349.41±19.12	320.07±14.60	401.86±33.49	357.23±4.43
47.4±0.7	353.31±5.55	355.79±08.45	375.25±19.66	321.00±14.36	401.02±31.00	352.09±4.31
50.7±0.6	325.43±4.15	325.63±08.02	300.52±14.55	315.88±11.33	281.67±22.61	323.23±3.41
53.9±0.6	274.43±4.06	252.84±08.05	253.39±14.08	243.19±10.96	194.16±22.79	266.61±3.35
59.9±0.6	170.87±2.56	174.55±05.69	174.53±10.41	138.47±07.39	132.17±18.88	168.75±2.73

decays by electron capture (95.9%) with a half-life of 5.4 hours to the excited states of ^{209}Po which itself de-excite with a half-life of 102 years by its characteristic gamma rays. The decay scheme of ^{209}At is shown in Fig. 4.11(b). The cross-sections for the reaction have been measured at eight incident α-particle energies considering the 0.195 MeV, 0.545 MeV, 0.781 MeV and 0.790 MeV gamma rays. The values of the parameters used in the calculation of cross-sections are given in Tables - 4.52 and - 4.53 and the cross-sections obtained using these values are tabulated in Table - 4.54.

Table - 4.52

Experimental data for $^{209}Bi(\alpha,4n)^{209}At$ reaction (First stack)

Half-life of product nucleus= 19440 sec.
Time of irradiation, t_1 = 3600 sec.
Incident flux, Φ = 5.7847×10^{11} = α-particles/cm^2-sec.
Number of target nuclei, N_o = 5.1536×10^{18}

Project. Energy E_α (MeV)	Gamma-Energy E_γ (MeV)	Absol. γ-intens. θ_γ (%)	Geometry dependent efficien. $\epsilon.G$	γ-self absorp. factor K	Time lapse t_2 (sec)	Record. time t_3 (sec)	Photo peak count (A)
37.7±0.6	0.195	22.8	0.01160	0.99819	30960	300	-
	0.545	94.4	0.00510	0.99974	30960	300	1180
	0.781	86.5	0.00342	0.99983	30960	300	716
	0.790	65.9	0.00340	0.99984	30960	300	481
38.9±0.6	0.195	22.8	0.01160	0.99819	33300	300	-
	0.545	94.4	0.00510	0.99974	33300	300	5463
	0.781	86.5	0.00342	0.99983	33300	300	3469
	0.790	65.9	0.00340	0.99984	33300	300	2959

Table - 4.53

Experimental data for $^{209}Bi(\alpha,4n)^{209}At$ reaction (Second stack)

Half-life of product nucleus = 19440 sec.

Time of irradiation, t_1 = 3600 sec.

Incident flux, Φ = 5.6524×10^{11} α-particles/cm^2-sec.

Number of target nuclei, N_o = 5.1536×10^{18}

Project. Energy E_α (MeV)	Gamma-Energy E_γ (MeV)	Absol. γ-intens. Θ_γ (%)	Geometry dependent efficien. $\epsilon.G$	γ-self absorp. factor K	Time lapse t_2 (sec)	Record. time t_3 (sec)	Photo peak count (A)
40.0±0.8	0.195	22.8	0.03900	0.99819	161640	272	747
	0.545	94.4	0.01620	0.99974	161640	272	1340
	0.781	86.5	0.01040	0.99983	161640	272	813
	0.790	65.9	0.01020	0.99984	161640	272	617
43.8±0.7	0.195	22.8	0.03900	0.99819	160140	270	1787
	0.545	94.4	0.01620	0.99974	160140	270	2712
	0.781	86.5	0.01040	0.99983	160140	270	1699
	0.790	65.9	0.01020	0.99984	160140	270	1256
47.4±0.7	0.195	22.8	0.03900	0.99819	159420	270	1981
	0.545	94.4	0.01620	0.99974	159420	270	3433
	0.781	86.5	0.01040	0.99983	159420	270	1958
	0.790	65.9	0.01020	0.99984	159420	270	1425
50.7±0.6	0.195	22.8	0.03900	0.99819	158220	270	3509
	0.545	94.4	0.01620	0.99974	158220	270	5326
	0.781	86.5	0.01040	0.99983	158220	270	3387
	0.790	65.9	0.01020	0.99984	158220	270	2504
53.9±0.6	0.195	22.8	0.03900	0.99819	156960	271	3116
	0.545	94.4	0.01620	0.99974	156960	271	5042
	0.781	86.5	0.01040	0.99983	156960	271	3087
	0.790	65.9	0.01020	0.99984	156960	271	2307
59.9±0.6	0.195	22.8	0.03900	0.99819	150360	450	2759
	0.545	94.4	0.01620	0.99974	150360	450	4209
	0.781	86.5	0.01040	0.99983	150360	450	2552
	0.790	65.9	0.01020	0.99984	150360	450	2025

Table - 4.54

Activation cross-sections for the $^{209}Bi(\alpha,4n)^{209}At$ reaction

E_α (MeV)	Cross-sections (mb) with gamma rays of				Weighted average cross-section (mb)
	0.195 MeV	0.595 MeV	0.781 MeV	0.790 MeV	
37.7±0.6	-	6.90±00.88	6.81±01.40	6.04±01.83	6.76±00.69
38.9±0.6	-	34.72±00.95	35.87±01.74	40.41±02.06	35.74±00.79
40.0±0.8	281.84±30.18	293.50±13.58	302.67±19.73	307.45±24.91	296.61±09.67
43.8±0.7	643.84±63.41	567.23±18.61	604.01±26.66	597.65±33.78	585.22±13.59
47.4±0.7	695.65±60.40	699.83±23.24	678.44±28.41	660.89±32.93	685.01±15.27
50.7±0.6	1180.62±41.38	1040.27±18.36	1124.45±25.56	1112.67±30.22	1087.24±13.97
53.9±0.6	998.67±34.29	938.09±17.68	976.24±24.03	976.51±28.78	961.54±11.96
59.9±0.6	422.22±20.35	373.92±09.33	385.35±13.44	409.27±15.76	390.42±06.58

4.6 Errors

The reliability and utility of experimental data in a particular measurement depends upon the various errors involved. The errors involved in the measurement of cross-sections consist of statistical and systematic errors. The various sources of errors which may creep in the present measurements, their estimation and steps to minimize them are described in the following paragraphs :

(1) The erratic behaviour of electronic equipments may introduce some errors in the measurement. It can be minimized by stabilizing the electronic equipments for a few hours before the start of the experiment.

(2) The determination of detector efficiencies may introduce some errors in the measurements. There may be some contribution to this error from any uncertainty in the strength of standard source, statistical count rate of the photopeaks, and in the absolute intensity of the relevant gamma ray. The error may be minimized by careful determination of the detector efficiency and drawing the efficiency curve by using a best polynomial fit using a standard computer program. The maximum uncertainty in the detector efficiency was estimated to be 2%.

(3) The measurement of target thickness may also introduce some errors. This error was minimized by cutting the target foils to the standard sizes and accurately weighing them using a microbalance. The estimated maximum error due to this factor

was less than 1%.

(4) Fluctuations in the alpha beam current may also introduce some errors in the current integrator reading due to incomplete charge collection at the 'Faraday cup'. The fluctuations were brought to a minimum by adjusting the necessary parameters in the operation of the cyclotron, particularly during a certain irradiation. The uncertainty due to this type of error was estimated to be less than 2%.

(5) The adopted values of stopping powers of the different targets also introduce some errors in the estimation of the incident alpha energies. Accuracy of stopping power values was not estimated by the authors[17].

(6) The inaccurate measurement of irradiation time, the time lapse between the stop of irradiation and start of counting as well as the counting time may introduce some errors. The estimated upper limit for this error is less than 1% in the present measurements.

(7) Some errors may also be introduced due to non-reproducibility of the geometries of irradiation and counting systems. However, this type of error was minimized by fixing the position of the target holder during irradiation and counting. A maximum error of 1% was estimated in the present measurements.

(8) Any error in the values of half-life and absolute gamma ray intensities may contribute some errors. In the present measurements, the errors were minimized by using latest available data[10].

(9) Gamma rays self absorption in the target is also a significant factor, especially in the target which has high Z values and are comparatively thick. This contribution was applied to each case.

(10) In addition to all the above systematic errors there will be statistical error in the counts under the photopeaks. This error varies from one case to another, depending upon the activities produced in the target foils. The statistical errors in the photopeak counts were estimated using the following relation[9)]

$$\sigma_u = \sqrt{x + y}$$

where σ_u is the net counts, x is the total counts and y is the background counts. This statistical error in the counts under the peak was estimated to be less than 1% to 35%. In some cases, these errors were as large as 59% because of low intensity of the induced activity.

References

1) S.M. Qaim : Radio Chemica Acta 25 (1978) 13, Inorg. Nucl. Chem. 36 (1974) 239.

2) W.J. Rubinson : J. Chem. Phys. 17 (1949) 542.

3) W.B. Lewis : Nucleonics No. 10, 12 (1954) 30.

4) M. Afzal Ansari : Ph.D. Thesis, Aligarh Muslim University, Aligarh (1982).

5) E. Bleuler and G.J. Goldsmith : Experimental Nucleonics (Holt, Rinchart and Winston, New York, 1952) 86.

6) E. Storm and H. Israel : Nucl. Data Tables 7 (1970) 565.

7) S.F. Mughabghab, M. Divadeenam and N.E. Holden : Neutron Cross-sections Vol. 1, Part-A Academic Press, Inc., N.Y. (1981) 89.

8) W.D. Hamilton : Electromagnetic Interaction in Nuclear Spectroscopy, (North Holland Publishing Company, U.K. 1975).

9) G.F. Knoll : Radiation Detection and Measurements (John Wiley and Sons, New York, 1979).

10) C.M. Lederer and V.S. Shirely : Table of Isotopes 7th Edition (John Wiley and Sons, New York, 1978).

11) C.L. Branquinho, S.M.A. Hoffmann, G.W.A. Newton, V.J. Robinson, H.Y. Wang and I.S. Grant : J. Inorg. Nucl. Chem. 41 (1979) 617.

12) W.W. Bowman and M. Blann : Nucl. Phys. A131 (1969) 513.

13) J. Ernst, R. Ibowski, H. Klampfl, H. Machner, T. Mayer-Kuckuk and R. Schanz : Z. Phys. Atoms and Nuclei, A308 (1982) 301.

14) H. Morinaga : Phys. Rev. 101 (1956) 100.

15) J.B. Ball, A.W. Fairhall and I. Halpern : Phys. Rev. 114 (1959) 305.

16) D.J. Frantsvog, A.R. Kunselman, R.L. Wilson, C.S. Zaidins and C. Detraz : Phys. Rev. C25 (1982) 770.

17) L.C. Northcliffe and R.F. Schilling : Nucl. Data Tables A7 (1970) 256.

18) R.K.Y. Singh : Ph.D. Thesis, Aligarh Muslim University, Aligarh (1985).

19) K.A. Keller, J. Lange and H. Munzel : Numerical Data and Functional Relationships in Science and Technology, New Series, Vol. 5C, Q-values and Excitation Functions of Nuclear Reactions, New York (1974).

20) A.H. Wapstra and K. Bos Atomic Data and Nuclear Data Tables 19 (1977) 177.

CHAPTER - V

RESULTS AND DISCUSSION

In order to test the validity of the various nuclear reaction theories and models, there is also need for extensive measurements of the excitation functions. A lot of work has been done on the study of excitation functions of α-particle induced reactions for various target nuclides[1]. One of the pioneer works is that of Weisskopf and Ewing[2], who have measured the excitation functions of (α,n) reactions for some heavy nuclei. Later, the measurements were extended to α-particle energies as high as 170 MeV, to explore different types of possible reactions[3-10]. However, the situation regarding it is still unsatisfactory as there are large discrepancies in the reported values[1] even for a single specific reaction. Moreover, the data are incomplete and contain large errors. The excitation functions, in the past, have often been analysed on the basis of compound nucleus model. In general, this mechanism of reaction could not account for the high energy tail portion of the excitation functions. With this view, for all the targets e.g., ^{55}Mn, $^{63,65}Cu$, $^{69,71}Ga$ and ^{209}Bi a total of 19 excitation functions have been measured between 7 and 60 MeV.

5.1 Experimental Results

The cross-sections measured for $^{55}Mn(\alpha,n)^{58}Co$, $^{55}Mn(\alpha,2n)^{57}Co$, $^{55}Mn(\alpha,3n)^{56}Co$, $^{55}Mn(\alpha,4n)^{55}Co$, $^{55}Mn(\alpha,\alpha n)^{54}Mn$ + $^{55}Mn(\alpha,2p3n)^{54}Mn$, $^{55}Mn(\alpha,\alpha 3n)^{52g}Mn$, $^{63}Cu(\alpha,n)^{66}Ga$, $^{63}Cu(\alpha,2n)^{65}Ga$ + $^{63}Cu(\alpha,pn)^{65}Zn$, $^{65}Cu(\alpha,n)^{68}Ga$, $^{65}Cu(\alpha,2n)^{67}Ga$, $^{65}Cu(\alpha,3n)^{66}Ga$, $^{69}Ga(\alpha,n)^{72}As$, $^{69}Ga(\alpha,2n)^{71}As$, $^{69}Ga(\alpha,3n)^{70}As$, $^{69}Ga(\alpha,p3n)^{69}Ge$, $^{71}Ga(\alpha,n)^{74}As$, $^{71}Ga(\alpha,4n)^{71}As$, $^{209}Bi(\alpha,3n)^{210}At$ and $^{209}Bi(\alpha,4n)^{209}At$ reactions are tabulated in Tables - 5.1 to 5.6. Our experimentally measured values alongwith earlier measurements[11-20] are displayed in Figs. 5.1 - 5.21 (with open circles). The horizontal bars in our results show the estimated total energy spread associated with each incident α-particle energy, while the vertical bars represent the total estimated error in cross-sections. If no error is depicted, the size of the circle includes the magnitude of the statistical error. Most of the previous reports do not show errors in their measurements, however, wheresoever errors are reported, they have been incorporated in the Figures. Further, it has also been observed that the maxima of the excitation functions are also shifted in individual sets of measurements by different groups. This is probably due to the choice of different stopping power tables used by each group. Moreover, the previous measurements are quite old[11-20] and were taken generally using NaI(Tl) scintillation detector and proportional counter.

For ^{55}Mn(Figs. 5.1 - 5.6) two earlier measurements are available in literature[11,12]. Measurements reported by

Table - 5.1

Experimental Cross-sections for the α-induced reactions on ^{55}Mn

E_α (MeV)	Reaction	Cross-sections σ(mb) (α,n)	(α,2n)	(α,3n)	(α,4n)	(α,αn)	(α,αn)+(α,2p3n)	(α,α3n)
	Product nucleus	^{58}Co	^{57}Co	^{56}Co	^{55}Co	^{54}Mn	^{54}Mn	^{52g}Mn
06.8±2.7		127.95±3.17	-	-	-	-	-	-
12.2±1.8		662.96±6.39	36.37±7.22	-	-	-	-	-
16.2±1.5		543.16±5.90	583.45±8.71	-	-	-	-	-
19.6±1.3		278.73±4.40	1013.52±8.45	-	-	22.37±12.99	-	-
22.5±1.2		114.72±3.05	958.85±9.56	-	-	96.20±16.35	-	-
25.2±1.2		65.88±2.58	870.94±9.36	3.40±01.24	-	125.54±12.99	-	-
27.8±1.1		54.18±2.47	870.32±9.15	24.28±01.98	-	180.12±13.95	-	-
30.2±1.0		40.82±2.31	683.68±8.83	57.95±02.44	-	212.34±14.43	-	-
35.5±0.9		16.30±2.25	199.97±7.43	98.62±05.30	-	165.69±13.71	-	-
40.3±0.8		12.49±2.47	174.63±7.39	191.59±06.54	0.99±0.11	169.77±13.95	-	-
44.7±0.7		10.24±2.73	118.14±7.22	197.02±09.28	3.59±0.17	-	143.30±15.87	1.28±0.17
48.9±0.7		8.14±3.00	60.39±7.35	95.04±07.05	6.26±0.21	-	71.65±14.67	10.05±0.36
52.8±0.7		-	46.85±7.69	60.74±07.19	7.28±0.25	-	106.50±17.31	22.35±0.67
56.5±0.6		-	40.01±6.66	46.99±08.61	8.73±0.30	-	118.99±23.80	37.67±1.03
59.95±0.6		-	34.55±8.71	43.94±11.13	9.97±0.32	-	124.27±24.04	46.77±1.58

Table - 5.2

Experimental cross-sections for the α-induced reactions on ^{63}Cu

E_α (MeV)	Cross-sections σ(mb)		
	Reaction	(α,n)	(α,pn)+(α,2n)
	Product nucleus	^{66}Ga	^{65}Zn + ^{65}Ga
16.8±1.6		329.97±3.80	229.56±83.17
18.8±1.5		192.84±1.90	249.53±63.22
20.7±1.4		207.72±1.90	363.50±63.63
22.5±1.3		140.54±1.54	516.58±54.07
24.3±1.3		83.73±1.06	932.54±78.61
25.9±1.2		52.58±0.33	1098.97±62.39
27.5±1.2		35.64±0.27	901.84±54.08
30.1±1.1		21.46±0.21	764.60±45.76
32.7±1.0		14.76±0.12	663.95±50.34
35.0±1.0		11.20±0.08	-
37.3±0.9		8.66±0.05	-
39.4±0.9		6.82±0.04	534.23±74.39

Table - 5.3

Experimental cross-sections for the α-induced reactions on ^{65}Cu

E_α (MeV)	Cross-sections σ(mb)		
Reaction	(α,n)	(α,2n)	(α,3n)
Product nucleus	^{68}Ga	^{67}Ga	^{66}Ga
16.8±1.6	556.27±43.08	58.37±1.86	-
18.8±1.5	329.99±44.15	216.97±3.83	-
20.7±1.4	256.46±58.40	424.18±7.44	-
22.5±1.3	218.79±59.77	520.22±8.90	-
24.3±1.3	-	545.76±9.21	-
25.9±1.2	-	579.33±9.64	-
27.5±1.2	-	573.48±9.08	-
30.1±1.1	-	528.71±8.66	3.28±0.15
32.7±1.0	-	469.70±2.44	38.06±1.32
35.0±1.0	-	329.14±5.26	88.70±1.69
37.3±0.9	-	270.13±4.63	150.25±1.73
39.4±0.9	-	191.11±3.30	193.26±1.90

Table - 5.4

Experimental cross-sections for the α-induced reactions on ^{69}Ga

E_α (MeV)	Cross-sections σ(mb)				
	Reaction	(α,n)	(α,2n)	(α,3n)	(α,p3n)
	Product nucleus	^{72}As	^{71}As	^{70}As	^{69}Ge
9.7±2.0		21.96±1.01	-	-	-
14.1±1.6		437.47±3.43	-	-	-
17.8±1.3		737.22±5.46	13.10±1.19	-	-
21.1±1.2		576.21±8.32	266.19±2.23	-	-
24.0±1.1		-	644.32±2.43	-	-
26.7±1.0		-	902.05±2.69	-	-
29.2±0.9		-	771.68±3.18	-	-
34.6±0.8		-	652.62±2.44	59.84±19.43	-
39.5±0.8		-	110.01±0.72	151.34±11.92	-
44.0±0.7		-	66.56±0.57	217.95±08.51	41.75±05.14
48.2±0.7		-	60.60±0.56	162.26±05.49	124.66±05.58
52.2±0.6		-	50.01±0.51	101.29±03.72	214.89±06.51
55.9±0.6		-	38.00±0.37	75.31±02.98	347.62±08.53
59.5±0.6		-	28.00±0.46	39.14±01.77	317.66±10.56

Table - 5.5

Experimental cross-sections for the α-induced reactions on ^{71}Ga

E_α (MeV)	Cross-sections σ(mb)		
	Reaction	(α,n)	(α,4n)
	Product nucleus	^{74}As	^{71}As
9.7±2.0		43.61±09.94	-
14.1±1.6		574.69±30.06	-
17.8±1.3		592.86±37.74	-
21.1±1.2		255.11±34.40	-
24.0±1.1		134.55±24.44	-
26.7±1.0		64.72±17.40	-
29.2±0.9		47.36±14.70	-
34.6±0.8		-	-
39.5±0.8		-	-
44.0±0.7		-	-
48.2±0.7		-	201.01±1.88
52.2±0.6		-	252.25±2.60
55.9±0.6		-	292.69±2.89
59.5±0.6		-	244.29±4.03

Table - 5.6

Experimental cross-sections for the α-induced reactions on ^{209}Bi

E_α (MeV)	Cross-sections σ(mb)		
	Reaction	(α,3n)	(α,4n)
	Product nucleus	^{210}At	^{209}At
29.8±0.7		15.51±0.21	-
31.2±0.7		20.47±0.25	-
31.5±0.9		58.74±1.49	-
32.6±0.7		312.65±0.91	-
33.9±0.6		646.49±3.67	-
35.2±0.6		791.81±4.86	-
35.9±0.8		1012.32±5.29	-
36.4±0.6		1123.43±6.91	-
37.7±0.6		1297.81±7.65	6.76±00.69
38.9±0.6		1154.60±7.93	35.74±00.79
40.0±0.8		647.00±4.17	296.61±09.67
43.8±0.7		357.23±4.43	585.22±13.59
47.4±0.7		352.09±4.31	685.01±15.27
50.7±0.6		323.23±3.41	1087.24±13.97
53.9±0.6		266.61±3.35	961.54±11.96
59.9±0.6		168.75±2.73	390.42±06.58

Matsuo et al.[11] cover upto 30 MeV α-particle energy for (α,n) reaction only, while the measurements by Tanaka et al.[12] cover upto 40 MeV α-particle energy for (α,n), (α,2n), (α,3n) and (α,αn) reactions. The data measured by Matsuo et al.[11] for (α,n) reaction (Fig. 5.1) show severe discrepancies in the lower as well as in the higher region with our data, while the measurements of Tanaka et al.[12], are in excellent agreement with ours. Excitation function for the reaction (α,α3n) has, to the best of our knowledge, been reported for the first time.

For ^{63,65}Cu(Figs. 5.7 - 5.12), it was found that earlier measurements of Lin et al.[13], Porile et al.[14], Hille et al.[15] Bryant et al.[16], Lebowitz et al.[17] and Graf et al.[18] are in general somewhat higher than our measurements, except the measurements by Porges[19]. The excitation function data reported by Porges[19] are, in general, lower than previous and present measurements. They differ by a factor of 4, at about E_α = 14 MeV, especially in the reactions ^{63}Cu(α,n)^{66}Ga and ^{65}Cu(α,n)^{68}Ga as shown in Figs. 5.7 and 5.10. Porges[19] has also reported the excitation function for ^{65}Cu(α,3n)^{66}Ga reaction, using natural Copper foils, but he has not discussed the procedure of separating the contributions from the reaction ^{63}Cu(α,n) which produces the same residual nucleus ^{66}Ga. Moreover, previous measurements differ from each other to a high extent, particularly the measurements by Porges[19] and those of Porile et al.[14]. The latter group has used a NaI(Tl) scintillation detector and proportional counter for their measurements.

Their results are in general higher than ours and other reported values.

The excitation functions measured for $^{69,71}Ga$ (Figs. 5.13 to 5.19) are $^{69}Ga(\alpha,n)$, $^{69}Ga(\alpha,2n)$, $^{69}Ga(\alpha,3n)$ $^{69}Ga(\alpha,p3n)$, $^{71}Ga(\alpha,n)$ and $^{71}Ga(\alpha,4n)$ reactions. The present measurements for $^{69,71}Ga$ are to the best of our knowledge, reported for the first time. For ^{209}Bi, an extensive study of $(\alpha,3n)$ and $(\alpha,4n)$ reactions (Figs. 5.20 - 5.21) have been done. Again, to the best of our knowledge, only one earlier measurement by Ramler et al.[20] has been reported in the literature upto 42 MeV. Our measurements have been extended upto 60 MeV α-particle energy. The values published by the authors[20] upto 42 MeV α-particle energy are in agreement with our results.

5.2 Model Calculations

Many of the reactions proceed mainly via compound nucleus formation[21]. Therefore, the experimental cross-sections may be compared with excitation functions calculated by means of the hybrid model, i.e., a combination of the precompound-compound nucleus model. In this model the spectra of emitted particles are calculated for each step in the energy dissipation process, induced by the interaction between projectile and target nucleons. The calculation starts with an initial number of excitons, i.e., particles above and holes below, the Fermi level induced by the primary interaction and proceeds to states with

an increasing exciton number. For each of these states the emission probability for the particles is calculated, and finally the integration spectra yield the cross-sections for the individual reactions. A more extensive description of the model is already given in Chapter - II.

For the calculations, the computer code 'ALICE/LIVERMORE-82,[22] has been used. These calculations combine theories of equilibrium reactions, according to Weisskopf and Ewing[2] and pre-equilibrium reactions, according to the hybrid[23] as well as the geometry dependent hybrid model[24] (GDH) of Blann. In the equilibrium calculations the evaporation of protons, neutrons, deuterons and α-particles has been allowed for. The Q-value for the formation of the compound nucleus and the neutron, proton, alpha, and deuteron binding energies for all nuclides of interest in the evaporation chain, have been calculated using the Myers-Swiatecki/Lysekil mass formula[25]. The pair-energy δ is calculated from the back shifted model. In these calculations pairing is as zero for even-even nuclides, $-\delta$ for odd-even and -2δ, for odd-odd nuclides respectively with $\delta = 11/\sqrt{A}$. The inverse cross-sections are calculated from the optical model subroutine of 'ALICE/LIVERMORE-82'[22], which uses the Becchetti and Greenlees[26] optical parameters. The intranuclear transition rates are calculated using the Pauli-corrected nucleon-nucleon (N-N) scattering cross-sections, and the adjustment of the mean free path for intranuclear transitions is done, keeping the so-called mean free path multiplier(k)

constant, and equal to 3.0.

The level density parameter influences the shape as well as the height of the calculated excitation functions[21]. For the calculations the level density formula proposed by Lang and Le couteur[27] is used. In general, for the level density parameter a value of $a = A/K$ is applied, where A denotes the nucleon number and K, a constant, for which values spread over a wide region have been given in the literature[28-30]. In our calculations a best fit has been obtained by using a value of 8 for ^{55}Mn, 10 for $^{63,65}Cu$ and $^{69,71}Ga$ and 12 for ^{209}Bi.

In pre-equilibrium reactions the initial exciton configuration is a crucial quantity[31]. The influence of this initial exciton configuration, on the results of the pre-equilibrium calculations, has been investigated by varying the initial exciton configuration n_o(n-p-h), which is described by the number of neutrons (n), and protons (p) in excited states, and the number of holes (h) after the first collision. The total exciton number n_o equals the sum of n,p and h. For α-induced reactions, the initial exciton number $n_o = 4$ or 5 was suggested by Blann[32]. However, it was found by many investigators[21,33-36] that $n_o = 4$ fits experimental data better than $n_o = 5$. We have performed the calculations with an initial exciton configuration $n_o = 4$, (2 neutrons, plus 2 protons, no hole i.e., pure particle state), which appears to give the best fit to our experimental data for α-induced reactions.

5.3 Discussion

The experimental excitation functions are compared with those predicted by theory, on the basis of the compound and pre-compound reaction mechanisms. Comparison with theory is made only for those reactions in which total cross-section (i.e., both isomers m and g) is measured in the present work. The excitation functions are represented by a solid curve for the cross-sections obtained by the consideration of both the compound and pre-compound contributions (GDH Model Calculation), and by a broken line for the compound nucleus (Weisskopf-Ewing calculation) cross-sections.

The agreement between the experimental and the theoretical excitation functions can be judged from their peak positions and widths. As can be seen from figures, the excitation functions calculated theoretically, have their peaks at energies, lower than the experimental ones. This is reasonable, since Weisskopf-Ewing calculations[2] refer to a lower limit for both these parameters[37], because of the angular momentum effects. Compound systems attained with incident particles of different masses, have appreciably different angular momenta, when excited to the same excitation energy. This, in principle can lead to differences in the excitation functions. If, in the last stages of the nuclear de-excitation, high angular momentum inhibits particle emission more than it does gamma-ray emission, then the peak of the excitation function, corresponding to the particle-emitting mode, will be shifted to the higher energy

side[38]. Such a shift could also be produced if the mean energy of the evaporated particles increases with increasing nuclear spin. The order of the magnitude of this shift can be obtained from nuclear rotational energy[38]. Blann et al.[39] have indicated that inclusion of angular momentum effects broadens the excitation functions.

Fig. 5.1 shows the theoretical and experimental excitation functions for the reaction $^{56}Mn(\alpha,n)^{58}Co$. This reaction produces two isomers of ^{58}Co, and both of them being unstable. Since the metastable state of ^{58}Co decays to its ground state with isomeric transitions, therefore, the measured cross-sections for ^{58}Co ground state gives the total cross-sections. It can be seen that there is good agreement between our results and the results of Tanaka et al.[32] with theory (GDH Model), while the results of Matsuo et al.[11] do not agree. Fig. 5.2, shows the theoretical and experimental excitation functions for the $^{55}Mn(\alpha,2n)^{57}Co$ reaction. It can also be seen that there is excellent agreement between our results and those obtained by Tanaka et al.[12] with theory (GDH Model). The experimentally measured and theoretically calculated excitation functions for the reaction $^{55}Mn(\alpha,3n)^{56}Co$ are shown in Fig. 5.3. In the lower energy side upto 40 MeV α-particle energy, our results agree with those of Tanaka et al.[12] but do not agree with theory. However, for the reaction $^{55}Mn(\alpha,4n)^{55}Co$ (Fig. 5.4) the theoretical cross-sections are surprisingly much higher than the measured one. This may probably be due to break-up

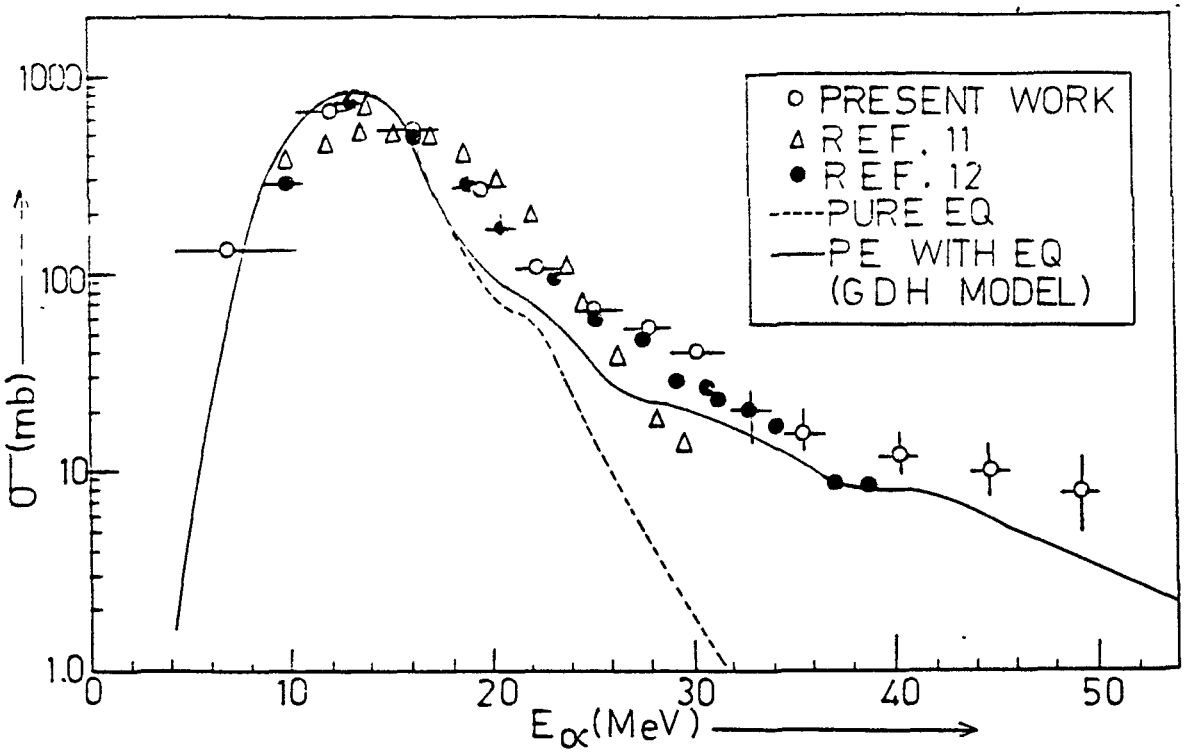

Fig. 5.1 Experimental and theoretical excitation functions for the reaction $^{55}Mn(\alpha,n)^{58}Co$.

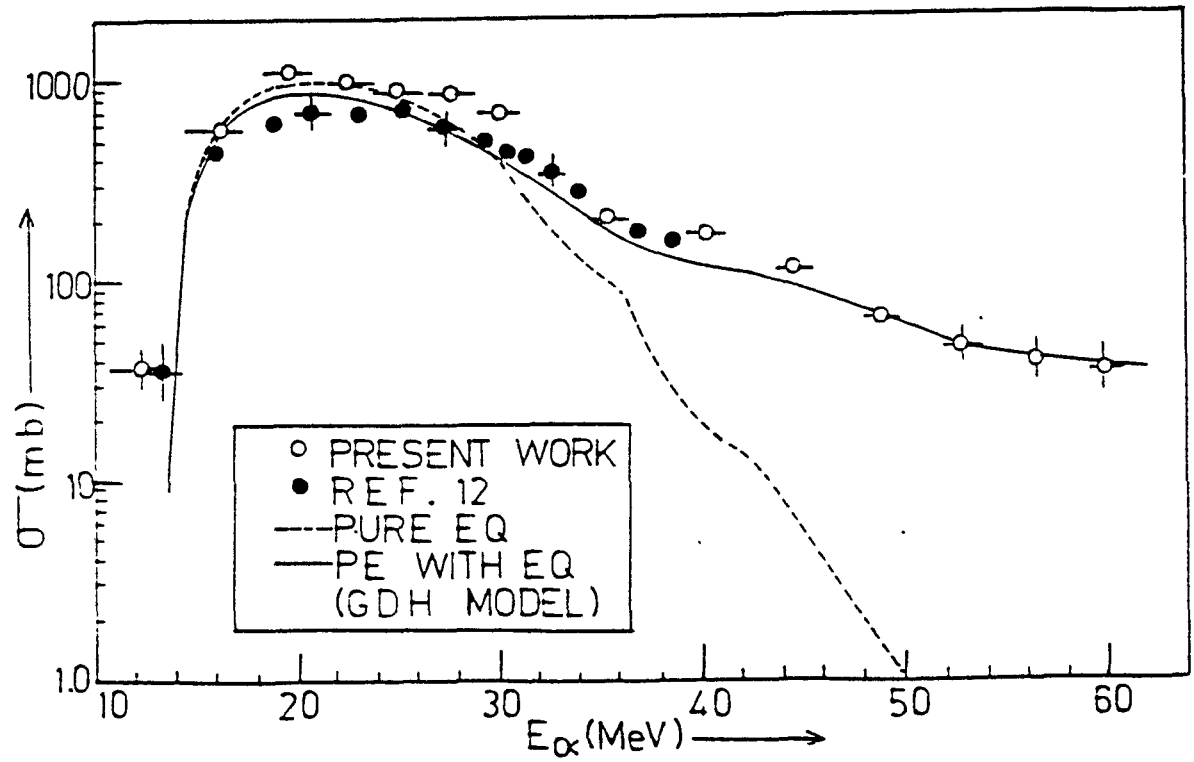

Fig. 5.2 Experimental and theoretical excitation functions for the reaction $^{55}Mn(\alpha,2n)^{57}Co$.

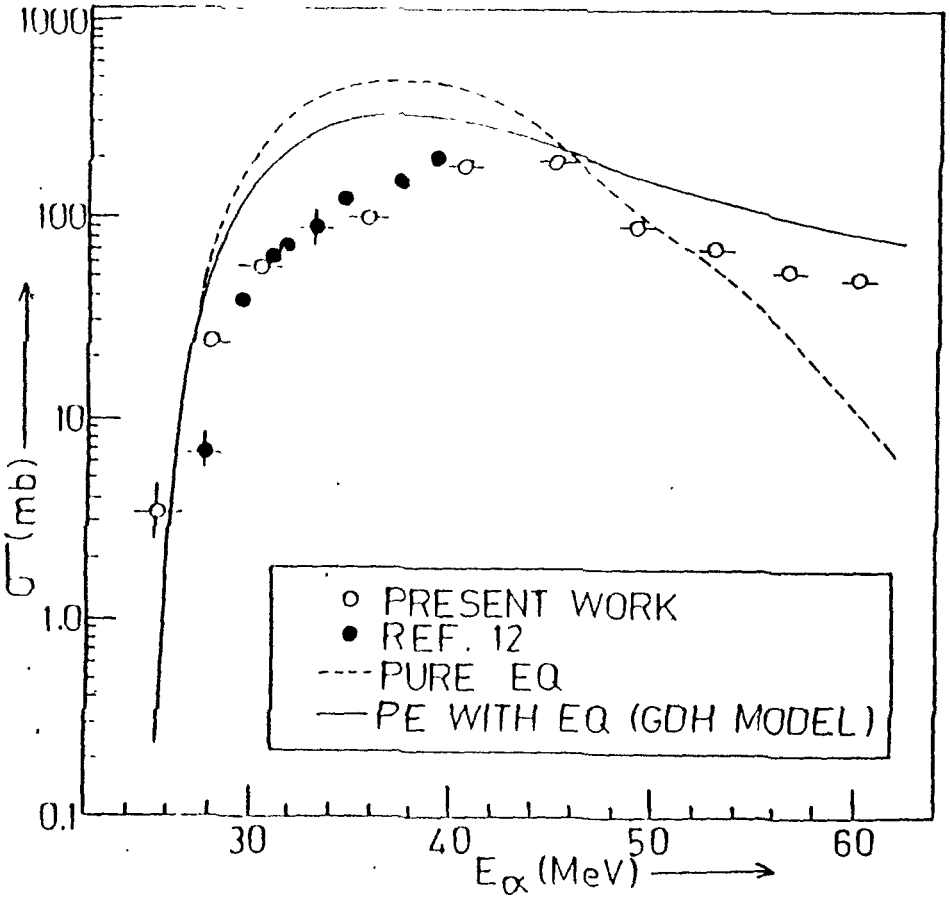

Fig. 5.3

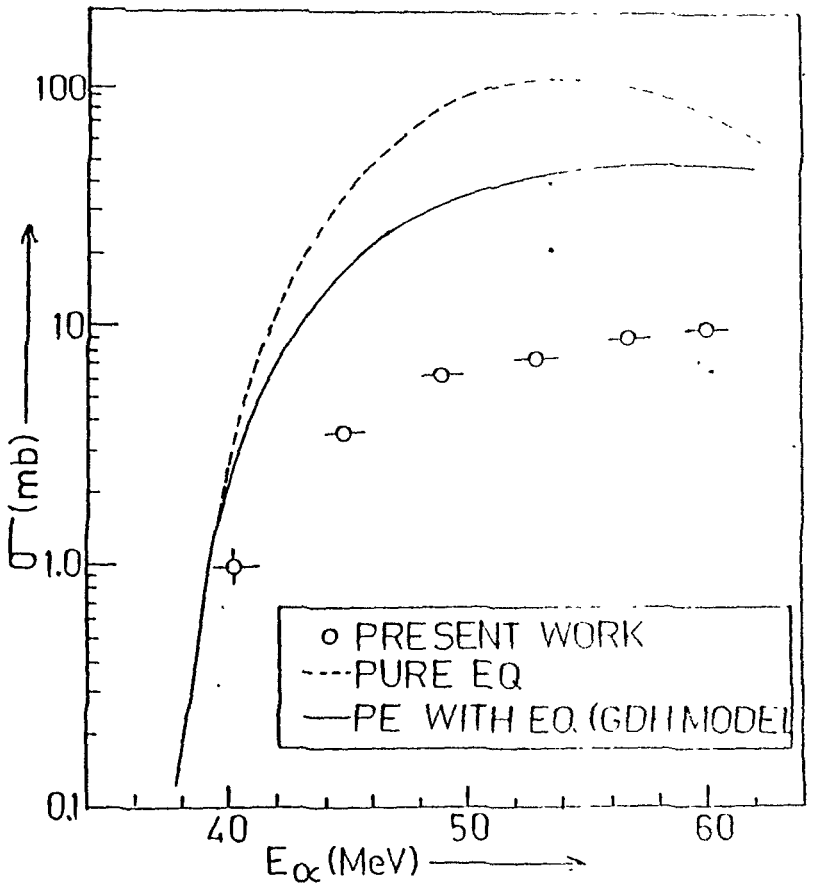

Fig. 5.4

Fig. 5.3 Experimental and theoretical excitation functions for the reaction $^{55}Mn(\alpha,3n)^{56}Co$.

Fig. 5.4 Experimental and theoretical excitation functions for the reaction $^{55}Mn(\alpha,4n)^{55}Co$.

reaction. Fig. 5.5, shows the experimental and theoretical results for the pair of reactions $^{55}Mn(\alpha,\alpha n)^{54}Mn$ and $^{55}Mn(\alpha,2p3n)^{54}Mn$, leading to the same residual nucleus ^{54}Mn. As explained earlier, the measured cross-section is the sum of these two reactions at the onset of the threshold energy of $^{55}Mn(\alpha,2p3n)^{54}Mn$ reaction, i.e., beyond 41.3 MeV. Below 40 MeV the experimental values are in agreement with theory (GDH Model), but above this energy, the picture changes drastically when looking the reaction, which is not adequately explained by theory. The dump between the αn and the 2p3n evaporation peaks is predicted to be much too deep by theory. In this case, we are observing massive contribution of pre-equilibrium α-emission which is not considered by theory. The excitation functions for the $^{55}Mn(\alpha,\alpha 3n)^{52}Mn$ reaction is measured only for the reaction leading to the ground state of ^{52}Mn. The results are shown in Fig. 5.6. Since we measured only the metastable state cross-sections, comparison of the results with theory is not feasible.

The measured excitation functions for the reactions $^{63}Cu(\alpha,n)^{66}Ga$ and $^{65}Cu(\alpha,3n)^{66}Ga$ are shown in Fig. 5.7. As the product nucleus is the same in both reactions, it is obvious that above the threshold energy of the $^{65}Cu(\alpha,3n)^{66}Ga$ reaction (i.e. 26.9 MeV), the experimentally measured cross-sections are the sum of the above two mentioned reactions. Therefore, the observed activity of 0.834 MeV and 1.039 MeV γ-rays, arising from the decay of residual nucleus ^{66}Ga, with

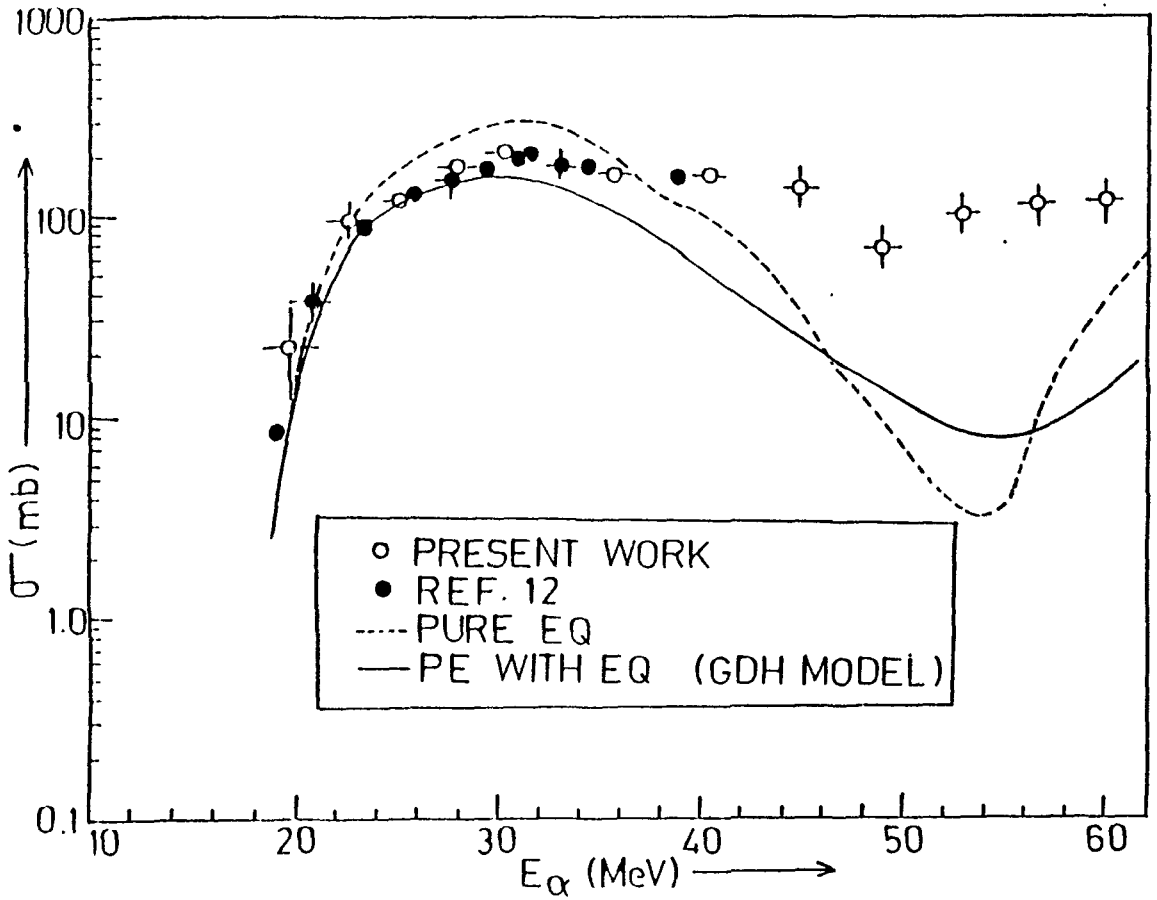

Fig. 5.5

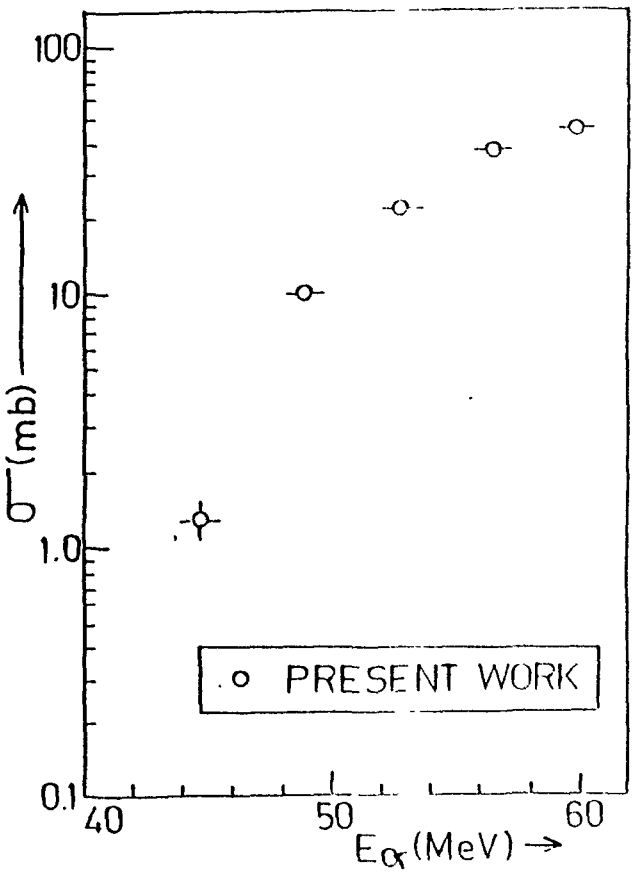

Fig. 5.6

Fig. 5.5 Experimental and theoretical excitation functions for the reactions $^{55}Mn(\alpha,\alpha n)^{54}Mn$ + $^{55}Mn(\alpha,2p3n)^{54}Mn$.

Fig. 5.6 Experimentally measured excitation function for the reaction $^{55}Mn(\alpha,\alpha 3n)^{52g}Mn$.

a half-life of 9.45 hours, into the irradiated samples, is the composite activity due to the two reactions, i.e., $^{63}Cu(\alpha,n)^{66}Ga$ and $^{65}Cu(\alpha,3n)^{66}Ga$. The two contributions can be separated pretty accurately, using either the known theoretical ratio of cross-sections, or, by substracting the contribution of one of the reactions measured with an enriched isotope. Efforts have been made to separate the contributions[40] for these two reactions using the theoretical excitation function for the reaction $^{63}Cu(\alpha,n)^{66}Ga$. Below the threshold for $^{65}Cu(\alpha,3n)^{66}Ga$ reaction (i.e. 26.9 MeV), the measured excitation function is due to $^{63}Cu(\alpha,n)^{66}Ga$ reaction only. Therefore, the measured excitation function for $^{63}Cu(\alpha,n)^{66}Ga$ reaction, below the threshold for $^{65}Cu(\alpha,3n)^{66}Ga$ reaction, has been first reproduced from theoretical calculations. The calculated excitation function has been then extended in the region of overlap, i.e., above 26.9 MeV, using the same set of parameters. The contribution of the extrapolated part of excitation function, beyond 26.9 MeV, for the $^{63}Cu(\alpha.n)$ reaction, has been subtracted from the composite decay curve, to get the counting rate for the $^{65}Cu(\alpha,n)$ reaction. This method for separating the two activities is justified, since the excitation functions for reactions $^{63}Cu(\alpha,n)^{66}Ga$ (Fig. 5.8) and for $^{65}Cu(\alpha,3n)^{66}Ga$ (Fig. 5.12), so resolved, are reproduced individually by theoretical calculations using the same set of parameters. The theoretically calculated and experimentally measured excitation functions for reactions $^{63}Cu(\alpha,2n)^{65}Cu$, and $^{63}Cu(\alpha,pn)^{65}Zn$ are

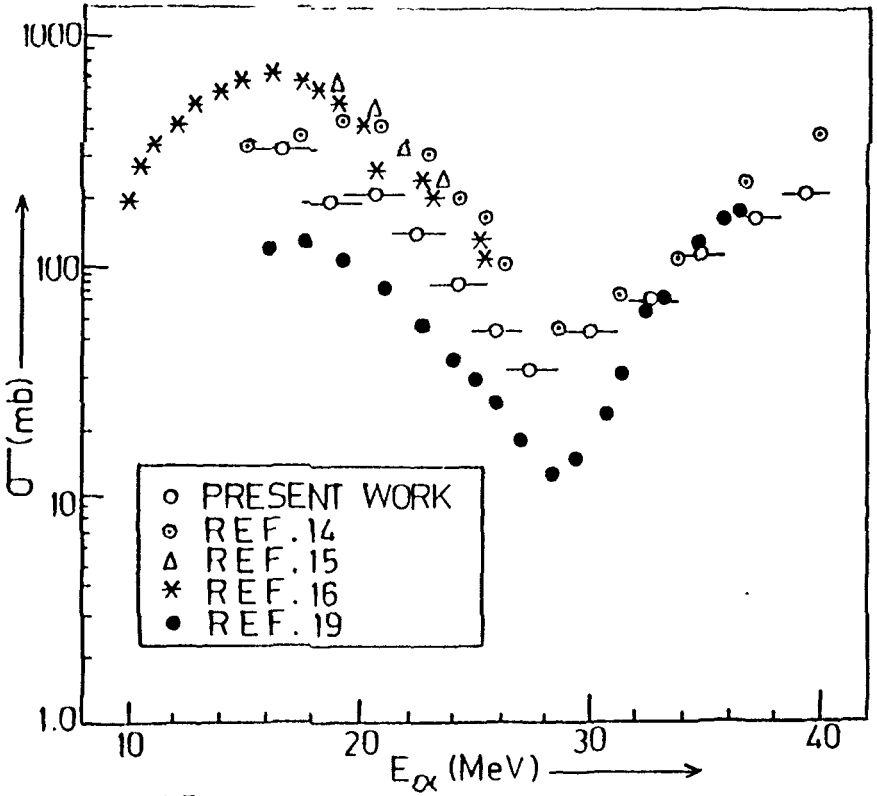

Fig. 5.7

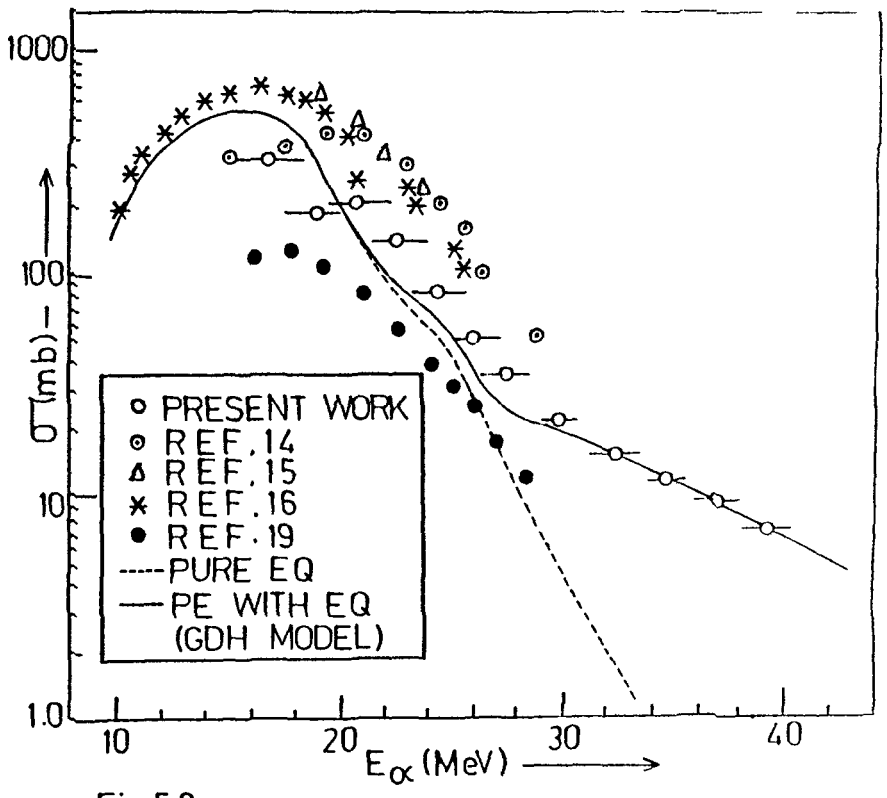

Fig. 5.8

Fig. 5.7 Experimentally measured excitation functions for the reactions $^{63}Cu(\alpha,n)^{66}Ga$ + $^{65}Cu(\alpha,3n)^{66}Ga$.

Fig. 5.8 Experimental and theoretical excitation functions for the reaction $^{63}Cu(\alpha,n)^{66}Ga$.

shown in Fig. 5.9. The excitation functions for these reactions have been measured as a cumulative sum of both the reactions, because the thresholds for both the reactions are close to each other, being 17.7 MeV and 13.4 MeV, respectively. One more reaction channel $^{65}Cu(\alpha,p3n)^{65}Zn$ opens at the offset of available α-particle energy (i.e. at 32.3 MeV), where as the same product nucleus ^{65}Zn is produced. By theoretical calculations we find that the cross-section for the reaction $^{65}Cu(\alpha,p3n)^{65}Zn$, is of the order of a few millibarns, upto 39.4 MeV energy and hence the contribution from the first two reactions, which is of the order of hundreds of millibarns, is predominant. The excitation function for the reaction $^{65}Cu(\alpha,n)^{68}Ga$, has also been measured and computed. Fig. 5.10 shows experimental data with the theoretically computed excitation function. The excitation functions (both experimental and theoretical), for the reaction $^{65}Cu(\alpha,2n)^{67}Ga$, are shown in Fig. 5.11. As can be seen from Figs. 5.8 - 5.12, our measured values are in better agreement with theory (GDH Model), while the earlier measurements[13-19] do not agree with theory, they are somewhat higher or lower than the calculated excitation functions.

Fig. 5.13, shows the theoretical and experimental excitation functions for the reaction $^{69}Ga(\alpha,n)^{72}As$. The excitation function for this reaction has been studied only upto 21.1 MeV α-particle energy, because above this energy, three more reaction channels, i.e., $^{69}Ga(\alpha,\alpha3n)^{66}Ga$ ($T_{1/2}$ = 26.01 hours,

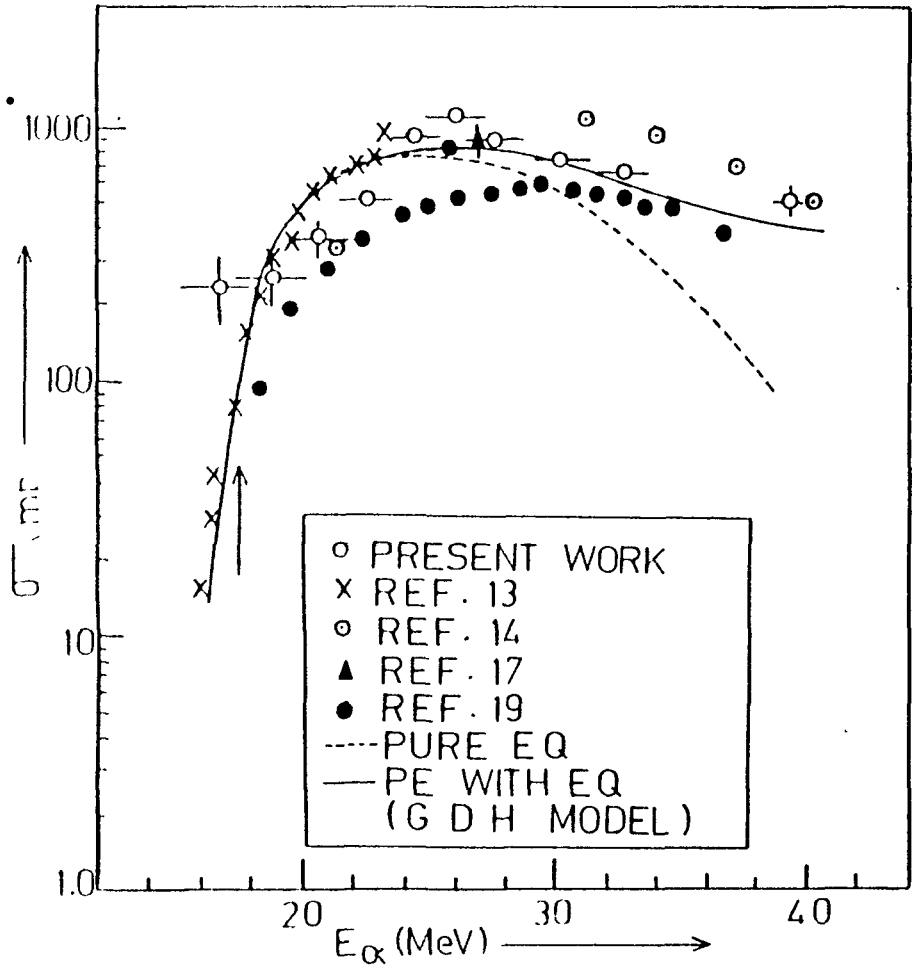

Fig 59

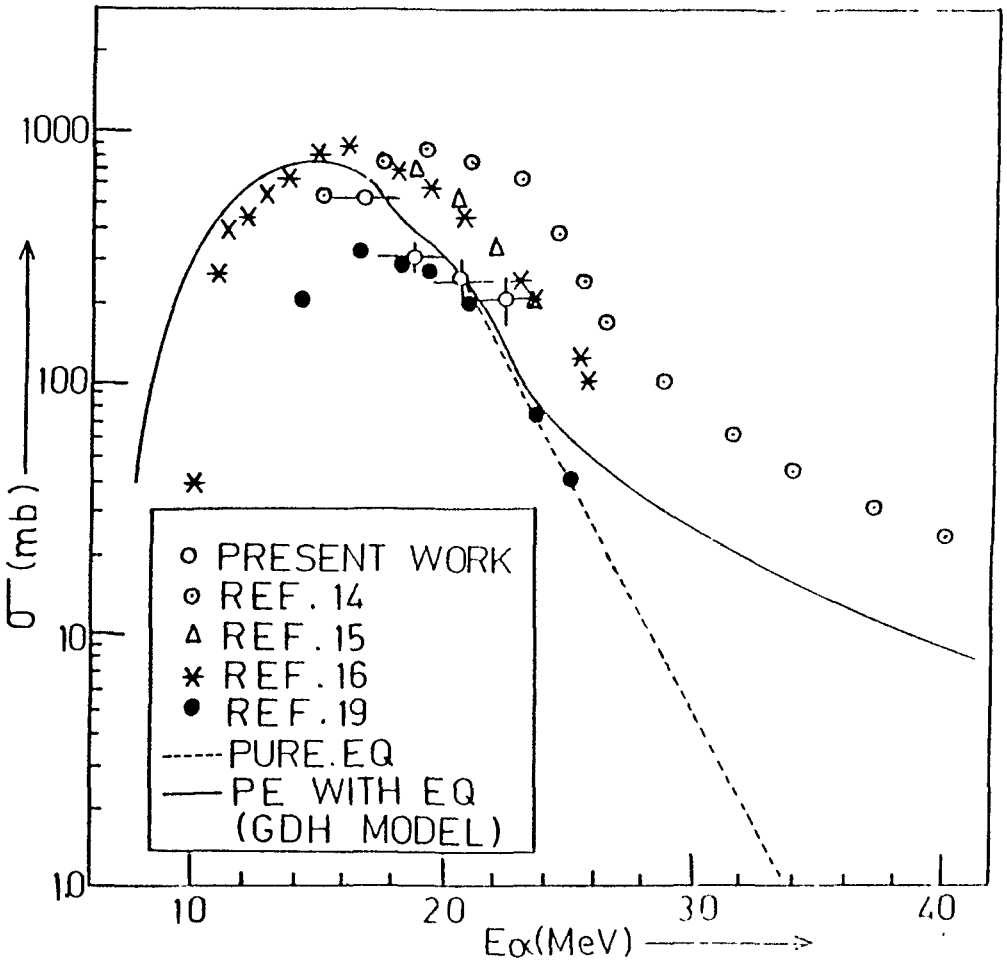

Fig. 5.10

Fig. 5.9 Experimental and theoretical excitation functions for the reactions $^{63}Cu(\alpha,2n)^{65}Ga$ + $^{63}Cu(\alpha,pn)^{65}Zn$.

Fig. 5.10 Experimental and theoretical excitation functions for the reaction $^{65}Cu(\alpha,n)^{68}Ga$.

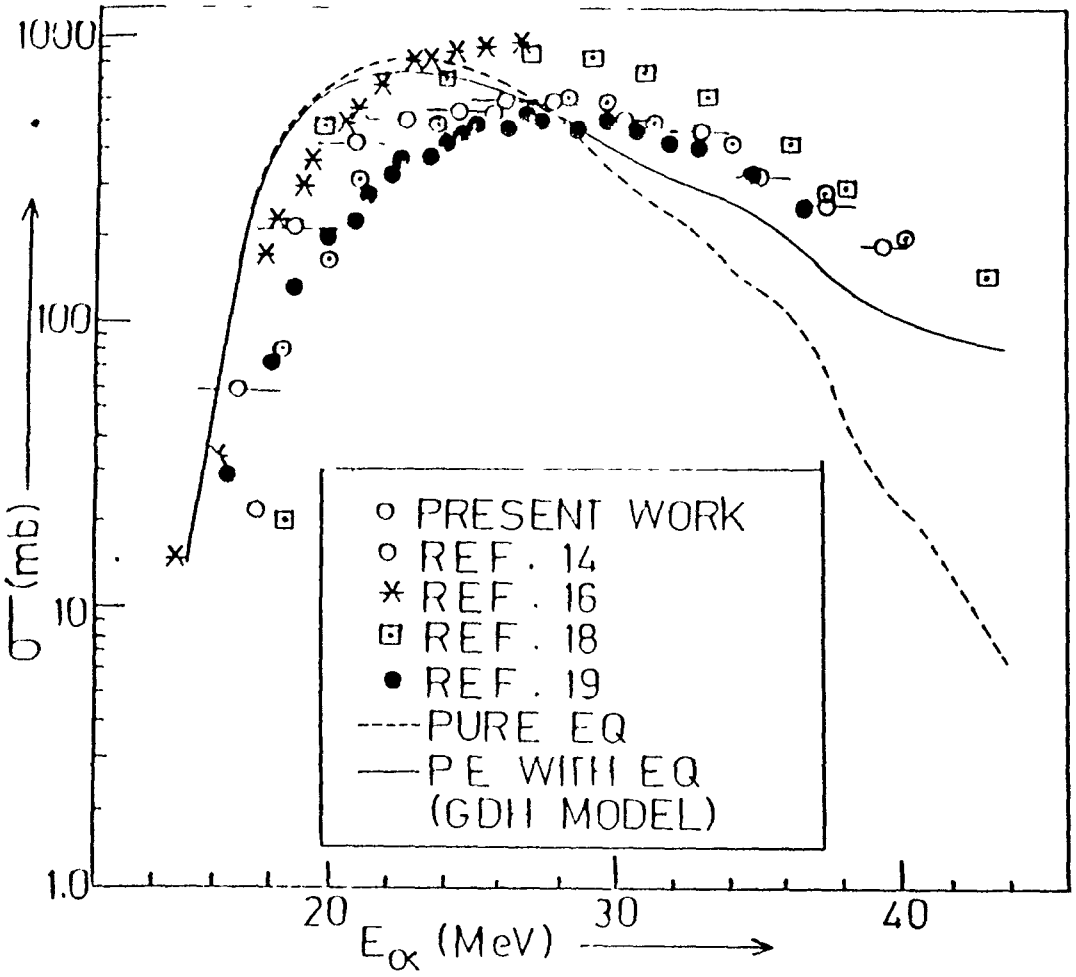

Fig 5 11

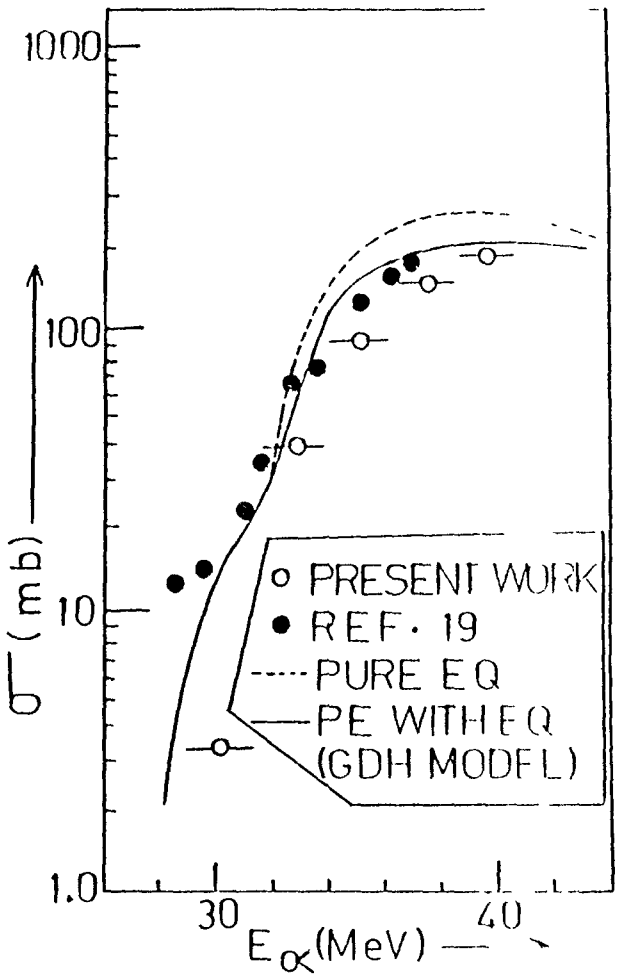

Fig. 5 12

Fig. 5.11 Experimental and theoretical excitation functions for the reaction $^{65}Cu(\alpha,2n)^{67}Ga$.

Fig. 5.12 Experimental and theoretical excitation functions for the reaction $^{65}Cu(\alpha,3n)^{66}Ga$.

Q = -26.03 MeV) and $^{71}Ga(\alpha,2pn)^{72}Ga$ ($T_{1/2}$ = 14.12 hours, Q = -21.78 MeV) occur at the same time and decay with the same gamma rays, i.e., 0.630 MeV and 0.834 MeV, as obtained in the case of the $^{69}Ga(\alpha,n)^{72}As$ reaction. The four reactions cannot be separated simultaneously. Fig. 5.14, shows the measured excitation functions for the reactions $^{69}Ga(\alpha,2n)$ and $^{71}Ga(\alpha,4n)$, leading to the same residual nucleus ^{71}As. The individual cross-section for $^{69}Ga(\alpha,2n)$ and $^{71}Ga(\alpha,4n)$ reactions, are separated at each energy, as explained earlier in cases of $^{63}Cu(\alpha,n)^{66}Ga$ and $^{65}Cu(\alpha,3n)^{66}Ga$ reactions. The theoretical and experimental excitation functions for the reactions $^{69}Ga(\alpha,2n)^{71}As$ and $^{71}Ga(\alpha,4n)^{71}As$ are shown in Figs. 5.15 and 5.19. It can be seen that there is agreement between theory (GDH Model) and experiment. Fig. 5.16 shows the present experimental values and the theoretical predictions for the reaction $^{69}Ga(\alpha,3n)^{70}As$ reaction. One more reaction channel $^{71}Ga(\alpha,5n)^{70}As$ opens at the offset of available α-particle energy (i.e., at 46.2 MeV), whereas the same product nucleus is produced. By theoretical calculations we find that the cross-section for the reaction $^{71}Ga(\alpha,5n)^{70}As$ is of the order of a few millibarns upto 60 MeV, and hence the contribution from the first reaction, i.e., $^{69}Ga(\alpha,3n)^{70}As$ is of the order of 5.5 millibarns is predominant. It can be seen that the trend of our experimental values is generally reproduced by the GDH model (theory). Fig. 5.17 shows the experimental and theoretical excitation functions for the $^{69}Ga(\alpha,p3n)^{69}Ge$

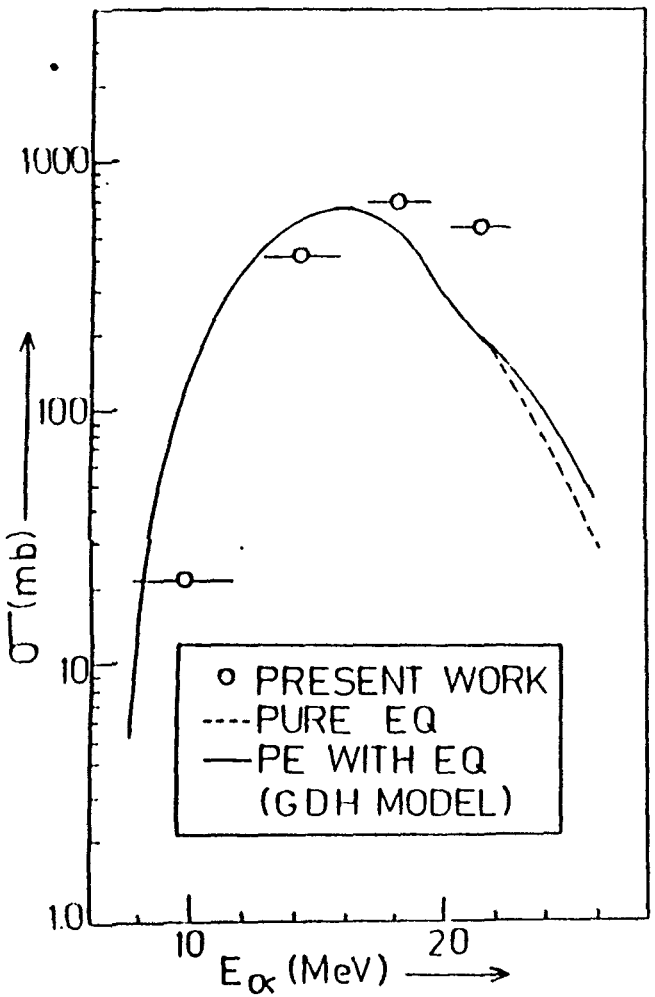

Fig. 5.13

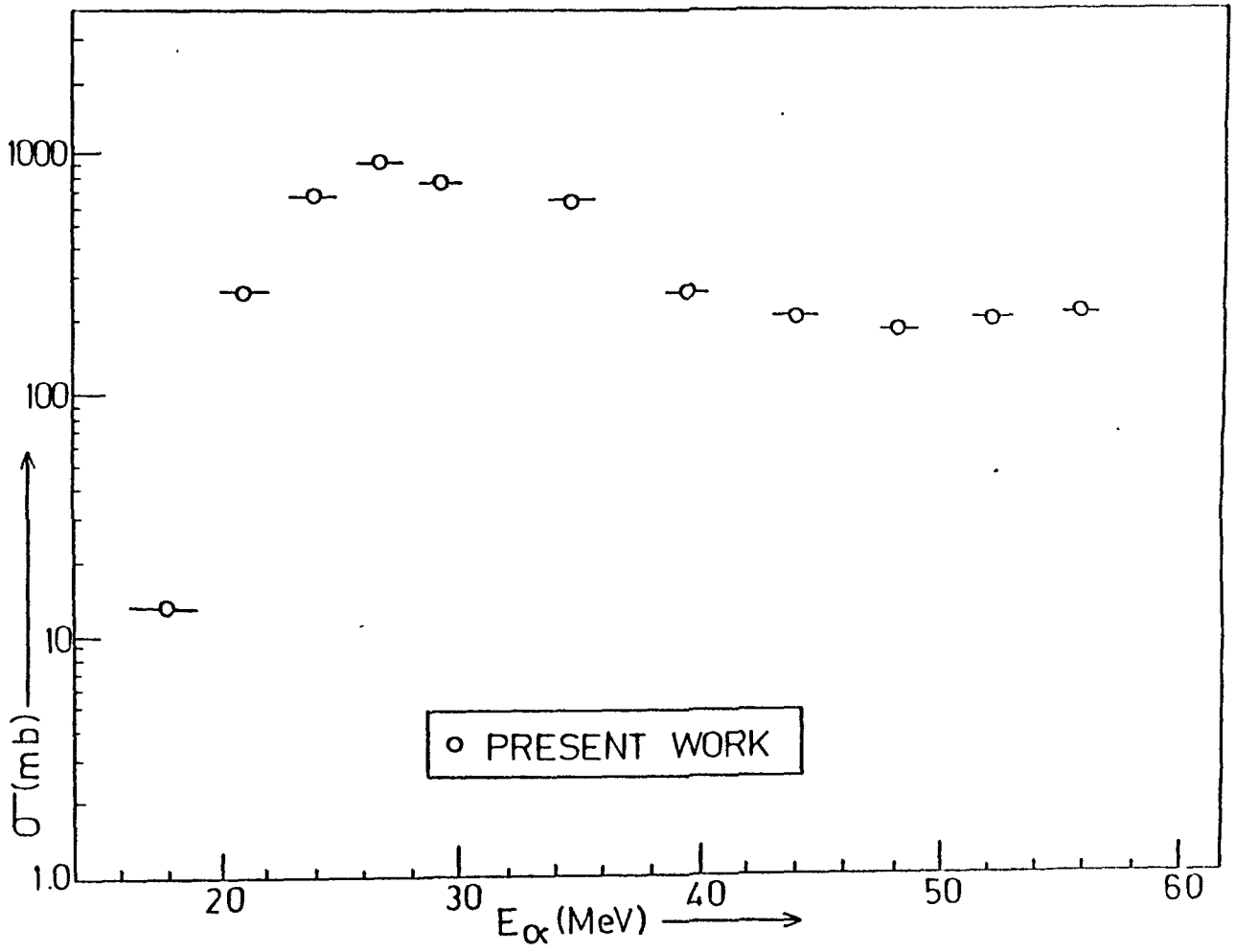

Fig. 5.14

Fig. 5.13 Experimental and theoretical excitation functions for the reaction $^{69}Ga(\alpha,n)^{72}As$.

Fig. 5.14 Experimentally measured excitation functions for the reactions $^{69}Ga(\alpha,2n)^{71}As$ + $^{71}Ga(\alpha,4n)^{71}As$.

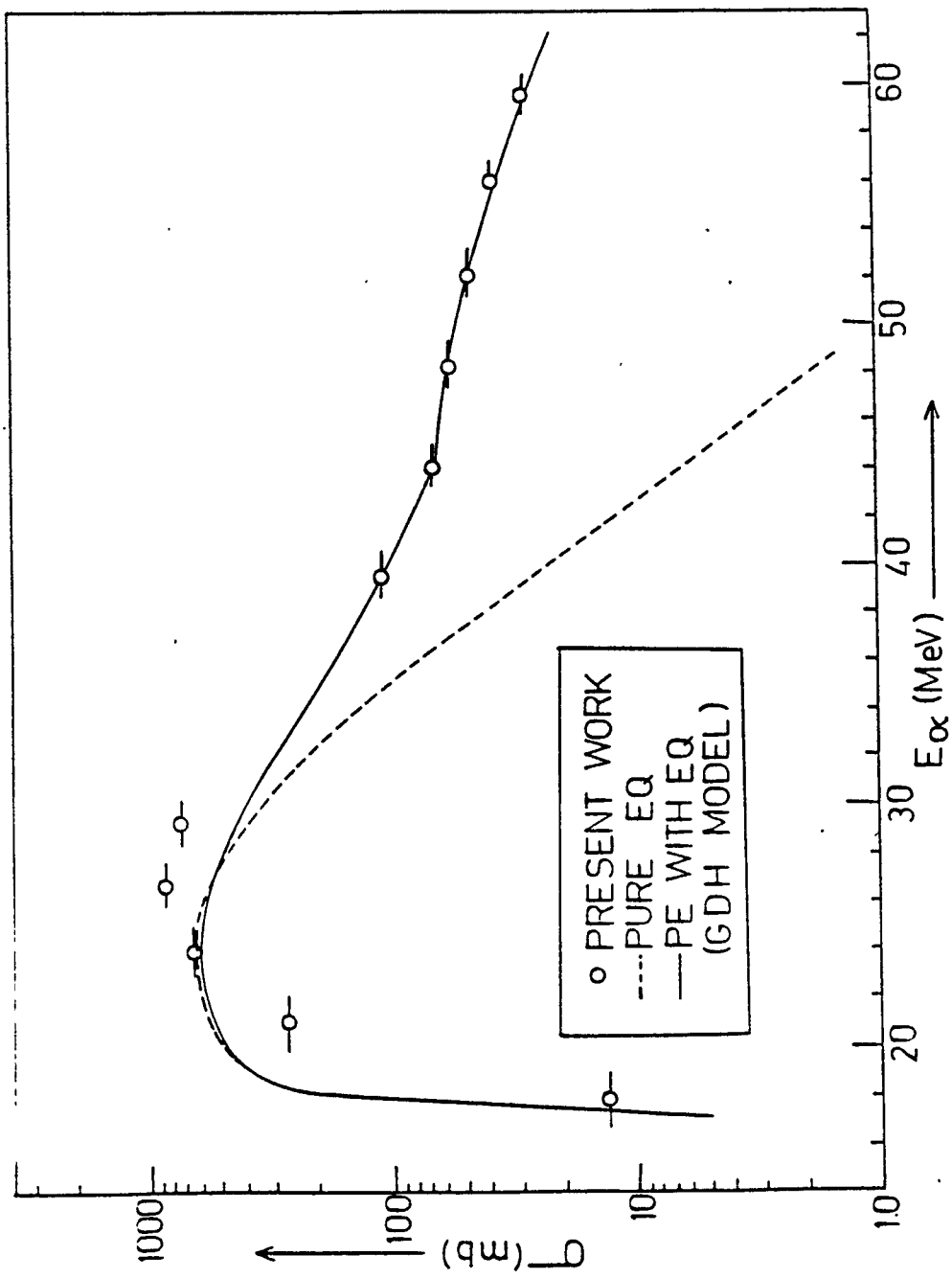

Fig. 5.15 Experimental and theoretical excitation functions for the reaction $^{69}Ga(\alpha,2n)^{71}As$.

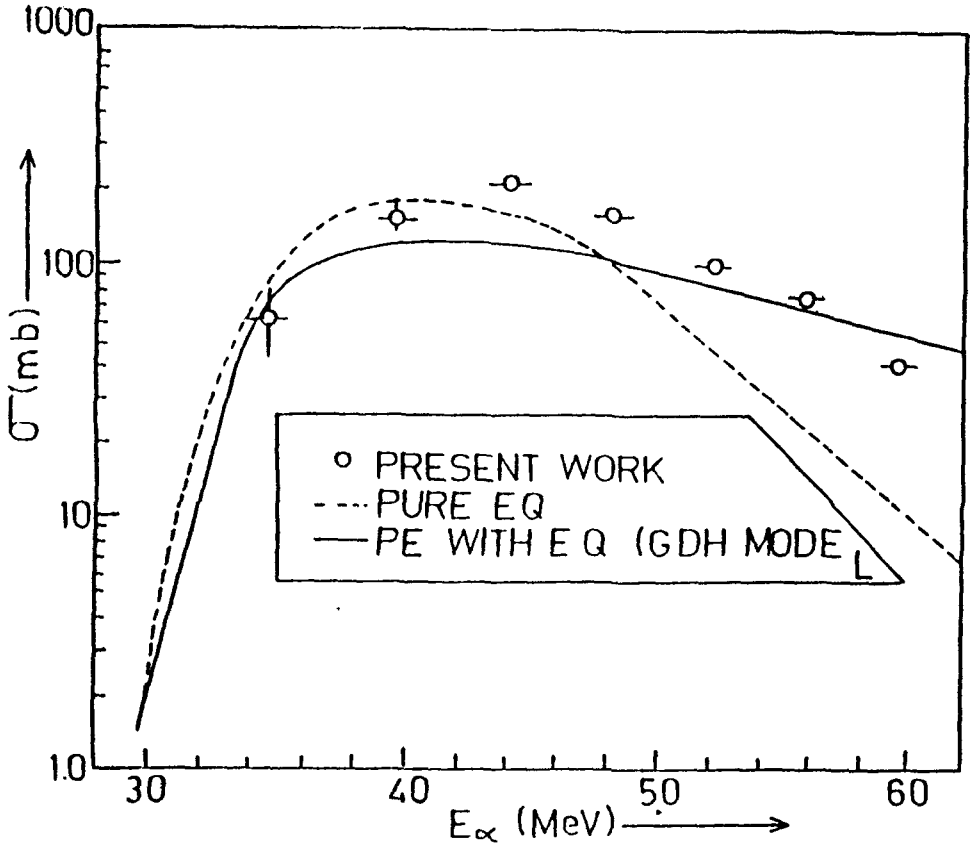

Fig. 5.16

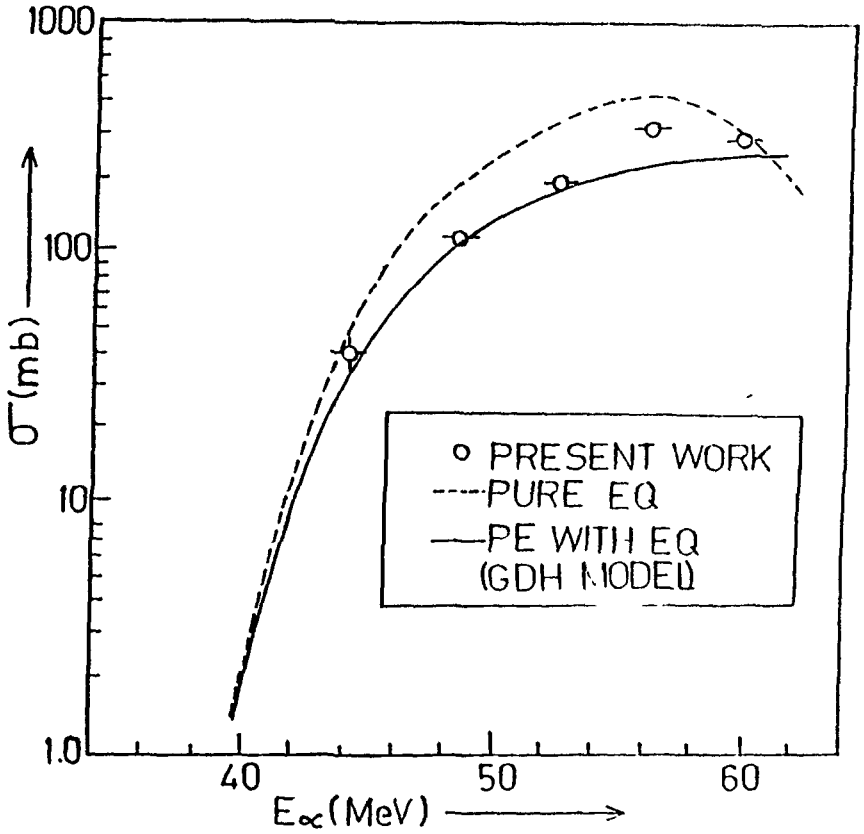

Fig. 5.17

Fig. 5.16 Experimental and theoretical excitation functions for the reaction $^{69}Ga(\alpha,3n)^{70}As$.

Fig. 5.17 Experimental and theoretical excitation functions for the reaction $^{69}Ga(\alpha,p3n)^{69}Ga$.

reaction. The same product nucleus ^{69}Ge is also produced by the $^{71}Ga(\alpha,p5n)$ reaction at the offset of the available α-particle energy (i.e. at 50.98 MeV). By theoretical calculations, it is important to note that the cross-section for the reaction $^{71}Ga(\alpha,p3n)^{69}Ge$ is <1 millibarns, upto 60 MeV, and hence the contribution from the $^{69}Ga(\alpha,p3n)^{69}Ge$ reaction, which is of the order of hundreds of millibarns is predominant. It can be seen that our results are in better agreement with GDH model calculations (theory). The theoretical and experimental excitation functions for the reaction $^{71}Ga(\alpha,n)^{74}As$ are shown in Fig. 5.18. It can be seen that there is good agreement between theory (GDH Model) and experiment.

The theoretical and experimental excitation functions for $^{209}Bi(\alpha,3n)^{210}At$ and $^{209}Bi(\alpha,4n)^{209}At$ reactions, are shown in Figs. 5.20 and 5.21. It can be seen that there is excellent agreement between our results and those obtained by Ramler et al.[20] with theoretical predictions (GDH Model).

In the present experiments, excitation functions for $^{55}Mn(\alpha,p)^{58}Fe$, $^{55}Mn(\alpha,pn)^{57}Fe$, $^{55}Mn(\alpha,5n)^{54}Co$, $^{63}Cu(\alpha,3n)^{64}Ga$, $^{63}Cu(\alpha,n\alpha)^{62}Cu$, $^{63}Cu(\alpha,2n\alpha)^{61}Cu$, $^{69}Ga(\alpha,4n)^{69}As$, $^{69}Ga(\alpha,p)^{72}Ge$, $^{69}Ga(\alpha,np)^{71}Ge$, $^{71}Ga(\alpha,p)^{74}Ge$, $^{71}Ga(\alpha,pn)^{73}Ge$, $^{209}Bi(\alpha,n)^{212}At$, $^{209}Bi(\alpha,2n)^{211}At$, $^{209}Bi(\alpha,p)^{212}Po$, $^{209}Bi(\alpha,pn)^{210}Po$ and $^{209}Bi(\alpha,5n)^{208}At$ reactions, could not be measured either because of the short half-life of the product nucleus, or, because of the low intensity of the induced activity.

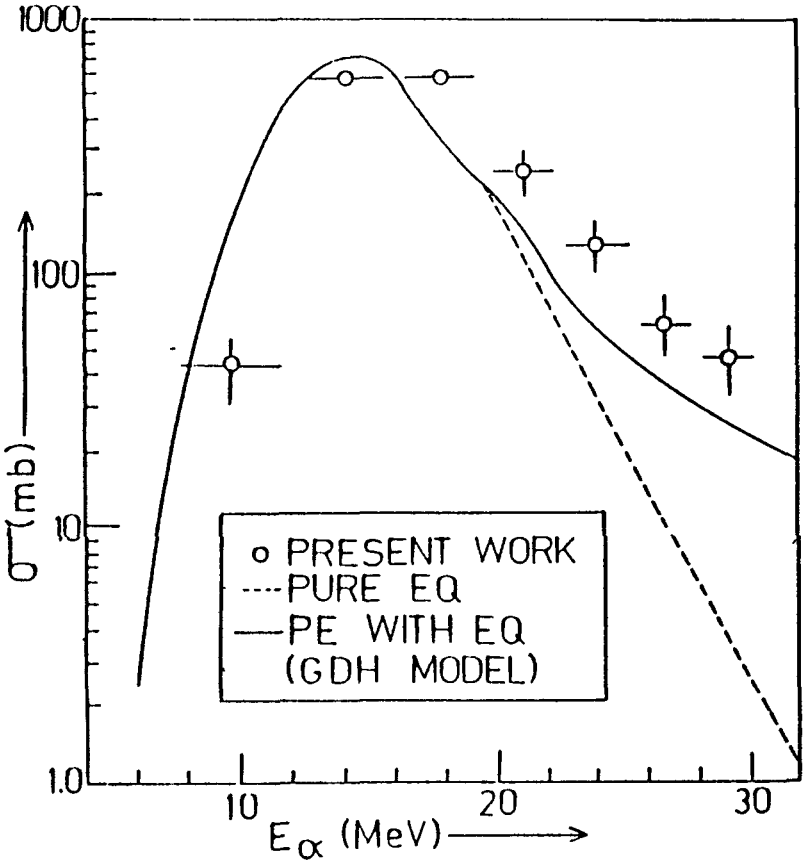

Fig. 5 18

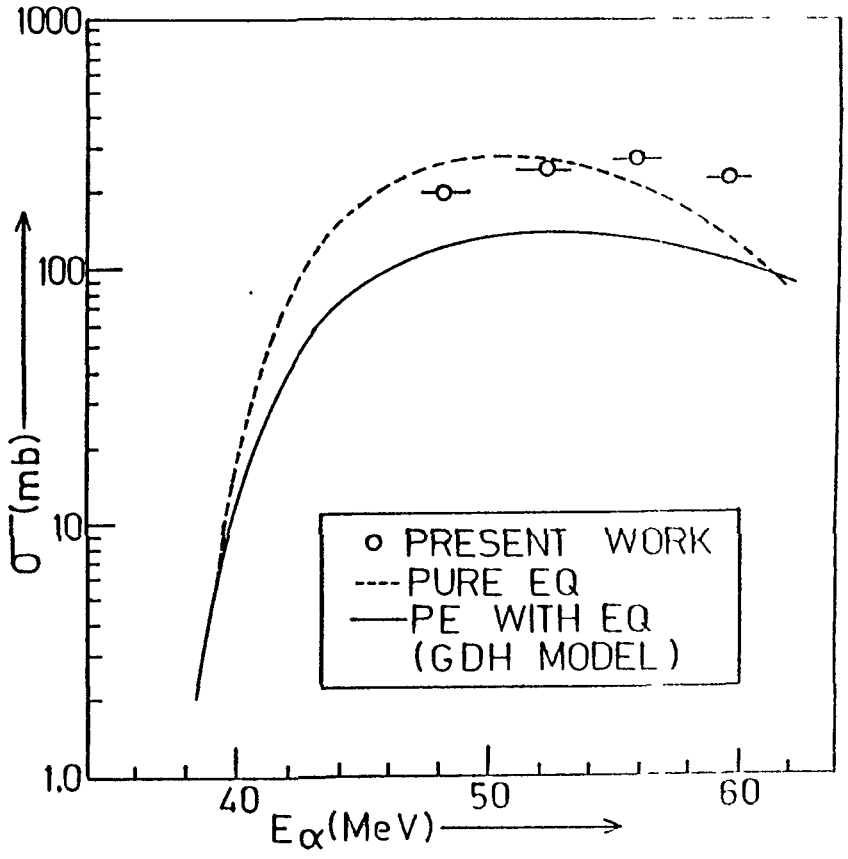

Fig. 5.19

Fig. 5.18 Experimental and theoretical excitation functions for the reaction $^{71}Ga(\alpha,n)^{74}As$.

Fig. 5.19 Experimental and theoretical excitation functions for the reaction $^{71}Ga(\alpha,4n)^{71}As$.

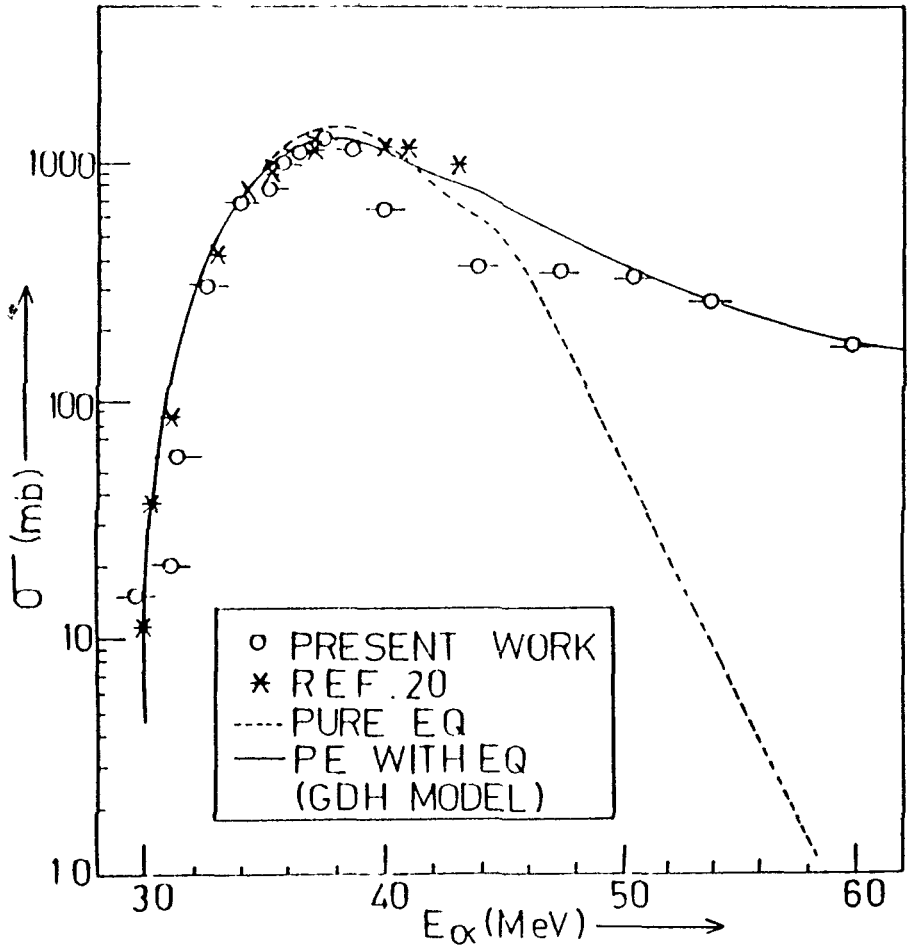

Fig 5.20

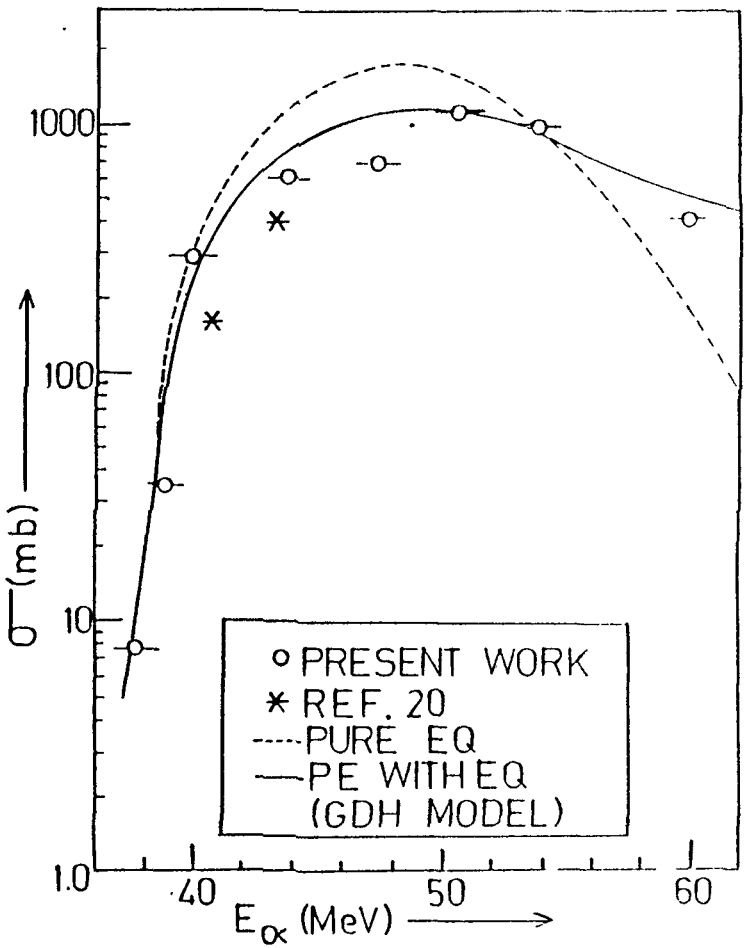

Fig. 5.21

Fig. 5.20 Experimental and theoretical excitation functions for the reaction $^{209}Bi(\alpha,3n)^{210}At$.

Fig. 5.21 Experimental and theoretical excitation functions for the reaction $^{209}Bi(\alpha,4n)^{209}At$..

5.4 Conclusions

From the present study of the excitation functions of α-induced reactions for ^{55}Mn, $^{63,65}Cu$, $^{69,71}Ga$ and ^{209}Bi, it is concluded that the quantitative agreement between the experimental and theoretical results is not very good in general, but qualitatively it is satisfactory, specially in the high energy tail portion of the excitation functions. Inspite of this quantitative disagreement, it is quite evident from Figs. 5.1 - 5.5, 5.8 - 5.13, 5.15 - 5.21, that pre-equilibrium (PE) emission of multiparticles is necessary before the system is equilibrated, and hence, the experimentally observed high energy tail of the excitation function can be explained only when the combination of semi-classically treated pre-equilibrium emission (geometry dependent hybrid model), followed by particle evaporation from the equilibrated system (Weisskopf-Ewing Model), is taken into account. The pure equilibrium reaction mechanism in its decay, is unable to explain the experimental data in the high energy tail portion of the excitation function. It is clear from the Figs. 5.1 - 5.5, 5.8 - 5.13, 5.15 - 5.21 that calculated values shown by broken lines(based on the pure equilibrium model) do not reproduce well the experimental data; they are reproduced well only when the pre-equilibrium emission is also taken into account, as shown by solid lines. We also infer that the initial exciton configuration $n_o = 4$ (2 neutrons plus 2 protons, no hole) gives the best fit to our experimental data and support the finding of

many earlier investigations[21,33-36].

The present analysis inoicates clearly the presence of significant pre-equilibrium contributions in α-induced reactions. Pre-equilibrium fraction (f_{PE}) is a measure of the relative weight of the pre-equilibrium contribution needed for the reproduction of experimental excitation functions and it reflects the relative importance of pre-equilibrium and equilibrium processes[40]. It is more meaningful to look for the total pre-equilibrium fraction of all type of emitted particles[41]. In a given target nucleus the total pre-equilibrium fraction, for all type of reactions, like (α,xpynα) reactions, are calculated using the 'ALICE/LIVERMORE-82'[22] code. Because of considerable contributions to pre-equilibrium fraction from the pre-equilibrium emission of charged particles, the calculated total pre-equilibrium fractions are not directly comparable with the measured excitation functions for (α,xn) type reactions. However, no definite trends for the variation of pre-equilibrium fraction with excitation energy, or, compound system mass number and changes in initial exciton number are reported[41], yet it is reasonable to assume that f_{PE} depends on the excitation energy of the compound system[32]. In the present calculations, f_{PE} is inherently energy dependent. This dependence is derived from consideration of the internal transition rates and of continuum decay rates[40,42]. The f_{PE} has been taken to be proprotional to the commulative sum of the probability of finding the particle in the continuum for

every possible configuration during the process of equilibration.

The calculated pre-equilibrium fractions for ^{55}Mn, $^{63,65}Cu$, $^{69,71}Ga$ and ^{209}Bi are shown in Fig. 5.22 as a function of bombarding energy (E_α) in the energy range $\lesssim$ 7-60 MeV. It is inferred from the Fig. 5.22, that the pre-equilibrium fraction increases very fast as the excitation energy of α-particle increases, and then at higher excitation energy, when the multiplicity of the out going particle increases, the pre-equilibrium fraction (f_{PE}) becomes more or less constant. As can be seen, in general, the pre-equilibrium threshold increases with the mass number of target isotopes, except in cases of ^{63}Cu and ^{71}Ga.

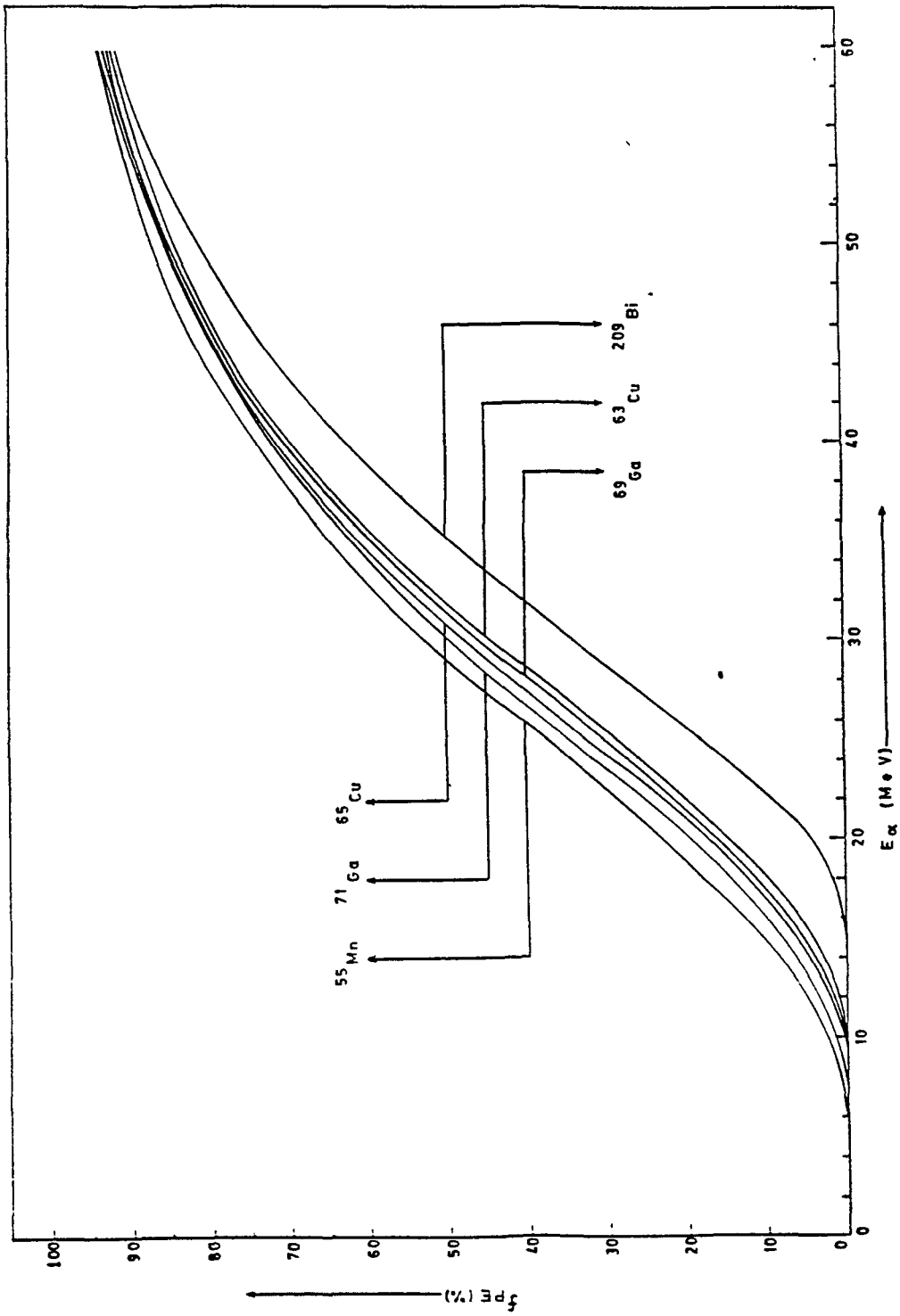

Fig. 5.22 Pre-equilibrium fraction (f_{PE}) of the total reaction cross-section as a function of α-particle energy.

References

1) EXFOR Library, Nuclear Data Section, I.A.E.A., Vienna (1986).

2) V.F. Weisskopf and D.H. Ewing : Phys. Rev. 57 (1940) 472.

3) J. Rama Rao, A.V. Mohan Rao, S. Mukherjee, R. Upadhyay, N.L. Singh, S. Agarwal, L. Chaturvedi and P.P. Singh : Nucl. Instr. Methods B24/25 (1987) 484.

4) W.W. Bowman and M. Blann : Nucl. Phys. A131 (1969) 513.

5) A. Djaloeis, P. Jahn, H.J. Probst and C. Mayer-Boricke : Nucl. Phys. A250 (1975) 149.

6) J.P. Didelez, P.M. Lieder, H. Beuscher, D.R. Haenni, H. Machner, M. Muller-veggian and C. Mayer-Boricke : Nucl. Phys. A341 (1980) 421.

7) J. Ernst, R. Ibowski, H. Klampfl, H. Machner, T. Mayer-Kuckuk and R. Schanz : Z. Phys. Atoms. and Nuclei. A308 (1982) 301.

8) E. Gadioli, E. Gadioli-Erba, J.J. Hogan and B.V. Jacak : Phys. Rev. C29 (1984) 76.

9) R. Michel and G. Brinkmann : Nucl. Phys. A338 (1980) 167.

10) J. Rama Rao, A.V. Mohan Rao, S. Mukherjee, R. Upadhyay, N.L. Singh, S. Agarwal, L. Chaturvedi and P.P. Singh : J. Phys. G; Nucl. Phys. 13 (1987) 535.

11) T. Matsuo, J.M. Matuszek, Jr., N.D. Dudey and T.T. Sugihara : Phys. Rev. B139 (1965) 886.

12) S. Tanaka, M. Furukawa, T. Mikumo, S. Iwata, M. Yagi, H. Amano : J. Phys. Soc. Japan 15 (1960) 545; Errata : J. Phys. Soc. Japan 15 (1960) 1357.

13) S.Y. Lin and J.M. Alexander : Phys. Rev. C16 (1977) 688.

14) N.T. Porile and D.L. Morrison : Phys. Rev. 116 (1959) 1193.

15) M. Hille, P. Hille, M. Uhl and W. Weisz : Nucl. Phys. A198 (1972) 625.

16) E.A. Bryant, D.R.F. Cochran and J.D. Knight : Phys. Rev. 130 (1963) 1512.

17) E. Lebowitz and M.W. Green : Int. J. App. Rad. Isotopes 21 (1970) 625.

18) H.P. Graf and H. Munzel : J. Inorg. Nucl. Chem. 36 (1974) 3647.

19) K.G. Porges : Phys. Rev. 101 (1956) 225.

20) W.J. Ramler, J. Wing, D.J. Henderson and J.R. Huizenga : Phys. Rev. 114 (1959) 154.

21) P. Misaelides and H. Munzel : J. Inorg. Nucl. Chem. 42 (1980) 937.

22) M. Blann and J. Bisplinghoff : 'ALICE/LIVERMORE-82', Lawrence Livermore Laboratory Report UCID-19614 (1982).

23) M. Blann : Phys. Rev. Lett. 27 (1971) 337; 27 (1971) 700(E); 27 (1971) 1550(E).

24) M. Blann : Phys. Rev. Lett. 28 (1972) 757.

25) W.D. Myers and W.J. Swiatecki : Ark. Fys. 36 (1967) 343.

26) F.D. Becchetti and G.W. Greenlees : Phys. Rev. 182 (1969) 1190.

27) J.M. Lang and K.J. Le Couteur : Proc. Phys. Soc. 67A (1954) 586.

28) D.G. Sarantites : Nucl. Phys. A93 (1967) 576.

29) G. Hurwitz, S.J. Spencer, R.A. Esterlund, B.D. Pate and J.B. Reynoldes : Nucl. Phys. 54 (1964) 65.

30) S. Fukushima, S. Hayashi, S. Kuma, H. Ikamura, K. Otozai, K. Sakamoto and Y. Yoshizawa : Nucl. Phys. 41 (1963) 275.

31) R. Michel and M. Galas : Nucl. Phys. A404 (1983) 77.

32) M. Blann : Ann. Nucl. Sci. 25 (1975) 123.

33) M. Blann and T.T. Komoto : Phys. Rev. C29 (1984) 1678.

34) I.A. Rizvi, M. Afzal Ansari, R.P. Gautam, R.K.Y. Singh and A.K. Chaubey : J. Phys. Soc. Japan 56 (1987) 3135.

35) R.K.Y. Singh : Ph.D. Thesis, Aligarh Muslim University, Aligarh (1985).

36) G.W.A. Newton, V.J. Robinson and E.M. Shaw : J. Inorg. Nucl. Chem. 43 (1981) 2227.

37) F.M. Lanzafame and M. Blann : Nucl. Phys. A142 (1970) 545.

38) D. Bodansky : Ann. Rev. Nucl. Sci. 12 (1962) 79.

39) M. Blann and G. Merkel : Phys. Rev. B137 (1965) 367.

40) R. Prasad and H.D. Bhardwaj : Internal Report IC/86/41 International Centre for Theoretical Physics, Trieste (Italy).

41) C.K. Cline and M. Blann : Nucl. Phys. A172 (1971) 225.

42) H.D. Bhardwaj and R. Prasad : Nucl. Instr. Method A242 (1985) 286.

List of Publications of the Author

1. Excitation Function Studies for $^{209}Bi(\alpha,3n)^{210}At$ Reaction.
   I.A. Rizvi, M. Afzal Ansari, R.P. Gautam and M.L. Sehgal,
   Proc. Nucl. Phys. Symposium (India) 28B C10 (1985) 36.

2. Alpha Induced Excitation Function Studies on Copper Isotopes.
   I.A. Rizvi, M. Afzal Ansari, R.K.Y. Singh, R.P. Gautam and A.K. Chaubey,
   Proc. Nucl. Phys. Symposium (India) 29B C11 (1986) 43.

3. Pre-equilibrium Particle Emission Process in Alpha Induced Silver Excitation Functions.
   R.P. Gautam, M. Afzal Ansari, R.K.Y. Singh, **I.A. Rizvi** and A.K. Chaubey,
   Proc. Nucl. Phys. Symposium (India) 29B P51 (1986) 245.

4. Excitation Function of $^{27}Al(\alpha,xn)$ Reaction between 50-63 MeV Range.
   I.A. Rizvi, A.K. Chaubey, Rajender Prasad and B.P. Singh
   Bulletin of the American Physical Society 31 (1986) p. 2.52 1304.

5. Excitation Function Studies of $(\alpha,xpyn)$ Reactions for $^{63,65}Cu$ and Pre-equilibrium Effects.
   I.A. Rizvi, M. Afzal Ansari, R.P. Gautam, R.K.Y. Singh and A.K. Chaubey,
   J. Phys. Soc. (Japan) 56 (1987) 3135.

6. Excitation Functions for Alpha-Induced Reactions on Gallium Isotopes.
   I.A. Rizvi, M. Afzal Ansari, Manoj Kumar, R.P. Gautam and A.K. Chaubey,
   Proc. Nucl. Phys. Symposium (India) 30B D29 (1987) 256.

7. Study of Isomer Ratio of ^{181}Ta in Neutron Capture.
R.K.Y. Singh, M. Afzal Ansari, I.A. Rizvi and R.P. Gautam,
Proc. Nucl. Phys. Symposium (India) 30B D37 (1987) 272.

8. Radiative Capture of Fast Neutrons in ^{160}Gd.
R.K.Y. Singh, M. Afzal Ansari, R.P. Gautam, I.A. Rizvi and S. Kailas,
Can. J. Phys. (Canada) 66 (1988) 330.

9. Pre-equilibrium Decay Process in the α-Induced Reactions on Silver Isotopes.
M. Afzal Ansari, R.K.Y. Singh, R.P. Gautam, I.A. Rizvi and A.K. Chaubey,
International Centre for Theoretical Physics (Italy)
Internal Report IC/88/50.

10. Multiparticle Emission in the Pre-equilibrium Decay of Light and Heavy Nuclei in α-Induced Reaction upto 60 MeV.
M. Afzal Ansari, I.A. Rizvi, M.K. Bardwaj and A.K. Chaubey,
International Centre for Theoretical Physics (Italy)
Internal Report IC/88/57.